

Event Generation for Next to Leading Order Chargino Production at the International Linear Collider

Dissertation
zur Erlangung des Doktorgrades
des Departments Physik
der Universität Hamburg

vorgelegt von
Tania Robens
aus Antwerpen

Hamburg
2006

Gutachter des Dissertation:	Prof. Dr. W. Kilian Prof. Dr. J. Bartels
Gutachter der Disputation:	Prof. Dr. W. Kilian Prof. Dr. B. Kniehl
Datum der Disputation:	24. 10. 2006
Vorsitzender des Prüfungsausschusses:	Prof. Dr. C. Hagner
Vorsitzender des Promotionsausschusses:	Prof. Dr. G. Huber
Dekan der Fakultät MIN:	Prof. Dr. A. Frühwald

Abstract

At the International Linear Collider (ILC), parameters of supersymmetry (SUSY) can be determined with an experimental accuracy matching the precision of next-to-leading order (NLO) and higher-order theoretical predictions. Therefore, these contributions need to be included in the analysis of the parameters.

We present a Monte-Carlo event generator for simulating chargino pair production at the ILC at next-to-leading order in the electroweak couplings. We consider two approaches of including photon radiation. A strict fixed-order approach allows for comparison and consistency checks with published semianalytic results in the literature. A version with soft- and hard-collinear resummation of photon radiation, which combines photon resummation with the inclusion of the NLO matrix element for the production process, avoids negative event weights, so the program can simulate physical (unweighted) event samples. Photons are explicitly generated throughout the range where they can be experimentally resolved. In addition, it includes further higher-order corrections unaccounted for by the fixed-order method. Inspecting the dependence on the cutoffs separating the soft and collinear regions, we evaluate the systematic errors due to soft and collinear approximations for NLO and higher-order contributions. In the resummation approach, the residual uncertainty can be brought down to the per-mil level, coinciding with the expected statistical uncertainty at the ILC. We closely investigate the two-photon phase space for the resummation method. We present results for cross sections and event generation for both approaches.

Zusammenfassung

Am Internationalen Linearbeschleuniger (International Linear Collider, ILC) können die Parameter supersymmetrischer Theorien (SUSY) mit einer experimentellen Genauigkeit gemessen werden, die der Präzision von theoretischen Vorhersagen von nächstführenden (next-to-leading, NLO) und höheren Ordnungen entspricht. Daher müssen diese Beiträge in die Analyse der Parameter eingeschlossen werden.

Wir präsentieren einen Monte Carlo Ereignis Generator für die Simulation von Chargino-Paarproduktion am ILC in NLO in den elektroschwachen Kopplungen. Wir betrachten zwei Ansätze für den Einschluss von Photon-Abstrahlung. Ein strikter Ansatz fester Ordnung (fixed-order) erlaubt den Vergleich und Konsistenztests mit publizierten semianalytischen Ergebnissen in der Literatur. Eine Version mit weicher und harter kollinearer Resummation von Photonabstrahlung, welcher die Resummation von Photonen mit dem Einschluss des NLO Matrix Elements für den Produktionsprozess kombiniert, vermeidet Ereignisse mit negativem Gewicht, sodass das Programm physikalische (ungewichtete) Ereignissamples simulieren kann. Photonen werden in dem Bereich, in dem sie experimentell aufgelöst werden können, explizit generiert. Ausserdem enthält die Methode weitere Korrekturen höherer Ordnung, die in der fixed-order Methode nicht eingeschlossen sind. Durch die Überprüfung der Abhängigkeit von den Cutoffs, die den weichen und den kollinearen Bereich abtrennen, evaluieren wir die systematischen Fehler, die infolge der weichen und kollinearen Näherung auftreten, für NLO Beträge sowie Beiträge höherer Ordnungen. Im Resummationsansatz kann die restliche Ungenauigkeit auf Promille-Niveau reduziert werden, welches der experimentellen statistischen Ungenauigkeit am ILC entspricht. Wir untersuchen den zwei-Photon Phasenraum der Resummationsmethode genau. Wir präsentieren Ergebnisse für Wirkungsquerschnitte und Ereignisgeneration für beide Ansätze.

Contents

1	Introduction	4
1.1	Standard Model (SM) and minimal supersymmetric extension	4
1.2	SUSY at colliders: discovery and precision	6
1.3	Next-to-leading order at Monte Carlo Generators	7
1.4	Outline	8
2	Chargino production at tree level	10
2.1	Born matrix element	10
2.2	Helicity amplitudes	11
2.3	Differential and total cross sections	12
2.4	Polarized incoming and outgoing particles	15
3	Chargino production at next-to-leading order (NLO)	18
3.1	Divergencies and infrared-safe cross sections in higher-order calculations .	18
3.2	Virtual corrections	20
3.3	Soft terms	20
3.4	Hard-collinear photons	21
3.5	Hard non-collinear photons	22
3.6	Fixed $\mathcal{O}(\alpha)$ results for total cross section	24
3.7	Resummation of higher logarithms: Initial state radiation	24
3.8	Further higher-order contributions	26
4	Inclusion of NLO corrected matrix elements in WHIZARD (fixed order)	29
4.1	Monte Carlo (event) generators	29
4.1.1	Monte Carlo integration	29
4.1.2	Event generation	30
4.1.3	WHIZARD	30
4.2	Calculating NLO matrix elements using <code>FeynArts</code> and <code>FormCalc</code>	30
4.3	Inclusion of the fixed order NLO contribution using a structure function .	31
4.4	Technicalities of the implementation	34
4.5	Drawback of the fixed-order method	35
4.6	Results	40
4.6.1	Cut dependencies	40
4.6.2	Total cross section	42
4.6.3	Event generation	42

5	Resumming photons	45
5.1	NLO and resummation at LEP and LHC	45
5.2	Resummation method	46
5.3	Implementation in WHIZARD	55
5.4	Difference to fixed order method	56
5.4.1	Negative weights	56
5.4.2	Higher-order photon contributions	57
6	Results	61
6.1	Cut dependencies	61
6.1.1	Energy cutoff dependence	61
6.1.2	Collinear cutoff dependence	63
6.2	Total cross section	64
6.2.1	Leading and first order results	64
6.2.2	Higher-order effects	65
6.3	Event Generation	67
7	Summary and Outlook	72
A	Conventions, SUSY overview, MSSM Lagrangian	75
A.1	Conventions	75
A.2	Poincaré and SUSY algebra	76
A.3	Expansion in component fields	77
A.4	General gauge-invariant Lagrangian and superpotential	79
A.5	MSSM field content and superpotential	81
A.6	Symmetry breaking and Lagrangian of the MSSM	81
B	Chargino and Neutralino Sector of the MSSM	84
B.1	Chargino mass eigenstates	84
B.2	Neutralino Mass Eigenstates	86
B.3	Chargino-Gauge-boson couplings	87
B.4	Lepton-slepton and quark-squark chargino couplings	90
B.5	Chargino-Neutralino-Gauge boson and Chargino-Neutralino-Higgs couplings	92
C	Point SPS1a'	95
D	Helicity eigenstates for massive fermions	96
E	Generic diagrams contributing to NLO Chargino production	99
F	Soft and collinear approximation; ISR structure function	106
F.1	Soft Photon Factor	106
F.2	Hard-collinear approximation	106
F.2.1	Finite mass effects in collinear radiation	106

F.2.2	Helicity dependent structure functions	111
F.2.3	Connection to leading log expressions	114
F.3	ISR structure function	115
F.3.1	Exact first order and soft solution	115
F.3.2	Exponentiation	117
G	Transformations and (Di)Gamma functions	119
G.1	The Fourier Transform	119
G.2	The Laplace Transform	119
G.3	The Mellin Transform	120
G.4	The Euler Gamma function $\Gamma(x)$	120
G.5	The Digamma function $\psi_0(x)$	120
H	References for Computer codes	122

1 Introduction

In this section, we will give a short overview of supersymmetry (SUSY) and its minimal realization, expectations, and results from experiments for SUSY particles, and the available computer tools. We also present an outline of the structure of this thesis.

1.1 Standard Model (SM) and minimal supersymmetric extension

The Standard Model

The Standard Model (SM) of particle physics [1, 2, 3, 4, 5] is a $SU(3)_c \times SU(2) \times U(1)$ gauge theory with the particle content listed in Table 1.1. The $SU(2) \times U(1)$ part of the theory is spontaneously broken by the nonzero vacuum expectation value of the Higgs boson [6, 7, 8, 9, 10] which gives masses to three of the $SU(2) \times U(1)$ gauge bosons. It describes current experimental data with high accuracy [11]. However, it suffers from a number of theoretical drawbacks. In general, the Standard Model can only be an effective low-energy theory as it does not describe gravity and is therefore valid at most up to the Planck scale. In addition, it suffers from the fine-tuning or naturalness problem: in the Standard Model, corrections to the mass of the Higgs boson are quadratically divergent. They can be regularized by a finite cutoff-parameter which can maximally be set to the Planck scale as the highest scale of the theory. However, the Higgs mass is theoretically bounded [12, 13, 14, 15, 16]. Therefore, extreme finetuning is needed to obtain the physical Higgs mass from the bare mass in the theory [17]. Similarly, the Standard Model alone does not provide an explanation for dark matter. From a more aesthetic point of view, it also does not allow for gauge coupling unification of all gauge

		$SU(3)_c$	$SU(2) \times U(1)$	
leptons	$(e, \mu, \tau)_L$		✓	
	$(e, \mu, \tau)_R$		✓	$(U(1) \text{ only})$
	$(\nu_e, \nu_\mu, \nu_\tau)_L$		✓	
quarks	$(u, d, c, s, t, b)_L$	✓	✓	
	$(u, d, c, s, t, b)_R$	✓	✓	$(U(1) \text{ only})$
gluons ($SU(3)$ gauge bosons)		✓		
W, Z ($SU(2) \times U(1)$ gauge bosons)			✓	

Table 1.1: Standard model particle content

groups [18]. Further problems are the origin of particle masses, possible symmetries between the leptonic and the quark sector, and so on.

Supersymmetry

Supersymmetric theories [19, 20] are one of the most promising candidates for the description of physics beyond the SM. They introduce a new symmetry as an extension of the Poincaré group which connects fermionic and bosonic degrees of freedom. This symmetry transforms the bosons/ fermions of the Standard Model into their fermionic/ bosonic superpartner with a different spin but otherwise identical quantum numbers. As the superpartners have not been directly observed in experiments, SUSY has to be broken such that all new particles obtain higher masses. The breaking most likely takes place in a “hidden sector” invisible to the Standard Model gauge groups and is then transferred to the visible sector. There are numerous suggestions for SUSY breaking mechanisms, including (minimal) supergravity [21, 22, 23], gauge-mediation [24, 25, 26], and anomaly-mediation [27, 28]. An additional symmetry (R-parity) only allows for the simultaneous creation/ annihilation of even numbers of SUSY particles. R-parity violation is strongly limited by experimental results from proton decay.

Supersymmetric theories address two main problems of the Standard Model: they allow for a natural solution for the fine-tuning problem. In addition, if R-parity is exactly conserved, the lightest supersymmetric particle (LSP) is a good dark matter candidate. Furthermore, they easily allow for the embedding of the $SU(3)_c \times SU(2) \times U(1)$ group in a grand unified theory and the unification of gauge couplings.

For more technical details on the construction of supersymmetric theories, cf. Appendix A.

Minimal Supersymmetric Standard Model

The Minimal Supersymmetric Standard Model (MSSM) is the minimal supersymmetric extension of the Standard Model [29, 22, 30, 31]. It contains a superpartner for each SM particle and an extended Higgs sector with the two Higgs doublets $H_u = \begin{pmatrix} H_u^+ \\ H_u^0 \end{pmatrix}$, $H_d = \begin{pmatrix} H_d^0 \\ H_d^- \end{pmatrix}$. The Lagrangian at the electroweak scale is given by

$$\mathcal{L}_{tot} = \mathcal{L}_{kin} + \mathcal{L}_{gauge} + \mathcal{L}_V + \mathcal{L}_{soft},$$

where \mathcal{L}_{kin} contains the kinetic terms of the free theory, \mathcal{L}_{gauge} are terms arising when imposing the gauge symmetry of the SM, \mathcal{L}_V is the Lagrangian part derived from the superpotential, and \mathcal{L}_{soft} are the soft SUSY breaking terms. For more details and the complete MSSM Lagrangian, cf. Appendix A. While \mathcal{L}_{kin} and \mathcal{L}_{gauge} only depend on SM parameters, new SUSY related parameters appear in the superpotential and the soft breaking terms. The unconstrained model contains in total 105 new parameters. The number of free parameters, however, can be constrained by imposing lepton number conservation, suppression of flavor changing neutral currents, and applying experimental

bounds on CP violation. The assumption of a specific breaking mechanism can reduce the number of new parameters even further. In the mSugra scenario of the MSSM, all parameters can be derived from 5 new parameters at the SUSY breaking scale. The parameters at the electroweak scale are then determined using renormalization group equations.

For recent reviews, see [32, 33, 34].

The Chargino and Neutralino Sector of the MSSM

A solid prediction of the MSSM is the existence of charginos $\tilde{\chi}_1^\pm, \tilde{\chi}_2^\pm$ and neutralinos $\tilde{\chi}_1^0, \tilde{\chi}_2^0, \tilde{\chi}_3^0, \tilde{\chi}_4^0$. These are the superpartners of the W^\pm and charged/neutral Higgs bosons H^\pm, H^0 rotated into their mass eigenstates. In grand unified theories (GUTs) the chargino masses tend to be near the lower edge of the superpartner spectrum, since the absence of strong interactions precludes large positive renormalizations of their effective masses. The precise measurement of chargino parameters (masses, mixing of $\tilde{\chi}_1^\pm$ with $\tilde{\chi}_2^\pm$, and couplings) is a key for uncovering any of the fundamental properties of the MSSM. These values give a handle for verifying supersymmetry in the Higgs and gauge-boson sector and thus the cancellation of power divergences. Charginos decay either directly or via short cascades into the LSP, which is the dark-matter candidate of the MSSM in case of R-parity conservation. Thus, a precise knowledge of masses and mixing parameters in the chargino/neutralino sector is the most important ingredient for predicting the dark-matter content of the universe. Finally, all SUSY parameters in the gaugino and higgsino sector of the MSSM can be determined from the measurements of the chargino production cross sections and masses and the lightest neutralino mass [35]. The high-scale evolution of the mass parameters should point to a particular supersymmetry-breaking scenario, if the context of a GUT model is assumed (cf. [36, 37]). In all these cases, a knowledge of parameters with at least percent-level accuracy is necessary.

1.2 SUSY at colliders: discovery and precision

In this section, we give a quick overview on SUSY searches at past and future colliders. We refer to [38] and [39, 40] and references therein for details.

Experimental bounds

Direct experimental searches for SUSY particles have been conducted at both LEP and the Tevatron. Neither experiment can claim a direct discovery for a SUSY particle, but both have determined lower mass limits [38]. While the combined LEP runs provide the most stringent mass limits for sleptons and gauginos, limits for squarks and gluinos can be obtained from CDF at the Tevatron and ALEPH at LEP. Most lower limits for visible SUSY particles (ie, not the LSP) are $\mathcal{O}(100 \text{ GeV})$. However, limits also depend strongly on the underlying SUSY scenarios and breaking mechanism. For a recent review for the mSugra parameter space, cf. [41]. Results from HERA give limits on R-parity violating scenarios [42, 43, 44].

Indirect constraints on the SUSY parameter space are in general given by (loop-induced) effects in electroweak precision data. The most stringent restrictions arise from the mass of the lightest Higgs boson. Further observables include the W boson mass, $\sin^2 \theta_W$, the flavour changing neutral current $b \rightarrow s \gamma$, and the anomalous magnetic moment of the muon ($a_\mu - 2$) [45].

Additional restrictions on the SUSY parameter space can be obtained from cosmological data, as dark matter searches.

LHC: discovery

The LHC as a hadron-hadron collider with a cm energy of $\sqrt{s} = 14 \text{ TeV}$ serves as a discovery machine for SUSY particles in most SUSY scenarios. The most dominant channels are pair production or associated production of gluinos and squarks. As supersymmetric particles usually decay via long decay chains, mass determination involves reconstruction from combined mass distributions. Analyses are parameter-point specific. For the mSUGRA point SPS1a(′)[46](cf. Appendix C), analyses for chargino, neutralino, squark, gluino, and slepton masses have been done [39, 47]. Relative errors for masses and cross sections are usually expected to lie in the % regime.

International Linear Collider (ILC): precision

The International Linear Collider (ILC) is a planned $e^+ e^-$ machine with a cm energy of 500 GeV (1 TeV). It provides much cleaner production channels and decay signatures with lower background than the LHC. In addition, direct pair production of sparticles in the slepton and chargino-/ neutralino sector is easily observable. If kinematically accessible, the sparticle content of the MSSM can be studied with high precision [48, 39]. Combining sparticle measurements from the ILC and the LHC leads to errors in the percent to per mille regime and significantly reduces the errors based on LHC measurements only [49, 39]. The same accuracy is reached in the respective fitting routines Sfit [50] and Fittino [51] for the reconstruction of the Lagrangian parameters at the weak scale.

Due to its low mass in most SUSY scenarios, the lighter chargino $\tilde{\chi}_1^\pm$ is likely to be pair-produced with a sizable cross section at a first-phase ILC with c.m. energy of 500 GeV. In many models, including supergravity-inspired scenarios such as SPS1a/SPS1a′ [46], the second chargino $\tilde{\chi}_2^\pm$ will also be accessible at the ILC, at least if the c.m. energy is increased to 1 TeV. Similar arguments hold for the neutralinos.

1.3 Next-to-leading order at Monte Carlo Generators

Several event generators [52, 53, 54, 55] already include the particle content of the MSSM and allow for event generation including sparticles at tree level. In Ref. [56], some of these have been presented and verified against each other, both for the SM and the MSSM.

To match the experimental accuracy for (SUSY) processes at (future) colliders, theoretical predictions with next-to-leading order (NLO) accuracy have to be implemented in the simulation tools (see e.g. [40]). The inclusion of higher-order corrections in Monte Carlo event generators has already been discussed for electroweak precision physics at LEP (cf. [57, 58, 59]). For the determination of the W-mass, Monte-Carlo event generators including higher-order corrections [60, 61] can reduce the theoretical uncertainties down to approximately 0.5% [62, 63, 11].

NLO calculations for the production of charginos and neutralinos at an e^+e^- collider are within the percent regime [64, 65, 66]. If SUSY is discovered, the experimental precision at the ILC requires to equally include these processes at next-to-leading order in a Monte Carlo event generator. Furthermore, it is essential for the simulation of physical (i.e., unweighted) event samples that the effective matrix elements are positive semidefinite over the whole accessible phase space. The QED part of radiative corrections does not meet this requirement in some phase space regions. This usually requires higher-order resummation for soft (and collinear) photonic contributions to the process. Methods for dealing with this problem have been developed in the LEP1 era [67, 68, 57]. Since the ILC precision actually exceeds the one achieved in LEP experiments, these higher-order effects from resummation can have the same order of magnitude as the experimental errors.

Similar techniques concern the event simulation of hadronic processes including partonic showers. The higher-order parton showers have to be matched with the exact NLO matrix element. Work along these lines has been done for e^+e^- [69, 70] and hadron colliders [71, 72, 73].

1.4 Outline

In this work, which is the extension of a recent publication [74], we present an extension of the Monte Carlo Event generator **WHIZARD** [52] which includes the $\mathcal{O}(\alpha)$ electroweak and SUSY corrections to chargino production at an e^+e^- collider. The fixed-order version, which we will discuss first, is limited to first order photon emission and suffers the well-known problem of negative weights for low cuts on the photon energy. We then introduce a method which combines the photon resummation already discussed at LEP with NLO matrix elements for the production process. It avoids negative events and therefore allows for lower energy cuts. In addition, it includes further higher-order corrections unaccounted for by the fixed-order method. We evaluate the systematic errors due to soft and collinear photon approximations and the cut-dependence of higher-order contributions. We present results for the cross section and event simulation for both methods.

In Chapter 2, we discuss chargino production at an e^+e^- collider at tree level, presenting the total and differential cross sections for any helicity combination. In Chapter 3, we present the analytic form of the infrared and cut-independent cross section for chargino production at next-to-leading order and the inclusion of resummed soft and

virtual photonic contributions. We sketch the treatment of $2 \rightarrow n$ processes including chargino decay in the double pole approximation.

In Chapter 4, we present a method to include the fixed $\mathcal{O}(\alpha)$ result in the Monte Carlo event generator **WHIZARD**. We give a brief overview on the technicalities of the inclusion and discuss the energy-cut-dependent problem of negative weights in certain points of phase space. We present first results for cutoff-independence, cross section integration and event generation in the allowed cut parameter regions.

In Chapter 5, we present our method of combining the completely resummed soft and virtual photonic contributions with the exact next-to-leading order contributions to chargino production. We explicitly discuss the description of collinear photonic contributions up to $\mathcal{O}(\alpha^2)$ and analytic differences between the resummation and the fixed order method. We present the results of our work in Chapter 6. In Chapter 7, we summarize and give an outlook on future work.

The appendices basically contain conventions, derivations of SUSY Feynman rules and the approximations used for the photonic contributions. We start with a general discussion of supersymmetric theories and the MSSM in Appendix A. The chargino- and neutralino-sector, especially the derivation of Feynman rules, is discussed in Appendix B. Appendix D gives an overview on the treatment of helicity states for massive particles needed for the discussion of the helicity-dependent Born cross section.

Appendix E shows all generic diagrams contributing to chargino production at NLO. Appendix F sketches the derivation of the collinear photon approximation and the initial state radiation (ISR) structure function [75]. We present the mSugra point SPS1a' in Appendix C and list some useful functions in Appendix G. Appendix H lists the references for all computer programs mentioned in this work.

2 Chargino production at tree level

In the MSSM, charginos $\tilde{\chi}^\pm$ are superpositions of superpartners of the charged gauge bosons W^\pm and the charged Higgs fields H^\pm . In the following, we use the mass-diagonalization matrices

$$U_{L,R} \begin{pmatrix} \widetilde{W}^- \\ \widetilde{H}^- \end{pmatrix} = \begin{pmatrix} \tilde{\chi}_1^- \\ \tilde{\chi}_2^- \end{pmatrix}_{L,R}$$

and the parameterization

$$U_{L,R} = \begin{pmatrix} \cos \Phi_{L,R} & \sin \Phi_{L,R} \\ -\sin \Phi_{L,R} & \cos \Phi_{L,R} \end{pmatrix}$$

for the case with no CP violation. For more details, cf. Appendix B.

2.1 Born matrix element

At an e^+e^- collider, charginos are produced by γ and Z exchange in the s -channel and $\tilde{\nu}_e$ exchange in the t -channel as shown in Figure 2.1. Neglecting the electron mass m_e , we can perform a Fierz transformation on the t -channel $\tilde{\nu}_e$ exchange. The sum of all contributions is then given by [76]:

$$\mathcal{M} = \frac{e^2}{s} Q_{\alpha\beta} [\bar{v}(e^+) \gamma_\mu P_\alpha u(e^-)] [\bar{u}(\tilde{\chi}_j^-) \gamma^\mu P_\beta v(\tilde{\chi}_i^+)], \quad (2.1)$$

with $\alpha, \beta = L, R$ and $P_{L/R} = \frac{1}{2}(1 \mp \gamma_5)$. The factors $Q_{\alpha\beta}$ have been explicitly calculated in [76] and are given by

$$\begin{aligned} Q_{LL} &= D_L \mp F_L \cos 2\Phi_L, & Q_{RL} &= D_R \mp F_R \cos 2\Phi_L, \\ Q_{LR} &= D'_L \mp F'_L \cos 2\Phi_R, & Q_{RR} &= D_R \mp F_R \cos 2\Phi_R, \end{aligned}$$

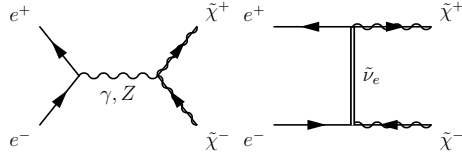


Figure 2.1: Feynman graphs for chargino pair production at the ILC.

for the production of $\tilde{\chi}_1^+ \tilde{\chi}_1^-$ and $\tilde{\chi}_2^+ \tilde{\chi}_2^-$ and

$$\begin{aligned} Q_{LL} &= F_L \sin 2\Phi_L, & Q_{RL} &= F_R \sin 2\Phi_L, \\ Q_{LR} &= F'_L \sin 2\Phi_R, & Q_{RR} &= F_R \sin 2\Phi_R \end{aligned}$$

for the production of $\tilde{\chi}_1^+ \tilde{\chi}_2^-$ and $\tilde{\chi}_2^+ \tilde{\chi}_1^-$ pairs. We here use the notations [76]

$$\begin{aligned} D_L &= 1 + \frac{D_Z}{s_W^2 c_W^2} \left(s_W^2 - \frac{1}{2} \right) \left(s_W^2 - \frac{3}{4} \right), & F_L &= \frac{D_Z}{4 s_W^2 c_W^2} \left(s_W^2 - \frac{1}{2} \right), \\ D_R &= 1 + \frac{D_Z}{c_W^2} \left(s_W^2 - \frac{3}{4} \right), & F_R &= \frac{D_Z}{4 c_W^2}, & D'_L &= D_L + \frac{D_{\tilde{\nu}}}{4 s_W^2}, \\ F'_L &= F_L - \frac{D_{\tilde{\nu}}}{4 s_W^2}, & D_Z &= \frac{s}{s - m_Z^2 + i\Gamma_Z}, & D_{\tilde{\nu}} &= \frac{s}{t - m_{\tilde{\nu}}^2}, \end{aligned} \quad (2.2)$$

where s_W^2 and c_W^2 denote the squared sine and cosine of the weak mixing angle.

2.2 Helicity amplitudes

The matrix element \mathcal{M} given by Eq. (2.1) can be decomposed into helicity amplitudes. We use the formalism introduced in [77] (see Appendix D for a short review on helicity eigenstates and an introduction to the used method). We define the \hat{e}_z direction as the flight direction of the electron and obtain

$$\begin{aligned} p_1(e^+) &= \begin{pmatrix} p_e \\ 0 \\ 0 \\ -p_e \end{pmatrix}, & p_2(e^-) &= \begin{pmatrix} p_e \\ 0 \\ 0 \\ p_e \end{pmatrix}, \\ p_3(\tilde{\chi}^-) &= \begin{pmatrix} E_\chi \\ p_\chi \sin \theta \\ 0 \\ p_\chi \cos \theta \end{pmatrix}, & p_4(\tilde{\chi}^+) &= \begin{pmatrix} E_\chi \\ -p_\chi \sin \theta \\ 0 \\ -p_\chi \cos \theta \end{pmatrix}, \end{aligned} \quad (2.3)$$

where p_e and p_χ are the magnitude of the electron/ positron and chargino three-momentum, respectively. θ is the angle between the electron and the negatively charged chargino. $\mathcal{M}(\sigma; \lambda_i \lambda_j) = 2\pi \alpha \langle \sigma; \lambda_i \lambda_j \rangle$ defines the matrix element for an electron with helicity σ and $\tilde{\chi}^\mp$ with helicity $\lambda_{i/j}$. The helicity amplitudes are then given by [78]:

$$\begin{aligned} \langle +; ++ \rangle &= - \left[Q_{RR} \sqrt{1 - \eta_+^2} + Q_{RL} \sqrt{1 - \eta_-^2} \right] \sin \theta, \\ \langle +; +- \rangle &= - \left[Q_{RR} \sqrt{(1 + \eta_+)(1 + \eta_-)} + Q_{RL} \sqrt{(1 - \eta_+)(1 - \eta_-)} \right] (1 + \cos \theta), \\ \langle +; -+ \rangle &= \left[Q_{RR} \sqrt{(1 - \eta_+)(1 - \eta_-)} + Q_{RL} \sqrt{(1 + \eta_+)(1 + \eta_-)} \right] (1 - \cos \theta), \\ \langle +; -- \rangle &= \left[Q_{RR} \sqrt{1 - \eta_-^2} + Q_{RL} \sqrt{1 - \eta_+^2} \right] \sin \theta, \end{aligned}$$

$$\begin{aligned}
\langle -; ++ \rangle &= - \left[Q_{LR} \sqrt{1 - \eta_+^2} + Q_{LL} \sqrt{1 - \eta_-^2} \right] \sin \theta, \\
\langle -; +- \rangle &= \left[Q_{LR} \sqrt{(1 + \eta_+)(1 + \eta_-)} + Q_{LL} \sqrt{(1 - \eta_+)(1 - \eta_-)} \right] (1 - \cos \theta), \\
\langle -; -+ \rangle &= - \left[Q_{LR} \sqrt{(1 - \eta_+)(1 - \eta_-)} + Q_{LL} \sqrt{(1 + \eta_+)(1 + \eta_-)} \right] (1 + \cos \theta), \\
\langle -; -- \rangle &= \left[Q_{LR} \sqrt{1 - \eta_-^2} + Q_{LL} \sqrt{1 - \eta_+^2} \right] \sin \theta,
\end{aligned}$$

with

$$\eta_{\pm} = \sqrt{\lambda} \pm (\mu_i^2 - \mu_j^2); \lambda = [1 - (\mu_i + \mu_j)^2] [1 - (\mu_i - \mu_j)^2]; \mu_i = \frac{m_{\chi_i}^2}{s}.$$

2.3 Differential and total cross sections

For the calculation of the differential cross section, we use the general formula for $2 \rightarrow 2$ particle processes:

$$d\sigma = \frac{1}{2w} \frac{d^3 k_1}{2k_1^0} \frac{1}{(2\pi)^2} \delta(k_2^2 - m_2'^2) \Theta(k_2^0) |\mathcal{M}|^2,$$

where k_i, k_i^0, m_i' are the momenta/ energy/ mass of the outgoing particles. The flux factor

$$w(s, m_1^2, m_2^2) = \sqrt{(s - m_1^2 - m_2^2)^2 - 4m_1^2 m_2^2}$$

depends on the center of mass energy \sqrt{s} and the masses of the incoming particles. For particles with very small masses with respect to the cm energy, $w = s$.

The differential cross section for a specific helicity state is then given by

$$\frac{d\sigma}{d\cos\theta} = \frac{\pi \alpha^2}{8s} \sqrt{\lambda} |\langle \sigma; \lambda_i \lambda_j \rangle|^2.$$

For chargino pair production, the differential cross section is

$$\frac{d\sigma}{d\cos\theta} = \frac{\pi \alpha^2}{2s} \sqrt{\lambda} \left\{ [1 - (\mu_i^2 - \mu_j^2)^2 + \lambda \cos^2 \theta] Q_1 + 4\mu_i \mu_j Q_2 + 2\sqrt{\lambda} Q_3 \cos \theta \right\} \quad (2.4)$$

with

$$\begin{aligned}
Q_1 &= \frac{1}{4} [|Q_{RR}|^2 + |Q_{LL}|^2 + |Q_{RL}|^2 + |Q_{LR}|^2], \\
Q_2 &= \frac{1}{2} \text{Re} [Q_{RR} Q_{RL}^* + Q_{LL} Q_{LR}^*], \\
Q_3 &= \frac{1}{4} [|Q_{RR}|^2 + |Q_{LL}|^2 - |Q_{RL}|^2 - |Q_{LR}|^2],
\end{aligned}$$

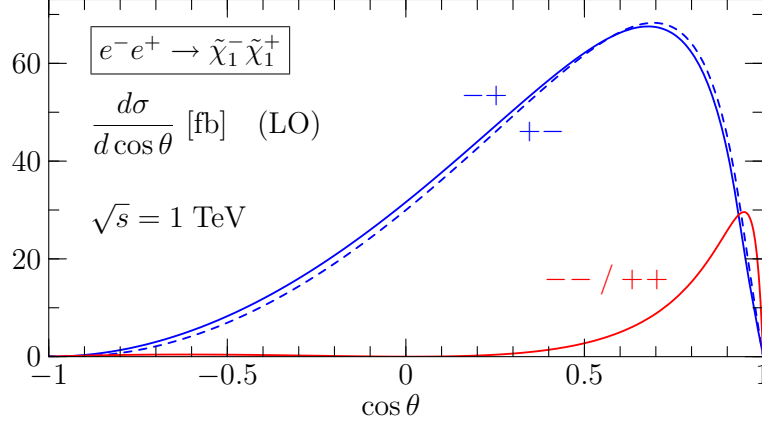


Figure 2.2: Chargino pair production at the ILC: Dependence of the differential distribution in polar angle $\cos\theta$ between e^- and $\tilde{\chi}_1^-$ for different helicity combinations. The labels indicate $\tilde{\chi}_1^-$ and $\tilde{\chi}_1^+$ helicity; the electron/positron helicity is fixed to $-+$.

where we averaged over initial and summed over final particle spins. Figure 2.2 shows the results for the differential cross section for the dominant helicity amplitudes for $\tilde{\chi}_1^+ \tilde{\chi}_1^-$ production for the point SPS1a' (cf. Appendix C). Independently of the SUSY parameters, processes with a left handed electron in the initial state are dominant, as diagrams with a γ and Z exchange interfere constructively. The same diagrams give destructive interference between the γ , Z exchange for righthanded initial electrons. This can easily be seen from Eqs. (2.2). We obtain

$$D_L \approx 1 + 0.727 D_Z, D_R \approx 1 - 0.67 D_Z, F_L \approx -0.01 D_Z, F_R \approx 0.33 D_Z.$$

For the cm values where chargino pair production is possible, $D_Z \geq 1$. Then, even without a possible enhancement from the t -channel sneutrino exchange and independent of the mixing parameters, $|Q_{RL}/Q_{LL}| \leq 0.33$. The ratio of $|Q_{RR}/Q_{LR}|$ strongly depends on the mixing parameters and the sneutrino mass. For the point SPS1a' and a cm energy of 1 TeV (400 GeV), $|Q_{RL}/Q_{LL}| = 3\%(1\%)$ and $|Q_{RL}/Q_{LL}| = 1\%_0(1\%)$ (neglecting contributions from the sneutrino exchange). We therefore only show the results for states with a left-handed electron in the initial state. Amplitudes with two charginos of the same helicity in the final state are suppressed by a factor $\propto \frac{m_{\tilde{\chi}}^2}{s}$. Figure 2.3 shows the helicity averaged/ summed differential cross section according to Eq. (2.4), Figure 2.4 the \sqrt{s} dependence of the corresponding total cross section.

For the same parameter point, we have compared the tree level results for $\tilde{\chi}_i^- \tilde{\chi}_j^+$ production using the analytic form [76] and several computer codes [52, 79, 80, 81]. The analytic and numeric results are in complete agreement. The values are given in Table 2.1.

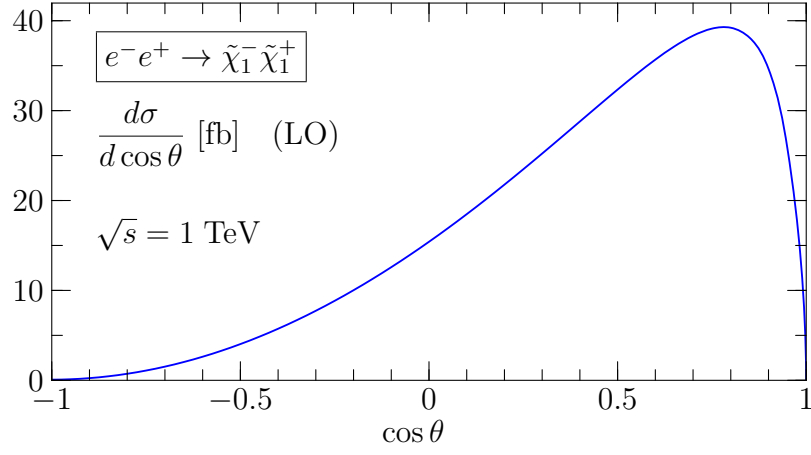


Figure 2.3: Chargino pair production at the ILC: Dependence of the spin summed and averaged differential distribution in polar angle $\cos \theta$ between e^- and $\tilde{\chi}_1^-$.

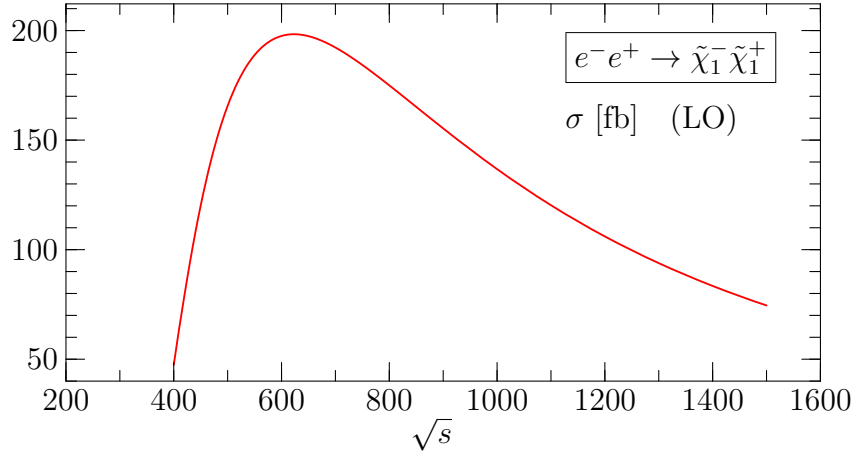


Figure 2.4: Chargino pair production at the ILC: unpolarized total cross section as a function of \sqrt{s} (averaged over initial and summed over final spins)

	$\sigma_{tot}[fb]$
$\tilde{\chi}_1^- \tilde{\chi}_1^+$	136.8
$\tilde{\chi}_1^- \tilde{\chi}_2^+$	10.97
$\tilde{\chi}_2^- \tilde{\chi}_2^+$	80.07

Table 2.1: Chargino total production cross sections for the SUSY parameter set SPS1a' and $\sqrt{s} = 1$ TeV.

2.4 Polarized incoming and outgoing particles

In [76, 78], the authors also list the analytic results for the $\tilde{\chi}^-$ polarization vector as well as the e^\pm -polarization dependent differential cross sections. Although not pursued further in this work, we reproduced these results and sketch the derivation for completeness.

Polarized outgoing particles

The polarization vector of the outgoing $\tilde{\chi}^-$ in its rest-frame is defined in the following coordinate system: z is given by the component parallel to the flight-direction of the chargino in the lab-frame, x is defined in the production plane, and y normal to the production plane. The $\tilde{\chi}^-$ polarization vector is then given by

$$\vec{\mathcal{P}} = tr(\vec{\sigma}\rho) = (\mathcal{P}_T, \mathcal{P}_N, \mathcal{P}_L),$$

where $\vec{\sigma}$ is the vector made of the Pauli-matrices σ_i , ρ the spin-density matrix, and

$$\begin{aligned} \mathcal{P}_L &= \frac{1}{4} \sum_{\sigma=\pm} \{ |\langle\sigma; ++\rangle|^2 + |\langle\sigma; +- \rangle|^2 - |\langle\sigma; -+ \rangle|^2 - |\langle\sigma; --\rangle|^2 \} / \mathcal{N}, \\ \mathcal{P}_T &= \frac{1}{2} Re \left\{ \sum_{\sigma=\pm} \langle\sigma; ++\rangle \langle\sigma; -+ \rangle^* + \langle\sigma; --\rangle \langle\sigma; +- \rangle^* \right\} / \mathcal{N}, \\ \mathcal{P}_N &= \frac{1}{2} Im \left\{ \sum_{\sigma=\pm} \langle\sigma; --\rangle \langle\sigma; +- \rangle^* - \langle\sigma; ++\rangle \langle\sigma; -+ \rangle^* \right\} / \mathcal{N}, \\ \mathcal{N} &= \frac{1}{4} \sum_{\lambda_i \lambda_j} [|\langle+; \lambda_i \lambda_j\rangle|^2 + |\langle-; \lambda_i \lambda_j\rangle|^2]. \end{aligned}$$

Polarized incoming particles

For the calculation of the differential and total cross sections depending on the polarization of the incoming particle beams, we start with

$$\mathcal{P} = (\mathcal{P}_T, 0, \mathcal{P}_L), \mathcal{P}' = (\mathcal{P}'_T \cos \eta, \mathcal{P}'_T \sin \eta, -\mathcal{P}'_L)$$

for the polarization vectors of the electron and positron, respectively, in a coordinate system where the z -axis is given by the momentum of the electron and the x -axis by

the electron's transverse polarization vector. η is the azimuthal angle of the positron transverse polarization vector with respect to the x-axis. We transform this into the lab-system, where the x-axis is defined by the scattering plane (cf. Eqs (2.3)):

$$\mathcal{P} = (\mathcal{P}_T \cos \Phi, -\mathcal{P}_T \sin \Phi, \mathcal{P}_L); \quad \mathcal{P}' = (\mathcal{P}'_T \cos(\eta - \Phi), \mathcal{P}'_T \sin(\eta - \Phi), -\mathcal{P}'_L);$$

Φ is the angle between the transverse polarization vector of the electron and the new x-axis.

The squared matrix element including an incoming particle with possible helicity eigenstates labeled by λ is given by [82]

$$\mathcal{M}^2 = \sum_{\lambda, \lambda'} \mathcal{M}(\lambda) \rho_{\lambda \lambda'} \mathcal{M}^\dagger(\lambda')$$

for particles and

$$\mathcal{M}^2 = \sum_{\lambda, \lambda'} \mathcal{M}(\lambda) \rho_{\lambda' \lambda} \mathcal{M}^\dagger(\lambda')$$

for antiparticles. The spin density matrix is given by $\rho = \frac{1}{2}(1 + \vec{\sigma} \cdot \vec{\mathcal{P}})$, and \mathcal{P} is defined such that $\vec{p} = |p| \hat{e}_z$. Taking this into account, the electron spin density matrix is

$$\rho_{\sigma_1 \sigma_2} = \frac{1}{2} \begin{pmatrix} 1 + \mathcal{P}_L & \mathcal{P}_T e^{i\Phi} \\ \mathcal{P}_T e^{-i\Phi} & 1 - \mathcal{P}_L \end{pmatrix}.$$

For the positron, we still have to perform a rotation around the x-axis such that $\vec{p}_{e^+} = |p_{e^+}| \hat{e}_{z, e^+}$ leading to

$$\mathcal{P}' = (\mathcal{P}'_T \cos(\eta - \Phi), -\mathcal{P}'_T \sin(\eta - \Phi), \mathcal{P}'_L)$$

which then gives

$$\rho_{\sigma'_1 \sigma'_2} = \frac{1}{2} \begin{pmatrix} 1 + \mathcal{P}'_L & \mathcal{P}'_T e^{i(\eta - \Phi)} \\ \mathcal{P}'_T e^{-i(\eta - \Phi)} & 1 - \mathcal{P}'_L \end{pmatrix}.$$

If we now calculate the sum over the squared helicity amplitudes using

$$\mathcal{M}^\dagger \mathcal{M} = \sum_{\sigma_1, \sigma_2, \sigma'_1 \sigma'_2; \lambda_i} \mathcal{M}^\dagger(\sigma_1 \sigma'_1; \lambda_i) \rho_{\sigma_1 \sigma_2} \rho_{\sigma'_1 \sigma'_2} \mathcal{M}(\sigma_2 \sigma'_2; \lambda_i)$$

and

$$\mathcal{M}(\sigma_i \sigma'_i; \lambda_j) = \mathcal{M}(\sigma_i; \lambda_j) \delta_{\sigma_i - \sigma'_i},$$

we obtain

$$\frac{d\sigma}{d\Omega} = \frac{\alpha^2}{16s} \sqrt{\lambda} \left[(1 - \mathcal{P}_L \mathcal{P}'_L) \Sigma_{unpol} + (\mathcal{P}_L - \mathcal{P}'_L) \Sigma_{LL} + \mathcal{P}_T \mathcal{P}'_T \cos(2\Phi - \eta) \Sigma_{TT} \right]$$

with

$$\begin{aligned} \Sigma_{unpol} &= 4 \left\{ [1 - (\mu_i^2 - \mu_j^2)^2 + \lambda \cos^2 \theta] Q_1 + 4\mu_i \mu_j Q_2 + 2\sqrt{\lambda} Q_3 \cos \theta \right\}, \\ \Sigma_{LL} &= 4 \left\{ [1 - (\mu_i^2 - \mu_j^2)^2 + \lambda \cos^2 \theta] Q'_1 + 4\mu_i \mu_j Q'_2 + 2\sqrt{\lambda} Q'_3 \cos \theta \right\}, \\ \Sigma_{TT} &= -4\lambda \sin^2 \theta Q_5, \end{aligned}$$

$$\begin{aligned}
Q'_1 &= \frac{1}{4} [|Q_{RR}|^2 - |Q_{LL}|^2 + |Q_{RL}|^2 - |Q_{LR}|^2], \\
Q'_2 &= \frac{1}{2} Re [Q_{RR} Q_{RL}^* - Q_{LL} Q_{LR}^*], \\
Q'_3 &= \frac{1}{4} [|Q_{RR}|^2 - |Q_{LL}|^2 - |Q_{RL}|^2 + |Q_{LR}|^2], \\
Q'_5 &= \frac{1}{2} Re [Q_{LR} Q_{RR}^* + Q_{LL} Q_{LR}^*]
\end{aligned}$$

and $\mu_{i,j}$ and λ as introduced in the last section. In [76, 78], the authors show that the measurement of the lightest chargino mass, the production cross sections, and spin-spin correlations suffice to completely determine the parameters of the chargino system in the tree level approximation.

3 Chargino production at next-to-leading order (NLO)

3.1 Divergencies and infrared-safe cross sections in higher-order calculations

Before discussing the $\mathcal{O}(\alpha)$ corrections to chargino production at an e^+e^- collider, we list some general features of the calculation of (virtual) higher-order corrections in perturbation theory.

In finite order calculations, divergences in the ultraviolet ($E \rightarrow \infty$) as well as infrared ($E \rightarrow 0$) regime can appear. The UV divergencies have to be regularized, which introduces a regularization parameter Λ . This leads to a parameter-dependence of the physical quantities with respect to the bare parameters in the Lagrangian. In bare perturbation theory, the bare parameters are then eliminated in relations between physically measurable quantities. If the underlying theory is meaningful, these relations should be cutoff-independent. Alternatively, the theory can be renormalized by absorbing the UV divergencies in a redefinition of the parameters and fields of the theory, thus giving a physical meaning to the parameters in the Lagrangian. The bare Lagrangian is split into the renormalized Lagrangian and a counterterm part,

$$\mathcal{L}_{bare} = \mathcal{L}_{ren} + \mathcal{L}_{ct},$$

where the Feynman rules resulting from \mathcal{L}_{ct} have to be included in all calculations of physical observables.

IR divergences arise in the case of zero-mass virtual gauge boson exchange. When virtual massive gauge bosons with the mass m_g are connected to an on-shell particle with the mass m , logarithms of the form

$$\log\left(\frac{m_g}{m}\right)$$

appear. This term gets infinite as $m_g \rightarrow 0$.

The IR divergence in QED can be regularized by introducing an infinitesimal gauge boson mass λ . According to the Bloch-Nordsieck theorem [83], the divergencies cancel if the emission of soft real photons is also taken into account. Infrared-safe observables therefore always include terms describing the emission of soft real photons. In the collinear approximation, where the transverse momentum of the emitted photon is neglected, the dominant contributions originating from the multiple emission of soft and virtual photons from the initial particles can be summed up into structure functions. This is discussed in Section 3.7.

In addition, collinear divergencies can appear when the (massless) gauge boson is emitted at a small angle relative to the emitting particle. In the collinear approximation the integration over the photon phase space leads to terms of the form

$$\log \frac{k_{\perp, max}}{m}$$

which diverge when $m = 0$. These singularities are regularized by keeping the physical nonzero mass m in this region of phase space, cf. Section 3.4.

An infrared-safe total cross section with a cm energy \sqrt{s} and n particles in the final state then includes the following contributions

- Born cross section:

$$\sigma_{Born}(s) = \int d\Gamma_n |\mathcal{M}_{Born}|^2, \quad (3.1)$$

- interference term between Born and first order terms describing the purely virtual contribution

$$\sigma_{virt}(s, \lambda^2) = \int d\Gamma_n [2\text{Re}(\mathcal{M}_{Born}(s)^* \mathcal{M}_{1-loop}(s, \lambda^2))] \quad (3.2)$$

- soft photon contribution

$$\sigma_s(s, \Delta E_\gamma, \lambda) = \int d\Gamma_n [f_{soft}(\Delta E_\gamma, \lambda) |\mathcal{M}_{Born}(s)|^2] \quad (3.3)$$

(The soft photonic approximation is explained in Section 3.3).

Here, λ denotes the photon mass and ΔE_γ is the soft photon energy cutoff separating the hard from the soft region. f_{soft} (3.6) denotes the soft photon factor.

The sum of the three contributions (3.1), (3.2), (3.3)

$$\sigma'(s, \Delta E_\gamma) = \sigma_{Born}(s) + \sigma_{virt}(s, \lambda^2) + \sigma_s(s, \Delta E_\gamma, \lambda)$$

is infrared-safe. However, it still depends on the soft photon cutoff ΔE_γ as the soft approximation only takes a part of the $m \rightarrow n + \gamma$ phase space into account. For a cutoff-independent result, the hard cross section

$$\sigma_{m \rightarrow (n+1)}(s, \Delta E_\gamma) = \int_{\Delta E_\gamma} d\Gamma_{(n+1)} |\mathcal{M}_{m \rightarrow n+1}(s)|^2$$

has to be added. This is usually split into a hard, collinear and a hard, non-collinear part

$$\sigma_{m \rightarrow n+1}(s, \Delta E_\gamma) = \sigma_{hard, non-coll}(s, \Delta E_\gamma, \Delta\theta_\gamma) + \sigma_{hard, coll}(s, \Delta E_\gamma, \Delta\theta_\gamma), \quad (3.4)$$

where the cutoff $\Delta\theta_\gamma$ separates the collinear from the non-collinear region. The hard-collinear part is treated in Section 3.4, the non-collinear in Section 3.5.

The total $\mathcal{O}(\alpha)$ cross section

$$\sigma_{tot}(s) = \sigma_{Born}(s) + \sigma_v(s, \lambda) + \sigma_s(s, \Delta E_\gamma, \lambda) + \sigma_{m \rightarrow (n+1)}(s, \Delta E_\gamma, \Delta\theta_\gamma) \quad (3.5)$$

is then cutoff-independent.

3.2 Virtual corrections

The one-loop corrections to the process $e^- e^+ \rightarrow \tilde{\chi}_i^- \tilde{\chi}_j^+$ with $i, j = 1, 2$ have been computed in the SUSY on-shell scheme in Ref. [64, 84]. An independent calculation in the \overline{DR} scheme has been presented in [66]. These calculations include the complete set of virtual diagrams contributing to the process with both SM and SUSY particles in the loop. The collinear singularity for photon radiation off the incoming electron/positron is regulated by the finite electron mass m_e . As an infrared regulator, the calculation introduces a fictitious photon mass λ . Both calculations use the **FeynArts/FormCalc** package [85, 80, 81, 86] for the evaluation of one-loop Feynman diagrams in the MSSM. A complete list of all generic one-loop diagrams (excluding tadpoles) contributing to the process $e^+ e^- \rightarrow \tilde{\chi}_1^+ \tilde{\chi}_1^-$ is given in Appendix E. The total number of diagrams is $\mathcal{O}(1500)$, with $\mathcal{O}(1000)$ self-energy diagrams for all contributing particles. It also includes $e^+ e^-$ -Higgs couplings which are absent if m_e is set to zero. We refer to [64, 84, 66] for details of the calculation.

3.3 Soft terms

The soft-photon factor has been derived in [87, 88, 89, 90]. We just sketch the derivation and refer to the literature for further details.

In the soft photon approximation, the radiation of a photon off an incoming or outgoing charged particle for an arbitrary process is considered in the limit $E_\gamma \rightarrow 0$, where only the terms contributing to the infrared singularity are kept. Then, the radiation can be described by a factor depending on the particle and photon momenta and the matrix element describing the radiation is proportional to the Born matrix element:

$$\mathcal{M}_{m \rightarrow n+\gamma} = f(p, k) \mathcal{M}_{m \rightarrow n},$$

where $p_{e^\pm}(k)$ denote the electron/positron (photon) four-vectors. For an incoming fermion, this factor is given by

$$f(p, k) = -e Q_F \frac{\varepsilon p}{kp}.$$

Here, Q_F is the charge of the fermion and ε the polarization vector of the photon. In addition,

$$\omega_k = \sqrt{\mathbf{k}^2 + \lambda^2}$$

is the energy of a photon regularized by the photon mass λ .
For cross sections, this leads to

$$\sigma_{m \rightarrow n+\gamma} = f_{soft} \sigma_{m \rightarrow n},$$

where

$$f_{soft} = -\frac{\alpha}{2\pi} \sum_{i,j} \int_{|\mathbf{k}| \leq \Delta \mathbf{E}_\gamma} \frac{d^3 k}{2\omega_k} \frac{(\pm) p_i p_j Q_i Q_j}{(p_i k)(p_j k)} \quad (3.6)$$

is summed over all charged incoming/ outgoing particles. The (\pm) in the numerator depends on the charge flow ($-$ for an incoming and $+$ for an outgoing charge). The integral appearing in f_{soft} has been calculated in [87] and is given in Appendix F.1. σ_{soft} is then given by

$$\sigma_{soft} = \int d\Gamma_2 f_{soft} |\mathcal{M}_{\text{Born}}(s)|^2. \quad (3.7)$$

3.4 Hard-collinear photons

If a photon is emitted off a particle of mass m with a small transverse momentum k_\perp , logarithms of the form

$$\log \frac{k_\perp}{m} \quad (3.8)$$

appear. Considering photon emission off electrons, these logarithms give rise to divergences if the electron mass is set to zero. Therefore, in order to regulate these collinear divergencies, the electron mass has to be taken into account in these regions of phase space. Similarly, numerical integration becomes tedious or even unreliable for very small transverse photon momenta. It is therefore customary to use an analytic collinear approximation for small k_\perp (or, alternatively, small emission angles θ_γ) when integrating over these regions of the photon phase space.

The explicit expression for the (hard) collinear photon approximation has been derived in [91, 92, 93]; cf. also Appendix F.2.

The hard-collinear contribution to the cross sections from the radiation of photons off one incoming particle is then given by convoluting the Born cross section with the structure function $f^\sigma(x; \Delta\theta_\gamma, \frac{m_e^2}{s})$, with $x = 1 - 2E_\gamma/\sqrt{s}$ being the energy fraction of the electron after radiation,

$$\begin{aligned} \sigma_{\text{hard,coll}}(s, \Delta E_\gamma, \Delta\theta_\gamma, m_e^2) &= \int_{\Delta E_\gamma, \Delta\theta_\gamma} d\Gamma_3 |\mathcal{M}_{2 \rightarrow 3}(s, m_e^2)|^2 \\ &= \sum_{\sigma=\pm} \int_0^{x_0} dx f^\sigma(x; \Delta\theta_\gamma, \frac{m_e^2}{s}) \int d\Gamma_2 |\mathcal{M}_{\text{Born}}^\sigma(xs, m_e^2)|^2. \end{aligned} \quad (3.9)$$

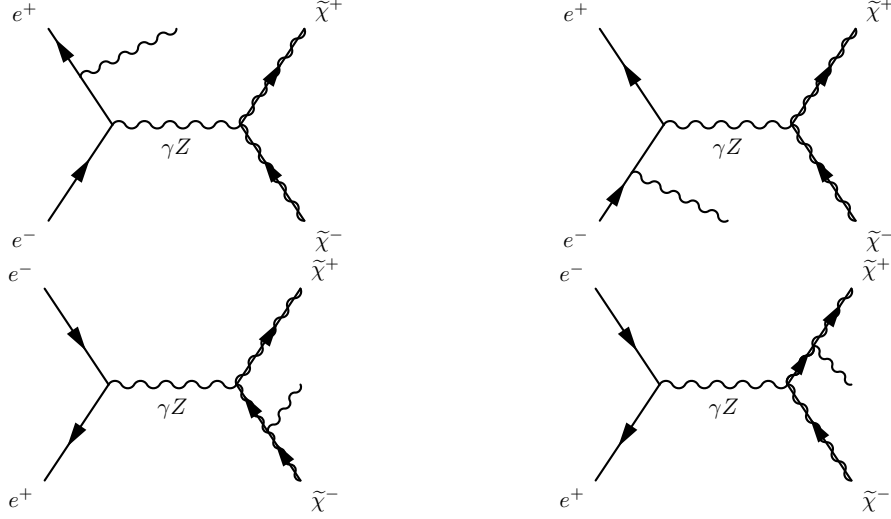


Figure 3.1: Matrix elements contributing to the $2 \rightarrow 3$ process. We only show the s channel contribution (t channel exchange analogously).

The two structure functions f^+, f^- are given by (F.5)

$$\begin{aligned} f^+(x) &= \frac{\alpha}{2\pi} \frac{1+x^2}{(1-x)} \left(\ln \left(\frac{s(\Delta\theta)^2}{4m^2} \right) - 1 \right), \\ f^-(x) &= \frac{\alpha}{2\pi} (1-x). \end{aligned}$$

They correspond to helicity conservation and helicity flip, respectively; each one is convoluted with the corresponding matrix element. The cutoff ΔE_γ is replaced by $x_0 = 1 - 2\Delta E_\gamma/\sqrt{s}$. In this approximation, positive powers of $\Delta\theta_\gamma$ are neglected. For radiation off both incoming particles, we have

$$\sigma_{\text{hard, coll}} = \sigma_{\text{hard, coll}}(e^+) + \sigma_{\text{hard, coll}}(e^-).$$

3.5 Hard non-collinear photons

The hard non-collinear contributions are added in form of the analytic $e^+ e^- \rightarrow \tilde{\chi}^+ \tilde{\chi}^- \gamma$ matrix element. In order to prevent double counting for soft and hard-collinear photons, which are already accounted for in σ_{soft} and $\sigma_{\text{hard, coll}}$, lower angular and energy cuts for the explicitly generated photon are set. Then,

$$\sigma_{\text{hard, non-coll}} = \int_{\Delta E_\gamma, \Delta\theta_\gamma} d\Gamma_3 |\mathcal{M}_{2 \rightarrow 3}(s)|^2. \quad (3.10)$$

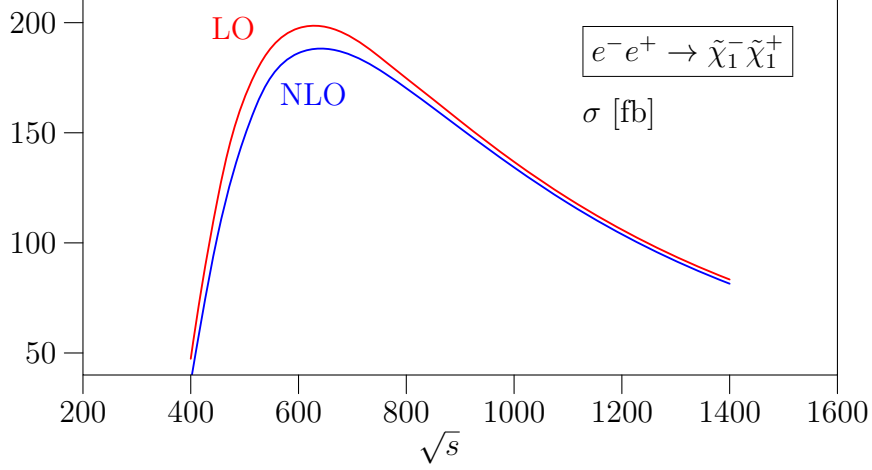


Figure 3.2: Born (LO) and fixed $\mathcal{O}(\alpha)$ (Eq. (3.11)) (NLO) corrected cross sections

In the non-collinear region, logarithms as (3.8), which are regulated by a finite photon mass, do no longer appear. For cm energies $\mathcal{O}(100 \text{ GeV})$ and larger, we can neglect contributions proportional to the electron mass and set $m_e = 0$.

The contributing Feynman diagrams for the s channel exchange are shown in Figure 3.1. The matrix elements can be easily obtained from Eq. (2.1) by substituting

$$\begin{aligned} \mathcal{M} = \bar{A}u(p) &\longrightarrow \mathcal{M}' = -\frac{e}{2pk} \bar{A}(\not{p} - \not{k} + m)\not{\epsilon}u(p), \\ \mathcal{M} = \bar{A}'v(p') &\longrightarrow \mathcal{M}' = -\frac{e}{2p'k} \bar{A}'(\not{p}' - \not{k} + m)\not{\epsilon}v(p'), \end{aligned}$$

where u or v are the spinors of the particle radiating off the photon with a momentum k^μ and the polarization vector ϵ^μ and A/A' symbolize the part of the matrix element untouched by the radiation.

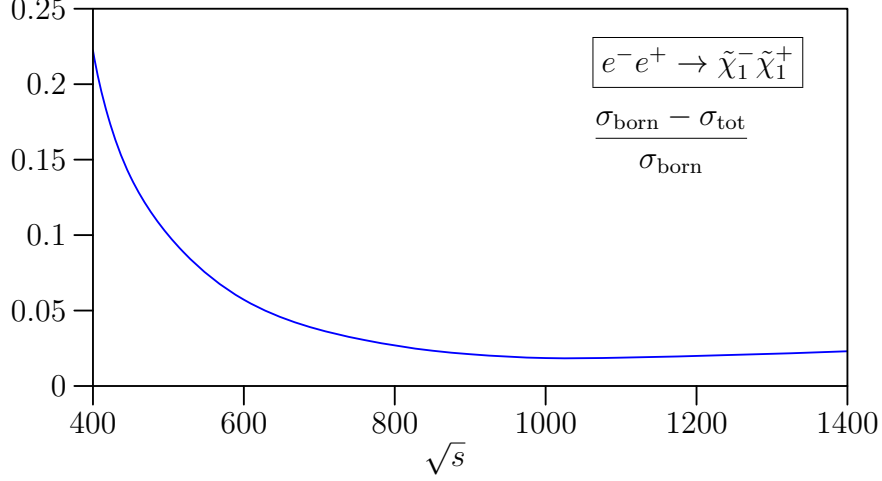


Figure 3.3: relative difference between Born and fixed-order result for total cross section:
 $\frac{\sigma_{Born} - \sigma_{tot}}{\sigma_{Born}}$

3.6 Fixed $\mathcal{O}(\alpha)$ results for total cross section

The total fixed-order $\mathcal{O}(\alpha)$ cross section (Eq. (3.5)) for the process $e^+ e^- \rightarrow \tilde{\chi}_1^+ \tilde{\chi}_1^-$, (γ) is then given by the sum of Eqs. (3.1), (3.2), (3.3), (3.4), (3.7)

$$\begin{aligned}
\sigma_{tot}(s) &= \sigma_{Born}(s) + \sigma_{soft}(s) + \sigma_{virt}(s, \lambda^2, m_e^2) + \sigma_{hard, coll}(s, \Delta E_\gamma, \Delta\theta_\gamma, m_e^2) \\
&+ \sigma_{hard, non-coll}(s, \Delta E_\gamma, \Delta\theta_\gamma) \\
&= \int d\Gamma_2 |\mathcal{M}_{Born}(s, \cos\theta)|^2 + \int d\Gamma_2 f_{soft} |\mathcal{M}_{Born}(s, \cos\theta)|^2 \\
&+ \int d\Gamma_2 [2\text{Re}(\mathcal{M}_{Born}(s)^* \mathcal{M}_{1-loop}(s, \lambda^2, m_e^2))] \\
&+ \sum_{i=1,2} \sum_{\sigma=\pm} \int_0^{x_0} dx_i f^\sigma(x_i; \Delta\theta_\gamma, \frac{m_e^2}{s}) \int d\Gamma_2 |\mathcal{M}_{Born}^\sigma(x_i, s, m_e^2)|^2 \\
&+ \int_{\Delta E_\gamma, \Delta\theta_\gamma} d\Gamma_3 |\mathcal{M}_{2 \rightarrow 3}(s)|^2
\end{aligned} \tag{3.11}$$

with the contributions introduced in the previous sections. For the mSugra point SPS1a' (cf. Appendix C), this leads to corrections $\mathcal{O}(20\%)$ near the threshold and in the 5% region for $\sqrt{s} \geq 600 \text{ GeV}$; cf. Figures 3.2 and 3.3.

3.7 Resummation of higher logarithms: Initial state radiation

The logarithms (3.8) which arise in the collinear emission of photons can become large for small m . In the collinear approximation, where the transverse momentum of a photon

with respect to the emitting particle is neglected, the divergencies originating from the emission of real collinear photons as well as their virtual counterparts can be summed up in splitting functions. The electron-electron splitting function in the leading logarithmic approximation is given by

$$P_{ee}(x) = \left(\frac{1+x^2}{1-x} \right)_+, \quad (3.12)$$

where only terms proportional to the collinear logarithm are kept. The $+$ -distribution is given by Eq. (F.6). The differential cross section taking the emission of one real and one virtual photon collinear photon into account then reads

$$d\sigma_{X+\gamma}(p) = \frac{\alpha}{2\pi} \log\left(\frac{Q^2}{m^2}\right) \int_0^1 dx P_{ee}(x) d\sigma_X(xp),$$

where p is the electron momentum, X symbolizes the final state of the reaction and Q is the scale of the process. The distribution function

$$f_{e,e}(x, Q^2) = \delta(1-x) + \frac{\alpha}{2\pi} \log\left(\frac{Q^2}{m^2}\right) P_{ee}(x)$$

gives the probability of finding an electron with the longitudinal momentum fraction x in an incoming electron, when the emittance of photons with the maximum transverse momentum Q^2 are taken into account. In the collinear limit, Q should be set equal to k_\perp and be small compared to p_0 .

If the coherent emission of more than one photon is considered, the splitting function is replaced by a distribution function D^{NS} . The dominant logarithmic contributions stem from the emission of photons with strong k_\perp -ordering such that $k_{\perp,1} \ll k_{\perp,2} \ll \dots$. The distribution function D^{NS} then obeys the evolution equation [94]

$$\frac{\partial}{\partial \eta} D^{NS}(x, \eta) = \frac{1}{4} \int_x^1 \frac{dz}{z} P(z) D^{NS}\left(\frac{x}{z}, \eta\right), \quad (3.13)$$

where

$$\eta = \int_{m^2}^{Q^2} \frac{ds'}{s'} \frac{2\alpha(s')}{\pi}.$$

In a first approximation, we can neglect the running of α and set it constant. In this case,

$$\eta = \frac{2\alpha}{\pi} \log\left(\frac{Q^2}{m^2}\right). \quad (3.14)$$

The first order solution of Eq. (3.13) is then

$$D^{NS}(x, \eta) = \delta(1-x) + \frac{\eta}{4} P_{e,e}(x) + \mathcal{O}(\eta^2),$$

where the $\delta(1-x)$ term corresponds to the tree level (= no photon emission) part. higher-order solutions can be found in the literature; cf. [75, 95, 96]. The exponentiated structure function $f_{\text{ISR}}(x; \Delta\theta_\gamma, \frac{m_e^2}{s})$ (Eq. (F.14)) includes photon radiation to all orders

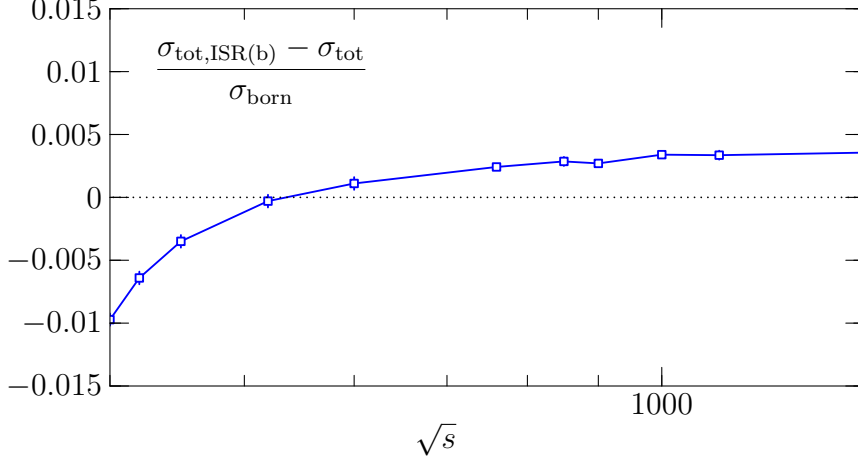


Figure 3.4: Relative effect of ISR higher-order initial state radiation: $\frac{\sigma_{tot,ISR(b)} - \sigma_{tot}}{\sigma_{Born}}$

in the soft regime at leading-logarithmic approximation and, simultaneously, correctly describes collinear radiation of up to three photons in the hard regime. It does not account for the helicity-flip part f^- of the fixed-order structure function. More details on this can be found in Appendix F.3.

Initial state radiation from both incoming particles is then given by

$$\sigma_{Born+ISR}(s, \Delta\theta_\gamma, m_e^2) = \int dx_1 f_{ISR}(x_1) \int dx_2 f_{ISR}(x_2) \int d\Gamma_2 |\mathcal{M}_{Born}(x_1, x_2, s)|^2. \quad (3.15)$$

In combining σ_{tot} (Eq. 3.11) and $\sigma_{Born+ISR}$ (Eq. 3.15), we have to subtract the $\mathcal{O}(1)$ and $\mathcal{O}(\alpha)$ contributions of $\sigma_{Born+ISR}$ as they are already accounted for by σ_{tot} . This way, the total cross section including all $\mathcal{O}(\alpha)$ contributions as well as higher-order initial state radiation, is given by

$$\begin{aligned} \sigma_{tot,ISR(b)} = & \sigma_{tot} + \sigma_{Born+ISR} - \sigma_{Born} \\ & - \left(\int dx_1 f_{ISR}^\alpha(x_1) \int d\Gamma_2 |\mathcal{M}_{Born}(x_1, s)|^2 + \int dx_2 f_{ISR}^\alpha(x_2) \int d\Gamma_2 |\mathcal{M}_{Born}(x_2, s)|^2 \right), \end{aligned} \quad (3.16)$$

where f_{ISR}^α is the $\mathcal{O}(\alpha)$ contribution of f_{ISR} . NLO results for total cross sections in the literature are typically presented in the form of Eq. (3.16). The effects of including higher-order ISR are in the per mille regime as can be seen from Figure 3.4.

3.8 Further higher-order contributions

Charginos usually decay via decay chains involving (at least) two final state particles. A complete NLO calculation therefore also includes factorizable corrections to the chargino

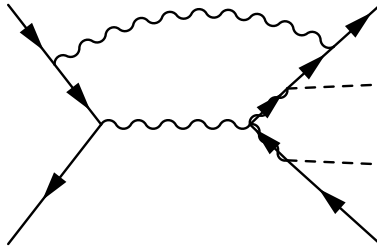


Figure 3.5: General example for a non-factorizing NLO contribution to the $2 \rightarrow 4$ process with s channel chargino production and unspecified final states

decays as well as non-factorizable corrections as e.g. in Figure 3.5.

A first step is the use of the double-pole approximation for the unstable particles. It includes (i) loop corrections to the SUSY production and decay processes, (ii) nonfactorizable, but maximally resonant photon exchange between production and decay, (iii) real radiation of photons, and (iv) off-shell kinematics for the signal process. Recent complete NLO calculations for SM W pair production at an e^+e^- collider [97] have explicitly verified the validity of this approximation in the signal region. A complete analysis also requires the consideration of (v) irreducible background from all other multi-particle SUSY processes, and (vi) reducible, but experimentally indistinguishable background from Standard Model processes. So far, no calculation provides all NLO pieces for a process involving SUSY particles.

In this work, we only consider the extension of the tree-level simulation of chargino production at the ILC by radiative corrections to the on-shell process, i.e., we consider (i) in the above list and consistently include real photon radiation (iii). This is actually a useful approximation since nonfactorizable NLO contributions are suppressed by $\mathcal{O}(\frac{\Gamma}{m})$ [98, 99] and in many MSSM scenarios the widths of charginos, in particular $\tilde{\chi}_1^\pm$, are quite narrow (cf. Table 3.1).

Chargino decays (ii), non-factorizing dominant contributions (iii), and finite-width effects (iv) will be covered in future work. NLO corrections to chargino decays for specific decay products are available from [84]. They are in the % regime and can easily be combined with the present analysis. The inclusion of background effects (v) and (vi) can easily be done using Monte Carlo Event generators [56]. Non-factorizing contributions and finite width effects can be treated in the double-pole approximation [100, 101, 60]. Here the propagators of the unstable particles are expanded around their poles, and only leading order contributions are kept. For W pair production at an e^+e^- collider, analytic results for non-factorizing contributions [102, 103, 104, 105] and a full double-pole approximation [106, 107, 108, 109, 60] are available in the literature.

At the production threshold, additional large corrections can arise from the Coulomb singularity [110, 111]. For on-shell particles, the cross section factorizes according to

$$\sigma_C = \frac{\alpha \pi}{2\beta} \sigma_{Born},$$

	Mass	Width
$\tilde{\chi}_1^+$	183.7 GeV	0.077 GeV
$\tilde{\chi}_2^+$	415.4 GeV	3.1 GeV

Table 3.1: Chargino masses and widths for the SUSY parameter set SPS1a’.

where β denotes the relative velocity of the produced particles. This expression diverges for $\beta \rightarrow 0$. At threshold, the Coulomb singularity needs to be resummed using effective field theories. If the produced particles are off-shell, the singularity is cut off at a relative velocity $\beta \propto \sqrt{\Gamma/m}$. For the masses and widths of charginos given in Table 3.1, this leads to corrections $\leq 1\%$ at threshold. Similarly, for W pair production [112, 113, 114, 115] and slepton production, [116], corrections are in the percent regime.

4 Inclusion of NLO corrected matrix elements in WHIZARD (fixed order)

4.1 Monte Carlo (event) generators

In general, Monte Carlo techniques make use of random numbers to numerically determine values of integrals or, given a probability distribution, simulate the outcome of physical events. For a general introduction of Monte Carlo techniques in particle and especially collider physics, see e.g. [117, 57, 118].

4.1.1 Monte Carlo integration

In Monte Carlo integration, the general idea is to use

$$I = \int_{x_1}^{x_2} f(x) dx \approx (x_2 - x_1) \langle f(x) \rangle,$$

where $\langle f(x) \rangle$ is determined by the averaged value of N random calls of x :

$$\langle f(x) \rangle = \frac{1}{N} \sum_{i=1}^N f(x_i).$$

According to the central limit theorem for large numbers, the error is then $\propto 1/\sqrt{N}$. The N -dependent error can be decreased by importance sampling, where more values of x are chosen in regions where $f(x)$ is largest, or similar techniques.

For the numerical calculation of cross sections with n final particles, we need to integrate

$$\sigma = \frac{1}{2s} \int |\mathcal{M}|^2 d\Pi_n, \quad (4.1)$$

where

$$\Pi_n = \left[\prod_{i=1}^n \frac{d^3 p_i}{(2\pi)^3 (2E_i)} \right] (2\pi)^4 \delta^{(4)} \left(p_0 - \sum_{i=1}^n p_i \right)$$

is the n -dimensional final state phase space. In Monte Carlo programs, the matrix element \mathcal{M} is either coded manually or generated by some (internal or external) automatic matrix element generator. Examples for external programs are **CompHEP** [119], **MadGraph** [120], or **O'Mega** [121]. The integral depends on $3n - 4$ independent variables. Of course, the multi-dimensional integration of phase space is non-trivial and equally requires refined techniques. Differential cross sections can be obtained accordingly.

4.1.2 Event generation

A physical event is defined by the specification of the n four-momenta of the final state particles, which require the generation of $3n - 4$ random numbers. In a straightforward Monte Carlo integration of σ (4.1), all events have the same a-priori probability. To obtain the final result σ , they are weighted with the corresponding differential cross section $d\sigma/(\prod dp_i)$.

A Monte Carlo Event generator, in contrast, should generate events according to their actual probability. This can be achieved by adapting the a-priori probability to the physical distribution or applying a hit-and-miss technique where each event is assigned the corresponding probability $P_i = d\sigma_{(i)}/d\sigma_{max}$ which is compared with a random number r between 0 and 1 and kept if $P_i \geq r$. Notice that this requires that $d\sigma_i \geq 0$. Although this condition is always fulfilled in leading order, NLO calculations might cause problems for certain points of phase space [57]; cf. Sections 4.5 and 5.1.

The events generated by the Monte Carlo program provide the same information as experimental data and can be analyzed using the respective detector simulation and analysis tools. Note that this equally allows for plotting of one- or multidimensional partial distributions, correlations, etc. without any further analytic calculation.

4.1.3 WHIZARD

WHIZARD [52] is a universal Monte Carlo event generator for multiparticle scattering processes. It interfaces several matrix event generators such as **CompHEP**, **MadGraph**, and **O'Mega**. In addition, it includes initial state radiation, beamstrahlung using the program **CIRCE** [122], and fragmentation and hadronization routines from **pythia** [55]. It is designed as a $2 \rightarrow n$ particle event generator. In one call, several processes can be combined such that background studies are simplified. Similarly, the results of several matrix element generators can be compared. For SUSY processes, this has recently been used for an extensive comparison [123]. Currently, it includes the Standard Model, MSSM, little Higgs models, and non-commutative geometry models. Similarly, it allows for user-modified spectra, structure functions, and cuts.

4.2 Calculating NLO matrix elements using **FeynArts** and **FormCalc**

FeynArts [124, 86] and **FormCalc** [81] are Mathematica- and Form-based programs for (higher-order) matrix element generation and the calculation of the respective total and differential cross sections. It includes the SM, the MSSM, and can be extended to any model desired by the user. Furthermore, it can generate Feynman diagrams in a Latex or postscript format. Both programs use **LoopTools** [81] for the calculation of n-point functions and other loop-related quantities. We will quickly discuss both **FeynArts** and **FormCalc** and refer to the respective manuals [80, 85] for more details.

FeynArts

FeynArts is a purely Mathematica-based program. For a given number of in- and outgoing particles and loops, it first generates the corresponding general topologies. After choosing a physical model and specifying the in- and outgoing particles, all amplitudes for the specified process are generated and given analytically (depending on the process, the output might be quite complex). The user can then apply numerous specifications, e.g. diagram selections or renormalization conditions. **FeynArts** equally creates the Latex or postscript output for all created or specifically selected diagrams.

FormCalc

FormCalc is a Form [125, 126]-based program with a Mathematica interface. It generates a Fortran code corresponding to the **FeynArts** amplitudes. The resulting program numerically integrates the total or (angular) differential cross section for the corresponding process. Currently, it contains the kinematics for $1 \rightarrow 2$, $2 \rightarrow 2$, and $2 \rightarrow 3$ particle reactions. In addition, it provides an easy input for e.g. mSugra parameters, loops over the cm energy or model parameters, or energy and angular cuts. It equally allows for different choices of multi-dimensional integration routines. The integrations are carried out according to the techniques described in Section 4.1.1.

Technically, the generated code consists of different process-dependent or independent modules. They contain e.g. routines for general features of the process, the process kinematics, the code for the Born and one-loop matrix element and, for SUSY processes, code for the SUSY spectrum-generation. The compilation creates libraries for the calculation of the matrix element (**squared_me.a**), the renormalization constants (**renconst.a**), and kinematics-dependent variables (**util.a**) which are linked to the main executable. Furthermore, the **LoopTools** library (**libooptools.a**) has to be included.

4.3 Inclusion of the fixed order NLO contribution using a structure function

In WHIZARD, there is an interface for arbitrary structure functions $f(x_1, x_2)$ that can be convoluted with the cross section according to

$$\sigma(s) = \int_0^1 dx_1 \int_0^1 dx_2 f(x_1, x_2) \sigma(x_1, x_2, s),$$

where x_i is the beam energy fraction. $f(x_1, x_2)$ can be the sum of two uncorrelated structure functions (one for each incoming beam) or a correlated structure function for two incoming beams. For more details, cf. [52].

We can therefore implement the fixed-order one-loop result σ_{tot} (Eq. (3.11)) using

$$\begin{aligned}\sigma_{tot}(s, m_e^2) = & \int dx f_{\text{eff}}(x_1, x_2; \Delta E_\gamma, \Delta\theta_\gamma, \frac{m_e^2}{s}) \int d\Gamma_2 |\mathcal{M}_{\text{eff}}(s, x_1, x_2; m_e^2)|^2 \\ & + \int_{\Delta E_\gamma, \Delta\theta_\gamma} d\Gamma_3 |\mathcal{M}_{2\rightarrow 3}(s)|^2,\end{aligned}\quad (4.2)$$

with the structure function

$$\begin{aligned}f_{\text{eff}}(x_1, x_2; \Delta E_\gamma, \Delta\theta_\gamma, \frac{m_e^2}{s}) = & \delta(1-x_1) \delta(1-x_2) \\ & + \delta(1-x_1) f(x_2; \Delta\theta_\gamma, \frac{m_e^2}{s}) \theta(x_0 - x_2) \\ & + f(x_1; \Delta\theta_\gamma, \frac{m_e^2}{s}) \delta(1-x_2) \theta(x_0 - x_1)\end{aligned}\quad (4.3)$$

and the effective squared amplitude

$$\begin{aligned}|\mathcal{M}_{\text{eff}}(s, x_1, x_2; m_e^2)|^2 = & [1 + f_{\text{soft}}(\Delta E_\gamma, \lambda^2) \theta(x_1, x_2)] |\mathcal{M}_{\text{Born}}(s)|^2 \\ & + 2\text{Re} [\mathcal{M}_{\text{Born}}(s) \mathcal{M}_{1\text{-loop}}(s, \lambda^2, m_e^2)] \theta(x_1, x_2)\end{aligned}\quad (4.4)$$

with $\theta(x_1, x_2) \equiv \theta(x_1 - x_0) \theta(x_2 - x_0)$. The parameter

$$x_0 = 1 - \frac{2 \Delta E}{\sqrt{s}}$$

separates the hard from the soft photon region. In addition to the introduction of the structure function f_{eff} , we replace the Born matrix element as computed by the matrix-element generator, **0'Mega**, by the effective matrix element \mathcal{M}_{eff} (4.4). The latter is computed by a call to the **FormCalc**-generated routine.

Technically, (4.2) is implemented by splitting the structure function into four different regions in the (x_1, x_2) space:

- $x_1 \geq x_0, x_2 \geq x_0$: (soft-soft)

This corresponds to the region where $f_{\text{eff}} = \delta(1-x_1) \delta(1-x_2)$. Both photons are in the soft photon regime; we set $x_i = 1$ and calculate the Born+virtual+soft cross sections:

$$\sigma_{\text{Born}} + \sigma_{\text{virt}} + \sigma_{\text{soft}} = \int d\Gamma_2 \{ (1 + f_{\text{soft}}) |\mathcal{M}_{\text{Born}}(s)|^2 + [2\text{Re} (\mathcal{M}_{\text{Born}}(s)^* \mathcal{M}_{1\text{-loop}}(s))] \}.$$

All matrix element contributions in this region as well as the soft photon factor are generated by a call to **FormCalc**. As we are mapping two δ functions to a finite (x_1, x_2) region, we need to divide the result by a normalization factor N such that $\frac{1}{N} \int_{x_0}^1 \int_{x_0}^1 dx_1 dx_2 = 1$.

- $x_i \geq x_0, x_j < x_0$ (soft-hard)

This corresponds to the region where $f_{eff} = \delta(1 - x_i) f(x_j; \Delta\theta_\gamma, \frac{m_e^2}{s})$. One of the photons is in the soft regime, while the other one is in the hard regime. For the soft photon, x is again set to 1. The hard-collinear contribution of the hard photon is then generated according to

$$\begin{aligned}\sigma_{hard,coll} &= \int (f^+(x) \sigma_{Born}^+(x, s) + f^-(x) \sigma_{Born}^-(x, s)) dx \\ &= \sum_{\sigma=\pm} \int_0^{x_0} dx f^\sigma(x; \Delta\theta_\gamma, \frac{m_e^2}{s}) \int d\Gamma_2 |\mathcal{M}_{Born}^\sigma(xs, m_e^2)|^2.\end{aligned}$$

Here, the matrix elements can be calculated using either **FormCalc** or **0'Mega**. The helicity-dependent form factors are implemented by a modification of the density matrix. In general,

$$|\mathcal{M}|^2 = \mathcal{M}^\dagger(\lambda) \rho_{\lambda\lambda'} \mathcal{M}(\lambda'),$$

where $\rho_{\lambda\lambda'}$ is the helicity-dependent density matrix for the incoming particles. For the inclusion of f^\pm , it is modified such that

$$\rho'_{\lambda\lambda} = f^+ \delta_{\lambda,\lambda'} \rho_{\lambda'\lambda'} + f^- \delta_{\lambda,-\lambda'} \rho_{\lambda'\lambda'},$$

where we assumed that λ, λ' can take the values of ± 1 as in fermionic cases. Taking the mapping of the δ function into account, we again have to divide the result by a normalization factor.

- $x_1 < x_0, x_2 < x_0$ (hard-hard)

Both photons are in the hard regime. In principle, this region would describe the radiation of two hard photons. As this is a second order effect, we set $f_{eff} = 0$ in this region.

As the soft photon approximation requires $x \approx 1$, we have to artificially split the interval $[0 : 1]$ such that $x \geq x_0$ is reached sufficiently often. This can be done by the introduction of an additional x_{del} and the projection

$$[0 : x_{del}] \longrightarrow [0 : x_0]; [x_{del} : 1] \longrightarrow [x_0 : 1].$$

We then have to multiply all results by the Jacobian of the transformation.

The hard, non-collinear part is added by a separate run of **WHIZARD** as given by eq. (3.10) with the explicitly generated matrix element $\mathcal{M}_{2 \rightarrow 3}$ applying the respective $\Delta E_\gamma, \Delta\theta_\gamma$ cuts. However, in **WHIZARD** it is equally possible to combine different processes in one run which then reproduces σ_{tot} as given in Eq. (3.11).

Implementing this algorithm in `WHIZARD`, we construct an unweighted event generator. With separate runs for the $2 \rightarrow 2$ and $2 \rightarrow 3$ parts, the program first adapts the phase space sampling and calculates a precise estimate of the cross section. The built-in routines apply event rejection based on the effective weight and thus generate unweighted event samples.

On the technical side, for the actual implementation we have carefully checked that all physical parameters and, in particular, the definition of helicity states are correctly matched between the conventions [77] used by `O'Mega` /`WHIZARD` and those used by `FormCalc` (cf. e.g. [127]). These differ by a complex phase in the definition of the two-component helicity eigenstates.

4.4 Technicalities of the implementation

The inclusion of the `FormCalc` generated NLO contributions described in Section 4.3 implies the modification of the `WHIZARD` as well as the `FormCalc` code. Here, we just sketch the general approach and refer to [128] for more details.

We used the `FormCalc` code for chargino production at NLO available from [64, 84]. `WHIZARD` already includes calls to other external programs, such as `CompHep`, `MadGraph`, and `O'Mega`. Here, libraries are created from the respective programs, which are then linked to the `WHIZARD` executable. The same is done here for the inclusion of the NLO `FormCalc` matrix element.

We therefore modify, in the `FormCalc` code, those modules calculating the matrix element as well as the soft photon factor (to create a `WHIZARD`-compatible in- and output) and the kinematics (in `FormCalc`, the routines setting the kinematics equally set the soft photon factor and give values to internal variables needed for the matrix element evaluation). In addition, we create a new interface setting the SM and MSSM variables to the values used by `WHIZARD`. We can therefore make use of the internal `WHIZARD` data reading routines and can equally use input in the Les Houches accord format [129]. A library `libformcalc.a` is then created and linked. The library equally contains the (modified) `FormCalc` libraries for the squared matrix element (`squared_me.a`), some kinematic variables (`util.a`), and the renormalization constants (`renconst.a`).

In `WHIZARD`, we add a routine `set_pars_formcalc` setting the SM and MSSM values used by `WHIZARD` in the `FormCalc` routines as well as a call to the (NLO)-generated matrix element subroutines `SquaredME` which depends on the cm energy and the four-vectors of the outgoing particles.

To summarize, we

- modify the file `2to2.F` from `FormCalc`, containing the $2 \rightarrow 2$ kinematics, for in- and output of the `WHIZARD` generated particle momenta,
- modify the file `squared_me.F` such that the helicity-dependent subroutine `SquaredME(result, spins, reset, matrix_Born, & matrix_loop, old_angles,`

`old_s`) can explicitly be called from WHIZARD,

- generate a new file `transer.f` for SM and MSSM value transfer,
- create the library `libformcalc.a` from the modified code, including also the unmodified libraries `renconst.a` and `util.a`,
- link `libformcalc.a` and `libooptools.a` to WHIZARD.

In WHIZARD , we

- add the respective routine `set_pars_formcalc` for variable transfer in the process-file,
- call the subroutines setting the case-to-case kinematic variables `SetEnergy` and `SquaredME` each time we need the `FormCalc` one loop matrix element and soft photon factor.

In addition, we included checks guaranteeing that the `FormCalc` loop-related routines are only called when necessary. For example, \sqrt{s} dependent quantities are recalculated only if \sqrt{s} actually changes.

The difference between the helicity bases for fermions used in WHIZARD and `FormCalc` (cf. Section 4.3) needs to be accounted for by the introduction of an additional phase of the matrix element. For the Born contribution, this has been checked for all possible helicity combinations.

The soft and collinear cuts ΔE_γ , $\Delta\theta_\gamma$ are added as variables in the file `cutpars.dat` in the `results` subdirectory of WHIZARD.

4.5 Drawback of the fixed-order method

For any fixed helicity combination and chargino scattering angle the differential cross section is positive if we include all contributions defined in Eq. (3.11). If the integration and simulation is split into a $2 \rightarrow 2$ and $2 \rightarrow 3$ part as implied by σ_{tot} (3.5), however, the fixed-order approach runs into the well-known problem of negative event weights [88, 130, 57]: The effective $2 \rightarrow 2$ matrix element in the soft-soft integration region,

$$|\mathcal{M}_{eff}|^2 = (1 + f_{soft}) |\mathcal{M}_{Born}(s)|^2 + 2 Re(\mathcal{M}_{Born}(s) \mathcal{M}_{1-loop}^*(s)), \quad (4.5)$$

is no longer positive definite if ΔE_γ becomes sufficiently small. If we lower the cutoff, this becomes negative within some range of scattering angle. We will investigate this effect closer and concentrate on the dominant helicity contribution with

$$\lambda_{e+} = 1, \lambda_{e-} = -1, \lambda_{\tilde{\chi}-} = 1, \lambda_{\tilde{\chi}+} = -1, \quad (4.6)$$

and consider the λ , ΔE_γ dependencies of $|\mathcal{M}_{eff}|^2$.

In the effective squared matrix element (4.5), we have

$$f_{soft} = f_{soft}(\lambda, \Delta E_\gamma); \mathcal{M}_{1-loop} = \mathcal{M}_{1-loop}(\lambda).$$

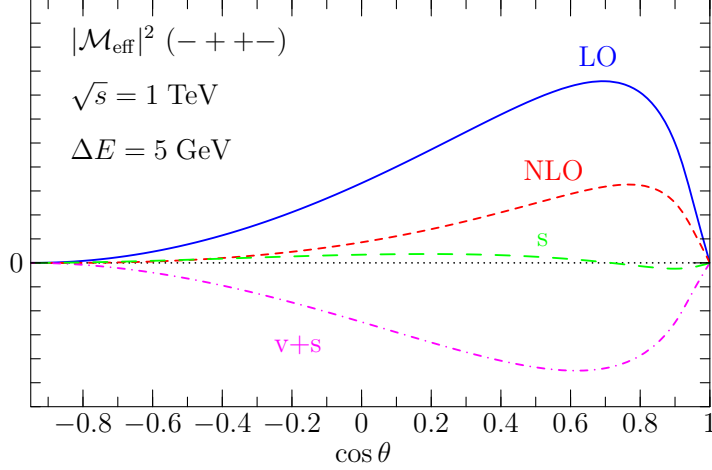


Figure 4.1: $|\mathcal{M}_{eff}|^2$ contributions for $\frac{\Delta E_\gamma}{\sqrt{s}} = 5 \cdot 10^{-3}$, LO: Born, NLO: $|\widetilde{\mathcal{M}}_{eff}|^2$, v denotes the virtual and s the soft contribution

The ΔE_γ dependence enters only in the soft factor

$$f_{soft} \propto \ln \left(\frac{\Delta E_\gamma}{\lambda} \right).$$

In the combination of virtual and soft photons in \mathcal{M}_{eff} , the $\log \lambda$ dependence cancels exactly.

As an example, we consider the angular behavior for a fixed helicity state with $\frac{\Delta E_\gamma}{\sqrt{s}} = 0.005$ (high cut) and $\frac{\Delta E_\gamma}{\sqrt{s}} = 0.0005$ (low cut), respectively. Figures 4.1 and 4.2 show all contributions to $|\mathcal{M}_{eff}|^2$ in these cases. \mathcal{M}_{Born} and $\mathcal{M}_{1-loop}(\lambda)$ are ΔE_γ independent and therefore do not change (for a fixed value for λ). With the high cut, we obtain $|\mathcal{M}_{eff}|^2 > 0$ for all values of θ , while for the lower cut, $|\mathcal{M}_{eff}|^2 < 0$ for $\cos \theta \leq 0.4$. In these regions of phase space, $\frac{\Delta E_\gamma}{\sqrt{s}}$ is small enough such that the virtual photon contributions are not sufficiently canceled by soft real photon contributions. Figure 4.3 shows the behavior of the $|\mathcal{M}_{eff}|^2$ for the helicity combination (4.6) as well as the subdominant contribution with $\lambda_{\tilde{\chi}^-} = \lambda_{\tilde{\chi}^+} = 1$.

If we insist on a positive weight Monte Carlo generator, an ad-hoc solution for the fixed $\mathcal{O}(\alpha)$ contribution would now be to set $\mathcal{M}_{eff}^2 = 0$ in the respective regions of phase space. However, for too low soft cuts, this leads to wrong results for the total and differential cross section, cf. Figure 4.4. An alternative approach uses subtractions in the integrand to eliminate the singularities before integration [131, 132, 133, 134, 101, 135]. The subtracted pieces are integrated analytically and added back or canceled against each other where possible. However, the subtracted integrands do not necessarily satisfy positivity conditions either.

Alternatively, we can include negative event weights. Such event samples are not a

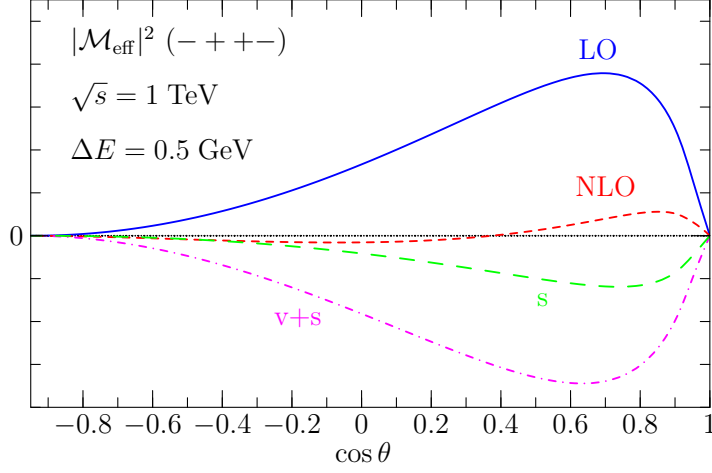


Figure 4.2: $|\mathcal{M}_{eff}|^2$ contributions for $\frac{\Delta E_\gamma}{\sqrt{s}} = 5 \cdot 10^{-4}$, LO: Born, NLO: $|\widetilde{\mathcal{M}}_{eff}|^2$, v denotes the virtual and s the soft contribution

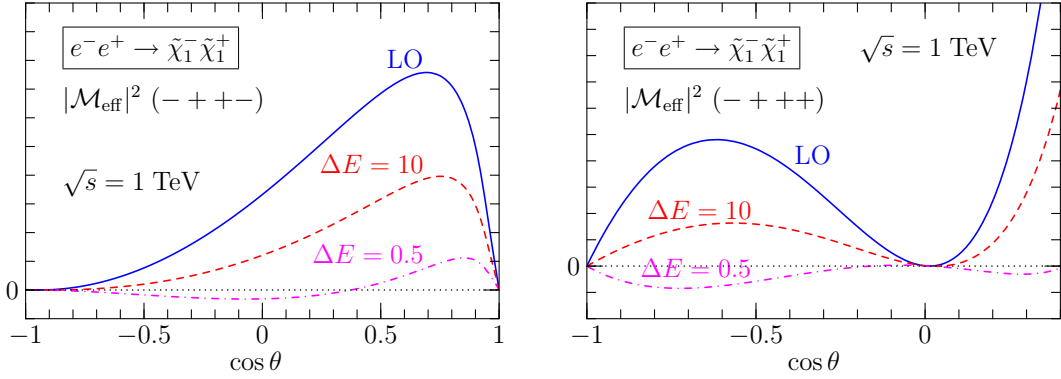


Figure 4.3: Effective squared matrix element (arbitrary units) for $e^-e^+ \rightarrow \tilde{\chi}_1^- \tilde{\chi}_1^+$ as a function of the polar scattering angle θ at $\sqrt{s} = 1$ TeV. Left figure: Helicity combination $- + + -$; right figure: $- + + +$. Solid line: Born term; dashed: including virtual and soft contributions for $\Delta E_\gamma = 10$ GeV; dash-dots: same with $\Delta E_\gamma = 0.5$ GeV.

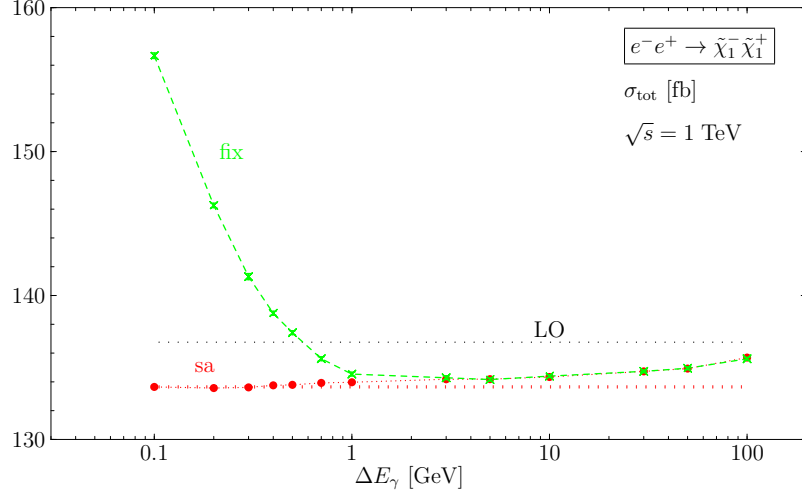


Figure 4.4: Total cross section as a function of the energy cutoff ΔE_γ using different calculational methods: (green, dashed) = fixed-order semianalytic result using **FeynArts/FormCalc**; (red, dotted) = fixed-order Monte-Carlo result using **WHIZARD**; semianalytic result for lowest numerically reachable ΔE_γ . Effects from setting $|\mathcal{M}_{eff}|^2 = 0$ where it becomes negative are visible for $\Delta E_\gamma/\sqrt{s} \leq 10^{-3}$. Statistical Monte-Carlo integration errors are shown. For the Monte-Carlo results, the collinear cutoff has been fixed to $\Delta\theta_\gamma = 1^\circ$. The rise of the fixed order result reflects the breakdown of the soft photon approximation; see Section 4.6.

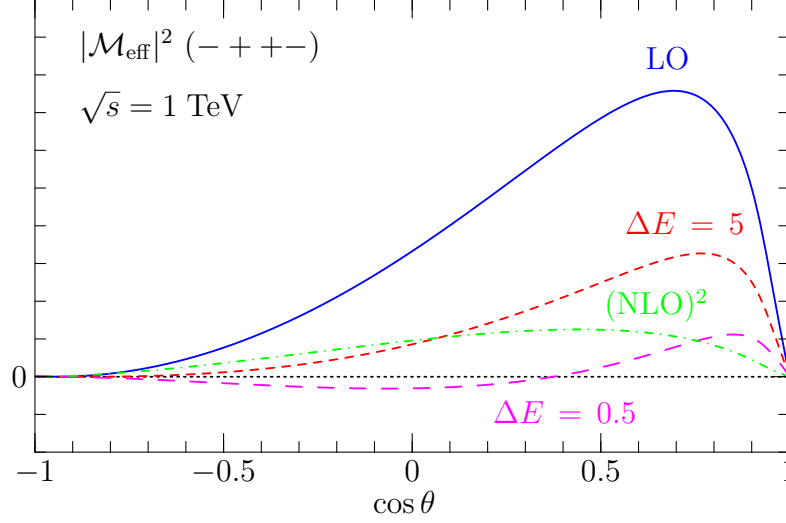


Figure 4.5: Effective squared matrix element and squared NLO contribution $|\mathcal{M}_{v+s}|^2$ as a function of the polar scattering angle θ at $\sqrt{s} = 1$ TeV. Helicity combination $- + + -$; Solid line: Born term; dashed: including virtual and soft contributions for $\Delta E_\gamma = 5$ GeV; long dashed: same with $\Delta E_\gamma = 0.5$ GeV; dash-dotted: $|\mathcal{M}_{v+s}|^2$, $\lambda = 5 \cdot 10^{-5}$ GeV

possible outcome of a physical experiment and imply further modification of the detector and analysis tools.

In general, experimental resolution at the ILC can well reach $\frac{\Delta E_\gamma}{\sqrt{s}} = 10^{-3}$ and lower values. From Figure 4.5, we see that, for a fixed λ , the 1-loop contribution $|\mathcal{M}_{1-loop}|^2$ is nearly the same order of magnitude as $|\mathcal{M}_{eff}|^2$. However, the soft contribution here is treated with the infrared cutoff λ ; setting $\lambda \rightarrow 0$ will always lead to the well-known infrared divergence $\sigma_{soft} \rightarrow \infty$. In principle, this can be canceled by the terms describing the emission of two soft photons equally regulated with the photon mass λ . Therefore, if we want to construct an event generator reaching the experimental cut requirements, we should take second and higher-order contributions into account.

For low enough soft energy cuts, the problem of negative event weights and negative soft cross sections remains as long as only finite order photon emissions are taken into account ([57] and references therein). This signals a breakdown of perturbation theory in this region of phase space and requires the inclusion of summed ISR contributions discussed in Section 3.7. We will present a method to combine this with the fixed-order corrections σ_{virt} in Chapter 5.

4.6 Results

4.6.1 Cut dependencies

In the kinematical ranges below the soft and collinear cutoffs, several approximations are made. In particular, the method neglects contributions proportional to positive powers of ΔE_γ and $\Delta\theta_\gamma$, so the cutoffs must not be increased into the region where these effects could become important. On the other hand, when decreasing cutoffs too much we can enter a region where the limited machine precision induces numerical instabilities. Therefore, we have to check the dependence of the total cross section as calculated by adding all pieces and identify parameter ranges for ΔE_γ and $\Delta\theta_\gamma$ where the result is stable but does not depend significantly on the cutoff values.

In the following, we will compare

1. **fixed order:** The implementation of σ_{tot} according to Eq. (4.2) in `WHIZARD` with both soft (ΔE_γ) and collinear ($\Delta\theta_\gamma$) cuts,
2. **semianalytic:** the NLO calculation presented in [64] using `FormCalc` in combination with the $2 \rightarrow 3$ part from `WHIZARD`. Here, only a soft cut ΔE_γ is applied.

Both programs use the same routine for the calculation of \mathcal{M}_{virt} and f_{soft} as well as the same SM and MSSM input parameters. Therefore, differences are due to the use of the collinear approximation and implementation differences described in Section 4.1.

Throughout this section, we set the process energy to $\sqrt{s} = 1$ TeV and refer to the SUSY parameter point SPS1a'. All $2 \rightarrow 2$ and $2 \rightarrow 3$ contributions are included, so the results would be cutoff-independent if there were no approximations involved.

Energy cutoff dependence

In Figures 4.4 and 4.6, we compare the numerical results obtained using the semianalytic calculation with our Monte-Carlo integration in the fixed-order scheme. The semianalytic result is not exactly cutoff-independent. Instead, it exhibits a slight rise of the calculated cross section with increasing cutoff; for $\Delta E_\gamma = 1$ GeV (10 GeV) the shift is about 2‰ (5‰) of the total cross section, respectively. This is an effect of the soft photon approximation, where the energy fraction x of the incoming electron/ positron is set to 1 in the soft regime. Therefore, for $x \approx 1$ the error is $\mathcal{O}(\Delta E_\gamma/\sqrt{s})$ with respect to σ_{Born} , cf. Figure 4.6. For $\Delta E_\gamma/\sqrt{s} \leq 10^{-5}$, we run into numerical problems with the exact $2 \rightarrow 3$ process. Otherwise, the errors of the semianalytic calculation are in the per mille regime and smaller.

The fixed-order Monte-Carlo result agrees with the semianalytic result, as it should be the case, as long as the cutoff is greater than a few GeV. For smaller cutoff values the Monte-Carlo result drastically departs from the semianalytic one because the virtual correction exceeds the LO term there, and therefore the $2 \rightarrow 2$ effective squared matrix element becomes negative in part of phase space as discussed in Section 4.5. There, the integrand is set to zero.

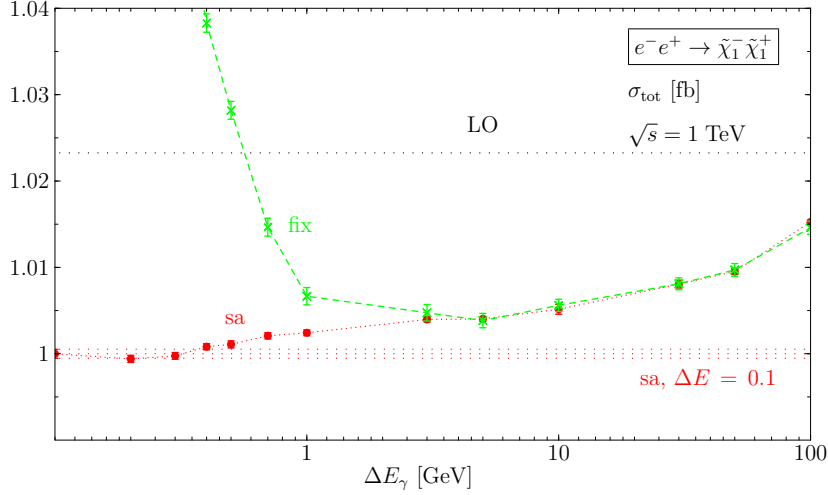


Figure 4.6: Total cross section as a function of the energy cutoff ΔE_γ using different calculational methods: fixed-order semianalytic result; fixed-order Monte-Carlo result using WHIZARD. Relative change with respect to σ_{tot} for $\Delta E_\gamma = 0.1$ GeV, no angular cut

Collinear cutoff dependence

The collinear cutoff $\Delta\theta_\gamma$ separates the region where, in the collinear approximation, higher-order radiation is resummed from the region where only a single photon is included, but treated with exact kinematics. We show the dependence of the result on this cutoff in Fig. 4.7. We see that, for $\Delta\theta \leq 1^\circ$, the collinear approximation holds. For $\Delta\theta = 1^\circ$, its errors are less than per mille. For larger $\Delta\theta$, the collinear approximation breaks down. Similar results are found in [84, 66].

Photon mass dependence

The infinitesimal photon mass λ is used in the FormCalc matrix element calculation for the regularization of infrared divergencies. The effective matrix element $|\mathcal{M}_{eff}|^2$ (Eq. 4.5) should then be independent of λ . Numerically, this has been tested for

$$5 \times 10^{-5} \text{ GeV} \leq \lambda \leq 10^{10} \text{ GeV}$$

for the FormCalc integration routines. In these regions, while the photon mass remains a parameter in the matrix element code, the result does not numerically depend on it, regardless which method has been used. It is of course more meaningful to choose small photon masses.

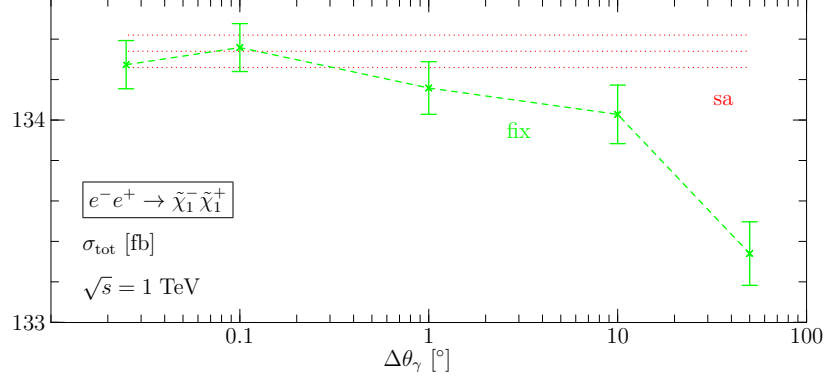


Figure 4.7: Total cross section dependence on the collinear cutoff $\Delta\theta_\gamma$ using different calculational methods: sa (red, dotted) = fixed-order semianalytic result fix (green, dashed) = fixed-order Monte-Carlo result σ_{tot} (3.11); The soft cutoff has been fixed to $\Delta E_\gamma = 10$ GeV, $\sqrt{s} = 1$ TeV

4.6.2 Total cross section

Fixing the cutoffs to $\Delta E_\gamma/\sqrt{s} = 5 \cdot 10^{-3}$, $\Delta\theta = 1^\circ$, we can use the integration part of the Monte-Carlo generator to evaluate the total cross section at NLO for various energies. They exactly reproduce the semianalytic results modulo the ΔE_γ -dependent % errors discussed in Section 4.6.1. For a discussion on the general behaviour of the fixed NLO cross section, cf. Chapter 3. The numerical results qualitatively agree with [64, 66]. However, we did not compare all SUSY parameters used here.

4.6.3 Event generation

The strength of the Monte-Carlo method lies not in the ability to calculate total cross sections, but to simulate physical event samples. We have used the WHIZARD event generator augmented by the effective matrix element (4.5) and structure function (4.3) to generate unweighted event samples for chargino production.

To evaluate the importance of the NLO improvement, in Figures 4.8 and 4.9 we show the binned distribution of the chargino production angle as obtained from a sample of unweighted events corresponding to 1 ab^{-1} of integrated luminosity for $\sqrt{s} = 1$ TeV and the SUSY parameter point SPS1a'. With cutoffs $\Delta\theta_\gamma = 1^\circ$ and $\Delta E_\gamma = 3$ GeV we are not far from the expected experimental resolution, while for the fixed-order approach negative event weights do not yet pose a problem.

The histograms illustrate the fact that NLO corrections in chargino production are not just detectable, but rather important for an accurate prediction, given the high ILC luminosity. The correction cannot be approximated by a constant proportionality factor K between the leading and next-to-leading order cross section (K -factor) but takes a different shape than the LO distribution. The correction is positive in the forward and backward directions, but negative in the central region. For comparison, Figure 4.9 also

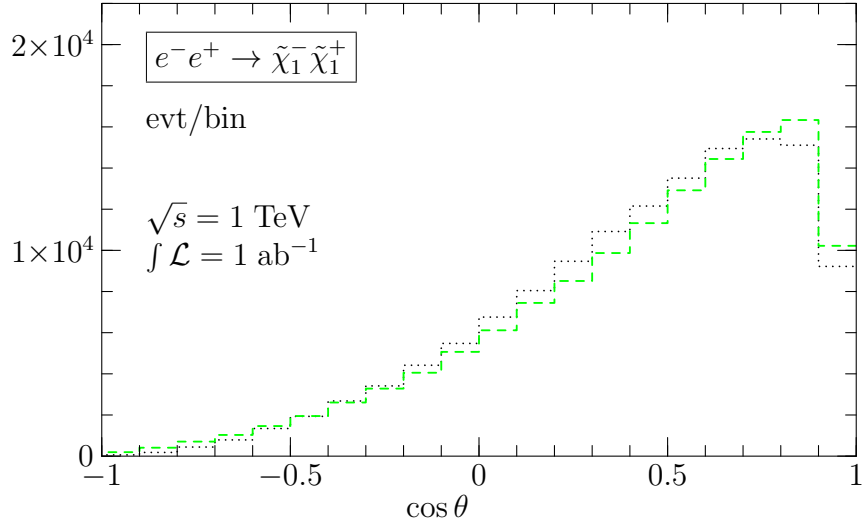


Figure 4.8: Polar scattering angle distribution for an integrated luminosity of 1 ab^{-1} at $\sqrt{s} = 1 \text{ TeV}$. Total number of events per bin, Born (dotted, black) and fixed order (dashed, green) result

shows the 1σ error from the Born result.

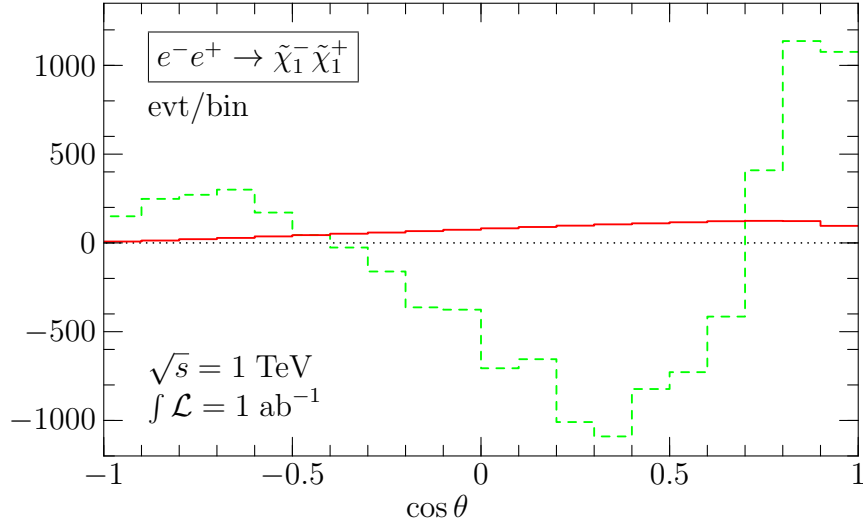


Figure 4.9: Polar scattering angle distribution for an integrated luminosity of 1 ab^{-1} at $\sqrt{s} = 1 \text{ TeV}$. Number of events per bin, difference between fixed order and Born (dashed, green). For comparison, the standard deviation from the Born result is also shown (solid, red)

5 Resumming photons

5.1 NLO and resummation at LEP and LHC

The principle of analytic photon resummation has already been discussed in Section 3.7. We will here shortly sketch the implementation of photon resummation in Monte Carlo generators at LEP as well as NLO matrix elements for hadronic machines and refer to the literature [57, 118] for more details.

Photon resummation at LEP

The problem of negative event weights discussed in Section 4.5 was, at LEP times, known as the k_0 problem. When slicing the Monte Carlo generator phase space in a $2 \rightarrow 2$ (Born, virtual, soft) and a $2 \rightarrow 3$ (hard) part as in the fixed order approach, event weights in the $2 \rightarrow 2$ part can become negative for $k_0 \rightarrow 0$. This holds true in any finite-order treatment of soft real and virtual photons. The solution is to sum photons up to an infinite order. In [57], different methods are proposed in order to include exponentiation in Monte Carlo event generators: ad hoc-exponentiation which estimates the energy loss due to photon radiation and modifies the Monte Carlo code accordingly, the use of (positive definite) structure functions convoluted with the Born cross section at a reduced cm energy, and YFS exponentiation [136] which correctly simulates the hard part, while using a structure function for soft and virtual photons. In Section 3.7 and in the following, we will use the structure-function method proposed by Jadach and Skrzypek [75]. Note, however, that none of these approaches includes non-photonic NLO contributions as σ_{virt} (Eq. 3.2).

NLO and parton showers for LHC

Recently, several computer codes attempt to include exact NLO matrix elements in Monte Carlo generators containing partonic showers, which are the QCD equivalent of the infinitely summed up photon contributions described above. These are basically directed to experiments at hadronic machines such as the LHC, cf. [71, 72, 118, 73]. A similar code treating jet production at e^+e^- colliders was proposed in [69, 70]. Basically, the NLO contributions are added by hand, while the corresponding first order parts from the parton showers are subtracted. In the following, we will pursue a similar approach for the inclusion of electroweak NLO corrections.

5.2 Resummation method

The shortcomings of the fixed-order approach described in Chapter 4 are associated with the soft-collinear region $E_\gamma < \Delta E_\gamma$, $\theta_\gamma < \Delta\theta_\gamma$, where the appearance of double logarithms $\frac{\alpha}{\pi} \ln \frac{E_\gamma^2}{s} \ln \theta_\gamma$ invalidates the perturbative series. However, in that region higher-order radiation can be resummed [94, 137, 138]. The exponentiated structure function f_{ISR} (F.14) that resums initial-state radiation,

$$\sigma_{\text{Born+ISR}}(s, \Delta\theta_\gamma, m_e^2) = \int dx f_{\text{ISR}}(x; \Delta\theta_\gamma, \frac{m_e^2}{s}) \int d\Gamma_2 |\mathcal{M}_{\text{Born}}(xs)|^2,$$

includes photon radiation to all order in the soft regime at leading-logarithmic approximation and, simultaneously, correctly describes collinear radiation of up to three photons in the hard regime. It does not account for the helicity-flip part f^- (F.5) of the fixed-order structure function; this may either be added separately or just be dropped since it is subleading.

We now combine the ISR-resummed LO result with the additional NLO contributions σ_{virt} given by Eq. (3.2). To achieve this and avoid double counting, we first subtract from the effective squared matrix element, for each incoming particle, the contribution of one soft real and virtual collinear photon that is contained in the ISR structure function. The soft photon has already been accounted for in the soft-photon factor, while the virtual part is contained in the interference term. Then

$$\begin{aligned} |\widetilde{\mathcal{M}}_{\text{eff}}(\hat{s}; \Delta E_\gamma, \Delta\theta_\gamma, m_e^2)|^2 &= \left[1 + f_{\text{soft}}\left(\frac{\Delta E_\gamma}{\lambda}\right) - 2f_{\text{soft,ISR}}(\Delta E_\gamma, \Delta\theta_\gamma, \frac{m_e^2}{s}) \right] |\mathcal{M}_{\text{Born}}(\hat{s})|^2 \\ &\quad + 2\text{Re} [\mathcal{M}_{\text{Born}}(\hat{s}) \mathcal{M}_{1\text{-loop}}^*(\hat{s}, \lambda^2, m_e^2)] \end{aligned} \quad (5.1)$$

with \hat{s} being the c.m. energy after radiation and $f_{\text{soft,ISR}}$ the integrated $\mathcal{O}(\alpha)$ contribution of f_{ISR} . This expression contains the Born term, the virtual and soft-collinear contribution with the leading-logarithmic part of virtual photons and soft-collinear emission removed, and soft non-collinear radiation of one photon; it still depends on the cutoff ΔE_γ . Convoluting this with the resummed ISR structure function,

$$\begin{aligned} \sigma_{\text{v+s,ISR}}(s, \Delta E_\gamma, \Delta\theta_\gamma, m_e^2) \\ = \int dx_1 f_{\text{ISR}}(x_1; \Delta\theta_\gamma, \frac{m_e^2}{s}) \int dx_2 f_{\text{ISR}}(x_2; \Delta\theta_\gamma, \frac{m_e^2}{s}) \int d\Gamma_2 |\widetilde{\mathcal{M}}_{\text{eff}}(\hat{s}; \Delta E_\gamma, \Delta\theta_\gamma, m_e^2)|^2, \end{aligned} \quad (5.2)$$

we obtain a modified $2 \rightarrow 2$ part of the total cross section.

In this description of the collinear region, there is no explicit cutoff ΔE_γ involved, and collinear virtual photons connected to at least one incoming particle are included. The cancellation of infrared singularities between virtual and real corrections is built-in for collinear photons. The main source of negative event weights is eliminated, and we

obtain a better behaviour for the integrand such that smaller energy cuts can be applied; cf. Section 5.4.1. Furthermore, the method is exact in $\mathcal{O}(\alpha)$ leading log terms. In the following, we will consider the description of one and more photons resulting from $\sigma_{v+s,ISR}$ in more detail.

In the resummation method, the emission of real and virtual photons is described in various ways: the soft approximation (cf. Sec. 3.3), initial state radiation (cf. Sec. 3.7), virtual contribution from interference term (cf. Section 3.2), and real emission given by exact (hard non-collinear) matrix element $\mathcal{M}_{2 \rightarrow 3}$ (cf. Sec 3.5). We will now consider the respective description of photons resulting from the resummation method in different points of phase space. Here, we go to infinite order for the photon emission from one incoming particle and to second order for the simultaneous photon emission from two incoming particles.

Radiation off one incoming particle

We first consider photon radiation from one particle only and use the exponentiated electron structure function f_{ISR} (F.14). In the following, we ignore the emission of the second photon contained in f_{soft} and only subtract the contribution of f_{ISR} for one photon. The corresponding effective matrix element for the radiation of only one photon is

$$|\widetilde{\mathcal{M}}_{\text{eff}}^{(1)}(\hat{s}; \Delta E_\gamma, \Delta\theta_\gamma, m_e^2)|^2 = \left[1 + f_{\text{soft}}\left(\frac{\Delta E_\gamma}{\lambda}\right) - f_{\text{soft},ISR}(\Delta E_\gamma, \Delta\theta_\gamma, \frac{m_e^2}{s}) \right] |\mathcal{M}_{\text{Born}}(\hat{s})|^2 + 2\text{Re} [\mathcal{M}_{\text{Born}}(\hat{s}) \mathcal{M}_{1\text{-loop}}^*(\hat{s}, \lambda^2, m_e^2)] \quad (5.3)$$

and the total cross section

$$\sigma_{v+s,ISR}^{(1)}(s, \Delta E_\gamma, \Delta\theta_\gamma, m_e^2) = \int dx f_{ISR}(x; \Delta\theta_\gamma, \frac{m_e^2}{s}) \int d\Gamma_2 |\widetilde{\mathcal{M}}_{\text{eff}}^{(1)}(x, s; \Delta E_\gamma, \Delta\theta_\gamma, m_e^2)|^2. \quad (5.4)$$

According to the exponentiation principle discussed in Appendix F.3.2, we can decompose $(\int) f_{ISR}$ in factors $F^{(l)}, F_l$ such that

$$\begin{aligned} \int_{x_0}^1 D^{NS}(x) dx &= \sum_{l=0}^n F^{(l)}(x_0) + \mathcal{O}(\eta^{n+1}), \\ D^{NS}(x) &= \sum_{l=0}^n F_l(x) + \mathcal{O}(\eta^{n+1}) \quad x < x_0, \end{aligned} \quad (5.5)$$

where $F^{(n)}(x_0)$ is the $\mathcal{O}(\eta^n)$ contribution to the integrated exact solution of the evolution equation (3.13) in the soft limit and $F_n(x)$ is the exact $\mathcal{O}(\eta^n)$ perturbative solution to it. In the structure function f_{ISR} (F.14) used in this work, F_n has been calculated up to $n = 3$. Using the scale $Q^2 = (\Delta\theta p_0)^2$, where p_0 is the energy of the electron, these factors exclusively describe collinear photons. We have

$$F^{(0)} = 1, \quad F^{(1)} = f_{\text{soft},ISR}; \quad F_0 = 0. \quad (5.6)$$

$|\widetilde{\mathcal{M}}_{eff}|^2$ mixes different orders of η . For a fixed order n , the photon contributions to $\sigma_{v+s,ISR}^{(1)}$ are given by

$$\begin{aligned}\sigma_\gamma^{(1)} &= F^{(n)}(x_0)\sigma_{Born}(s) + \int_0^{x_0} F_n(x)\sigma_{Born}(x,s)dx + F^{(n-1)}\hat{\sigma}(s) \\ &+ \int_0^{x_0} F_{n-1}(x)\hat{\sigma}(x,s)dx - F^{(1)}(x_0)F^{(n-1)}(x_0)\sigma_{Born}(s) \\ &- F^{(1)}(x_0)\int_0^{x_0} F_{n-1}(x)\sigma_{Born}(x,s)dx,\end{aligned}\tag{5.7}$$

where

$$\hat{\sigma} = \int d\Gamma_2 f_{\text{soft}}|\mathcal{M}_{\text{Born}}(x,s)|^2 + 2\text{Re}[\mathcal{M}_{\text{Born}}^*(x,s)\mathcal{M}_{1\text{-loop}}(x,s)]$$

contains all contributions from virtual photon emission according to the exact $\mathcal{M}_{1\text{-loop}}$ calculation as well soft photon emission in the soft approximation.

We will now consider the results for soft-collinear photons, distinguishing between multiple photon emissions where the last emitted photon does or does not obey the transverse momentum ordering $k_{\perp,n-1} \ll k_{\perp,n}$:

- k_{\perp} ordering obeyed

If the first $n-1$ emitted photons are soft (i.e. their total energy is lower than ΔE_γ), this part of $\sigma_\gamma^{(1)}$ is given by

$$F^{(n)}(x_0)\sigma_{Born}(s) + F^{(n-1)}\hat{\sigma}(s) - F^{(1)}(x_0)F^{(n-1)}(x_0)\sigma_{Born}(s) = F^{(n-1)}\hat{\sigma}(s),$$

and by

$$\begin{aligned}&\int_0^{x_0} \left(F_n(x) - F^{(1)}(x_0)F_{n-1}(x)\right)\sigma_{Born}(x,s)dx + \int_0^{x_0} F_{n-1}(x)\hat{\sigma}(x,s)dx \\ &= \int_0^{x_0} F_{n-1}(x)\hat{\sigma}(x,s)dx\end{aligned}$$

otherwise. The last soft-collinear photon is described by the soft photon approximation, all others by f_{ISR} .

- no k_{\perp} ordering

The terms $\propto F^{(n)}$, F_n , which describe the emission of n k_{\perp} -ordered photons, are missing in $\sigma_\gamma^{(1)}$. This results in

$$F^{(n-1)}\left(\hat{\sigma}(s) - F^{(1)}(x_0)\sigma_{Born}(s)\right) + \int_0^{x_0} F_{n-1}(x)\left(\hat{\sigma}(x,s) - F^{(1)}(x_0)\sigma_{Born}(x,s)\right)dx.\tag{5.8}$$

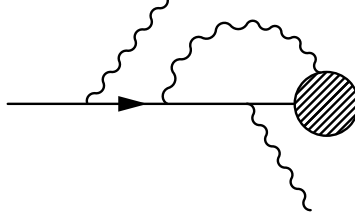


Figure 5.1: Example for mixed real and virtual photon emissions described by f_{ISR} . All photons are collinear and k_\perp -ordered

We only obtain differences between the exact and the leading log contribution for the last radiated photon, multiplied with the f_{ISR} contribution for the first $n - 1$ photons.

If only hard-collinear photons are emitted, they are all described by f_{ISR} . For virtual photons, the same relations hold as for soft real photons: in the case of k_\perp ordering of the last photon, it is given by the contribution to M_{1-loop} . Otherwise, the emission of the virtual last photon is again described by difference terms according to Eq. (5.8). Note that the radiation of a non-collinear soft photon as well as a non-collinear virtual photon is not touched by the subtraction mechanism. Here, the respective contribution to $\sigma_\gamma^{(1)}$ is simply

$$F^{(n-1)} \hat{\sigma}_{rest}(s) + \int_0^{x_0} F_{n-1}(x) \hat{\sigma}_{rest}(x, s) dx, \quad (5.9)$$

where $\hat{\sigma}_{rest}$ contains all non-collinear virtual and non-photon contributions.

In general, f_{ISR} describes a combination of real and virtual photon emissions, e.g. graphs given in Figure 5.1, as the electron splitting function P_{ee} (3.12) combines the radiation of both a real and a virtual photon in order to cancel the IR divergence. Both soft real and virtual photons are contained in the soft contributions to the factors $F^{(n)}$ and F_n . For example, we can split $F^{(n)}$ according to

$$F^{(n)}(x_0) = (F^{(1)})^n = (F_{soft} + F_{virt})^n. \quad (5.10)$$

This describes the emission of n collinear photons in an arbitrary combination of soft and virtual contributions. The only requirement is the k_\perp ordering of their transverse momenta and $\sum_{\text{real } \gamma} E_\gamma \leq \Delta E_\gamma$.

Radiation off two incoming particles

Figure 5.2 shows the diagrams contributing to the emission of two photons off two incoming particles for the s channel γ , Z exchange (we omitted diagrams resulting from the crossing symmetry for the radiated photons). As discussed in the last section, virtual photons are contained in the soft parts of f_{ISR} (cf. Eq. (5.10)). We now consider the

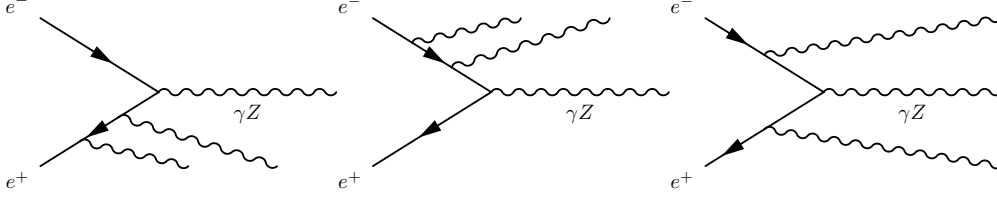


Figure 5.2: Diagrams contributing to the radiation of two photons, either from one incoming particle, or both incoming particles, for the s channel γ, Z exchange. Missing are diagrams from crossing symmetry of radiating photons. The t channel $\tilde{\nu}$ -exchange behaves analogously

contributions to $\sigma_{virt+ISR}$ (5.2) from up to two photon emissions. In the remainder of this section, $\sigma = \sigma_{Born}$.

In general, the photonic $\mathcal{O}(\alpha^n)$ contributions to $\sigma_{v+s,ISR}$ are given by

$$\begin{aligned}
& \sum_{l=0}^n \left(\int_0^{x_0} dx_1 \int_0^{x_0} dx_2 F_l(x_1) F_{n-l}(x_2) \sigma(x_1 x_2 s) + \int_0^{x_0} dx_1 F_l(x_1) F^{(n-l)}(x_2) \sigma(x_1 s) \right. \\
& \quad \left. + \int_0^{x_0} dx_2 F_{n-l}(x_2) F^{(l)}(x_1) \sigma(x_2 s) + F^{(l)}(x_1) F^{(n-l)}(x_2) \sigma(s) \right) \\
& + \sum_{l=0}^{n'-1} \left(\int_0^{x_0} dx_1 \int_0^{x_0} dx_2 F_l(x_1) F_{n'-l}(x_2) \left(\hat{\sigma}(x_1 x_2 s) - 2 F^{(1)} \sigma(x_1 x_2 s) \right) \right. \\
& \quad + \int_0^{x_0} dx_1 F_l(x_1) F^{(n'-l)}(x_2) \left(\hat{\sigma}(x_1 s) - 2 F^{(1)} \sigma(x_1 s) \right) \\
& \quad + \int_0^{x_0} dx_2 F_{n'-l}(x_2) F^{(l)}(x_1) \left(\hat{\sigma}(x_2 s) - 2 F^{(1)} \sigma(x_2 s) \right) \\
& \quad \left. + F^{(l)}(x_1) F^{(n'-l)}(x_2) \left(\hat{\sigma}(s) - 2 F^{(1)} \sigma(s) \right) \right).
\end{aligned}$$

For $\mathbf{n} = \mathbf{0}$, we obtain (recall Eq (5.6)) the Born contribution (3.1):

$$\begin{aligned}
& \int_0^{x_0} dx_1 \int_0^{x_0} dx_2 F_0(x_1) F_0(x_2) \sigma(x_1 x_2 s) + \int_0^{x_0} dx_1 F_0(x_1) F^{(0)}(x_2) \sigma(x_1 s) \\
& + \int_0^{x_0} dx_2 F_0(x_2) F^{(0)}(x_1) \sigma(x_2 s) + F^{(0)}(x_1) F^{(0)}(x_2) \sigma(s) \\
& = \sigma(s).
\end{aligned}$$

Setting $\mathbf{n} = \mathbf{1}$ gives the additional terms

$$\begin{aligned}
& \left(\int_0^{x_0} dx_1 \int_0^{x_0} dx_2 F_1(x_1) F_0(x_2) \sigma(x_1 x_2 s) + \int_0^{x_0} dx_1 F_1(x_1) F^{(0)}(x_2) \sigma(x_1 s) \right. \\
& + \int_0^{x_0} dx_1 F_0(x_1) F^{(1)}(x_2) \sigma(x_1 s) + F^{(1)}(x_1) F^{(0)}(x_2) \sigma(s) \Big) + (x_1 \leftrightarrow x_2) \\
& + \int_0^{x_0} dx_1 \int_0^{x_0} dx_2 F_0(x_1) F_0(x_2) \left(\hat{\sigma}(x_1 x_2 s) - 2 F^{(1)} \sigma(x_1 x_2 s) \right) \\
& + \int_0^{x_0} dx_1 F_0(x_1) F^{(0)}(x_2) \left(\hat{\sigma}(x_1 s) - 2 F^{(1)} \sigma(x_1 s) \right) \\
& + \int_0^{x_0} dx_2 F_0(x_2) F^{(0)}(x_1) \left(\hat{\sigma}(x_2 s) - 2 F^{(1)} \sigma(x_2 s) \right) \\
& + F^{(0)}(x_1) F^{(0)}(x_2) \left(\hat{\sigma}(s) - 2 F^{(1)} \sigma(s) \right) \\
& = \int_0^{x_0} dx_1 F_1(x_1) \sigma(x_1 s) + \int_0^{x_0} dx_2 F_1(x_2) \sigma(x_2 s) + \hat{\sigma}(s),
\end{aligned}$$

where we used Eq. (5.6), the fact that $F^{(1)}$ only depends on x_0 such that $F^{(1)}(x) = F^{(1)}(x_0)$, and

$$-2 F^{(1)} = -F^{(1)}(x_1) - F^{(1)}(x_2). \quad (5.11)$$

for the subtraction terms in $|\mathcal{M}_{eff}|^2$.

We see that the $n = 1$ term corresponds exactly to the $2 \rightarrow 2$ part of the leading log $\mathcal{O}(\alpha)$ contribution of the fixed order calculation (3.11).

For $\mathbf{n} = \mathbf{2}$, we obtain the additional terms

$$\begin{aligned}
& \left(F^{(2)}(x_2) \sigma(s) + \int_0^{x_0} dx_2 F_2(x_2) \sigma(x_2 s) \right) + (x_1 \leftrightarrow x_2) \\
& + \int_0^{x_0} dx_1 \int_0^{x_0} dx_2 F_1(x_1) F_1(x_2) \sigma(x_1 x_2 s) + \int_0^{x_0} dx_1 F_1(x_1) F^{(1)}(x_2) \sigma(x_1 s) \\
& + \int_0^{x_0} dx_2 F_1(x_2) F^{(1)}(x_1) \sigma(x_2 s) + F^{(1)}(x_1) F^{(1)}(x_2) \sigma(s) \\
& \left(+ \int_0^{x_0} dx_2 F_1(x_2) \left(\hat{\sigma}(x_2 s) - 2 F^{(1)} \sigma(x_2 s) \right) \right. \\
& \left. + F^{(1)}(x_2) \left(\hat{\sigma}(s) - 2 F^{(1)} \sigma(s) \right) \right) + (x_1 \leftrightarrow x_2), \quad (5.12)
\end{aligned}$$

where we again used Eq. (5.6). To really understand the Feynman diagrams to which the different contributions in (5.12) correspond and the cancellations, we have to take Eq. (5.11) into account. We first consider the case of two photons radiating off the same incoming particle, e.g. the one depending on x_1 . The relevant contributions are given

by

$$\begin{aligned}
& F^{(2)}(x_1) \sigma(s) + \int_0^{x_0} dx_1 F_2(x_1) \sigma(x_1 s) \\
& + \int_0^{x_0} dx_1 F_1(x_1) \left(\hat{\sigma}(x_1 s) - F^{(1)}(x_1) \sigma(x_1 s) \right) + F^{(1)}(x_1) \left(\hat{\sigma}(s) - F^{(1)}(x_1) \sigma(s) \right).
\end{aligned} \tag{5.13}$$

A comparison shows that this exactly corresponds to the $n = 2$ case of only 1 particle radiating off photons (cf. Eq. (5.7)). Therefore, the description of photon radiation given for this case also applies here.

The mixed case is more complicated. The relevant terms are given by

$$\begin{aligned}
& \int_0^{x_0} dx_1 \int_0^{x_0} dx_2 F_1(x_1) F_1(x_2) \sigma(x_1 x_2 s) + \int_0^{x_0} dx_1 F_1(x_1) F^{(1)}(x_2) \sigma(x_1 s) \\
& + \int_0^{x_0} dx_2 F_1(x_2) F^{(1)}(x_1) \sigma(x_2 s) + F^{(1)}(x_1) F^{(1)}(x_2) \sigma(s) \\
& + \int_0^{x_0} dx_2 F_1(x_2) \left(\hat{\sigma}(x_2 s) - F^{(1)}(x_1) \sigma(x_2 s) \right) + F^{(1)}(x_2) \left(\hat{\sigma}(s) - F^{(1)}(x_1) \sigma(s) \right) \\
& + \int_0^{x_0} dx_1 F_1(x_1) \left(\hat{\sigma}(x_1 s) - F^{(1)}(x_2) \sigma(x_1 s) \right) + F^{(1)}(x_1) \left(\hat{\sigma}(s) - F^{(1)}(x_2) \sigma(s) \right).
\end{aligned} \tag{5.14}$$

If at least one of the radiated photons is hard, the relevant terms are given by (for e.g. x_1 hard and x_2 hard or soft):

$$\begin{aligned}
& \int_0^{x_0} dx_1 \int_0^{x_0} dx_2 F_1(x_1) F_1(x_2) \sigma(x_1 x_2 s) + \int_0^{x_0} dx_1 F_1(x_1) F^{(1)}(x_2) \sigma(x_1 s) \\
& + \int_0^{x_0} dx_1 F_1(x_1) \left(\hat{\sigma}(x_1 s) - F^{(1)}(x_2) \sigma(x_1 s) \right) \\
& = \int_0^{x_0} dx_1 \int_0^{x_0} dx_2 F_1(x_1) F_1(x_2) \sigma(x_1 x_2 s) + \int_0^{x_0} dx_1 F_1(x_1) \hat{\sigma}(x_1 s),
\end{aligned}$$

i.e. we obtain the usual description (hard photon: leading log, soft photon: soft approximation, virtual photon: one-loop description from interference term). However, if both photons are soft, we have to closer investigate the phase space slicing. The soft-soft terms are given by

$$F^{(1)}(x_2) \hat{\sigma}(s) + F^{(1)}(x_1) \hat{\sigma}(s) - F^{(1)}(x_1) F^{(1)}(x_2) \sigma(s). \tag{5.15}$$

We now split $\hat{\sigma}$ into

$$\hat{\sigma} = F^{(1)} \sigma + \Delta F^{(1)} \sigma + \hat{\sigma}_{rest}, \tag{5.16}$$

where $\hat{\sigma}_{rest}$ contains all non-collinear virtual and non-photonic (ie, weak and SUSY) contributions, and $\Delta F^{(1)}$ is the difference between the soft approximation f_{soft} (3.6)

and the first order contributions of the integrated leading log structure function $f_{soft,ISR}$ (F.18):

$$\Delta F^{(1)} = f_{soft}^{1\gamma} - f_{soft,ISR}. \quad (5.17)$$

In an ideal case, we would have

$$(F^{(1)} + \Delta F^{(1)})(x_1) (F^{(1)} + \Delta F^{(1)})(x_2) \sigma.$$

Up to $\mathcal{O}((\Delta F^{(1)})^2)$ terms, this corresponds to eq. (5.15). In this accuracy, both photons are described by f_{soft} . The same holds for virtual-soft and virtual-virtual emissions, where the virtual part is (up to similar corrections) described by the interference term. Finally, we have to consider whether these contributions correspond to the photon-photon diagrams as given in Figure 5.2. We obtain 6 diagrams (for each diagram, there is one with the outgoing photons crossed). However, as we have two indistinguishable photons in the final state, we obtain an additional factor $\frac{1}{2}$ so that the approximation above directly corresponds to the contributions we expect for the process $e^+ e^- \rightarrow \tilde{\chi} \tilde{\chi} \gamma \gamma$. The same holds of course for any convoluting of the Born cross section with $\int dx_1 \int dx_2 D^{NS}(x_1) D^{NS}(x_2)$.

As in the case of only one particle emitting photons (Eq. (5.9)), (5.2) also includes collinear photonic corrections to the Born/one-loop interference $\hat{\sigma}_{rest}$ in leading log accuracy. The corresponding convolution with f_{ISR} is completely unaffected by the subtraction mechanism, which only accounts for the soft parts.

The complete result is supplemented by the $2 \rightarrow 3$ part,

$$\sigma_{tot,ISR}(s, m_e^2) = \sigma_{v+s,ISR} + \int_{\Delta E_\gamma, \Delta \theta_\gamma} d\Gamma_3 |\mathcal{M}_{2 \rightarrow 3}(s)|^2. \quad (5.18)$$

A final improvement is to also convolute the $2 \rightarrow 3$ part with the ISR structure function which defines

$$\begin{aligned} \sigma_{tot,ISR+}(s, m_e^2) &= \int dx_1 f_{ISR}(x_1; \Delta \theta_\gamma, \frac{m_e^2}{s}) \int dx_2 f_{ISR}(x_2; \Delta \theta_\gamma, \frac{m_e^2}{s}) \\ &\times \left(\int d\Gamma_2 |\widetilde{\mathcal{M}}_{\text{eff}}(\hat{s}; \Delta E_\gamma, \Delta \theta_\gamma, m_e^2)|^2 + \int_{\Delta E_\gamma, \Delta \theta_\gamma} d\Gamma_3 |\mathcal{M}_{2 \rightarrow 3}(\hat{s})|^2 \right). \end{aligned} \quad (5.19)$$

This introduces another set of higher-order corrections, namely those where after an arbitrary number of collinear photons, one hard non-collinear photon is emitted. This additional resummation does not double-count. It catches logarithmic higher-order contributions where ordering in transverse momentum can be applied. Other, logarithmically subleading contributions are missed. In $\mathcal{O}(\alpha)$, σ_{tot} (3.11) is exactly reproduced by $\sigma_{tot,ISR}$; only the helicity flip-part of the hard-collinear radiation is not taken into account (which can become important for completely polarized initial particle states).

For $n = 2$, $\sigma_{tot,ISR}$ now also contains diagrams where the last radiated photon is hard, non-collinear, and obeying or not obeying the strong k_\perp ordering.

Leading and higher-orders: summary

We can therefore summarize that $\sigma_{tot,ISR+}$ (5.19) reproduces σ_{tot} (3.11) up to $\mathcal{O}(\alpha)$. For terms $\mathcal{O}(\alpha^2)$ and higher, $\sigma_{tot,ISR+}$ contains all contributions of $\hat{\sigma}_{rest}$ convoluted with f_{ISR} for both incoming particles, i.e. the radiation of infinitely summed up soft or virtual collinear photons and up to 3 hard-collinear photons off all non-photonic and non-collinear virtual contributions of the interference term. The same holds if the last radiated photon is non-collinear and hard, as the contribution is then given by the $2 \rightarrow 3$ part of (5.19). For the emission of a last soft or virtual collinear photon, we carefully have to check the contributions resulting from the subtraction. For $\mathcal{O}(\alpha^2)$, at least one of the photons is always described by the ISR structure function. But when the Born term is convoluted with the ISR function, there are also two-photon contributions described solely by the ISR. We have to distinguish between the cases where (i) the two photons are attached to the same or (ii) to different incoming particles. In case (i), we consider the three terms (cf. Eq. (5.13))

$$\mathcal{O}(\alpha^2)_{ISR} - \mathcal{O}(\alpha)_{ISR} \mathcal{O}(\alpha)_{ISR}^{\text{soft}} + \mathcal{O}(\alpha)_{ISR} \mathcal{O}(\alpha)_{\text{soft}}. \quad (5.20)$$

The first term contains all pairs of collinear photons from the ISR, k_\perp -ordered; the last term contains a first photon from ISR and a second one from the soft-photon factor or the interference term. The term in the middle is the subtraction to avoid double-counting of soft photons. Here both photons are from the ISR, the first one with arbitrary energy, the second one real soft or virtual.

If the second of the considered photons is real soft or virtual, and both are k_\perp -ordered, then there is an exact cancellation between the first two terms. For non k_\perp -ordered photons, the first term gives no contribution, and there is a cancellation between the second and third term, which results in a difference between the soft approximation/interference term contribution expression and the ISR leading logarithmic approximation term given by $\Delta F^{(1)}$ (5.17).

In the case (ii), we write the terms schematically as (cf. Eq. (5.14))

$$\mathcal{O}(\alpha)_{1,ISR} \mathcal{O}(\alpha)_{2,ISR} + \mathcal{O}(\alpha)_{1,ISR} \left(\mathcal{O}(\alpha)_{2,\text{soft}} - \mathcal{O}(\alpha)_{2,ISR}^{\text{soft}} \right) + \left(\mathcal{O}(\alpha)_{1,\text{soft}} - \mathcal{O}(\alpha)_{1,ISR}^{\text{soft}} \right) \mathcal{O}(\alpha)_{2,ISR}.$$

Since there are always two different structure functions involved, k_\perp -ordering is absent, and after a cancellation of soft terms one is left with

$$\Delta F^{(1)}(x_1) \mathcal{O}(\alpha)_{2,ISR} + \mathcal{O}(\alpha)_{1,ISR} \Delta F^{(1)}(x_2) + \mathcal{O}(\alpha)_{1,ISR} \mathcal{O}(\alpha)_{2,ISR},$$

which is up to the missing terms $\Delta F^{(1)}(x_1) \Delta F^{(1)}(x_2)$ equivalent to a soft approximation/interference term description for both legs.

Remark: Soft approximation for matrix elements

In the soft approximation as well as the exponentiation in structure functions, it is assumed that

$$\mathcal{M}(x \geq x_0) \approx \mathcal{M}(x = 1), \quad \sigma(x \geq x_0) \approx \sigma(x = 1) \quad (5.21)$$

and therefore (cf. Eq. (5.5))

$$\int_{x_0}^1 dx f_{ISR}(x) \sigma(x, s) \approx \left(\int_{x_0}^1 dx f_{ISR}(x) \right) \sigma(s) = (1 + F^{(1)}) \sigma(s) + \mathcal{O}(\eta^2) \quad (5.22)$$

for the exponentiation; f_{soft} is derived similarly. This holds true up to errors proportional to $\int_{x_0}^1 dx (\partial\sigma/\partial x)_{x=1} f_{ISR}(x) (1-x)$. Some of these contributions, however, are accounted for in the actual WHIZARD implementation of the resummation method; cf. Section 5.3.

To take them into account, we have to substitute $f_{soft}\sigma(s')$ by

$$f_{soft}\sigma(s') + \left(\int_{x_0}^1 f_{ISR}(x) \sigma(x, s') \right)_{\mathcal{O}(\alpha)} - f_{soft,ISR}\sigma(s') \quad (5.23)$$

for any s' in all expressions. The last two terms only cancel up to $\mathcal{O}(\frac{\partial\sigma}{\partial x}|_{x=1} \Delta x)$. Equally, $F^{(l)}$ should be read as

$$F^{(l)} \sigma(s) \equiv \left(\int_{x_0}^1 f_{ISR}(x) \sigma(x, s) \right)_{\mathcal{O}(\alpha^l)} \quad (5.24)$$

for all higher-order terms.

5.3 Implementation in WHIZARD

The implementation of $\sigma_{tot,ISR+}$ in the Monte Carlo event generator WHIZARD is similar to the implementation of the fixed $\mathcal{O}(\alpha)$ correction described in Section 4.3. We use f_{ISR} (F.14) as a user-defined structure function for each incoming beam with the scale $Q = p_0 \cos \theta$ such that only collinear photons are described (cf. Section F.2.3). We then integrate over the x_1, x_2 dependent effective matrix element $\widetilde{\mathcal{M}}_{eff}$ (5.1) according to Eq. (5.2). Note that, in contrast to the fixed order method, there is no (x_1, x_2) phase space slicing involved. Therefore, in the integration over the f_{ISR} soft region, the x -dependence of the matrix element is actually taken into account, so that in the code implementation additional contributions as given in (5.23) and (5.24) appear. Note, however, that f_{soft} (3.6) in $\widetilde{\mathcal{M}}_{eff}$ still sets $x = 1$ throughout the soft region. The effects of this can be seen in the ΔE_γ dependence of $\sigma_{tot,ISR(+)}$ as discussed in Chapter 6.

The $2 \rightarrow 3$ part of $\sigma_{tot,ISR+}$,

$$\int dx_1 f_{ISR}(x_1; \Delta\theta_\gamma, \frac{m_e^2}{s}) \int dx_2 f_{ISR}(x_2; \Delta\theta_\gamma, \frac{m_e^2}{s}) \times \int_{\Delta E_\gamma, \Delta\theta_\gamma} d\Gamma_3 |\mathcal{M}_{2 \rightarrow 3}(\hat{s})|^2$$

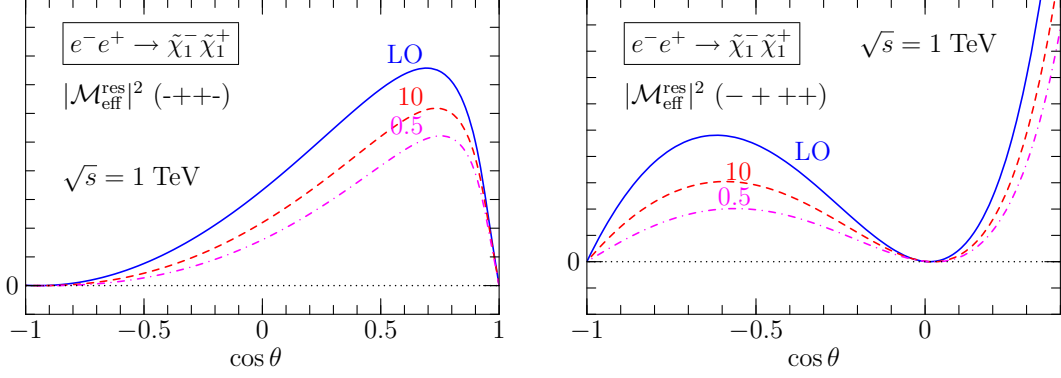


Figure 5.3: Effective squared matrix element (arbitrary units) with the one-photon ISR part subtracted, for $e^-e^+ \rightarrow \tilde{\chi}_1^- \tilde{\chi}_1^+$ as a function of the polar scattering angle θ at $\sqrt{s} = 1$ TeV. Left figure: Helicity combination $- + + -$; right figure: $- + + +$. Solid line: Born term; dashed: including virtual and soft contributions for $\Delta E_\gamma = 10$ GeV; dotted: same with $\Delta E_\gamma = 0.5$ GeV. The collinear cutoff is fixed at $\Delta\theta_\gamma = 1^\circ$.

is again generated in a separate run of WHIZARD, applying the soft and collinear cuts ΔE_γ , $\Delta\theta_\gamma$ and convoluted with the structure function f_{ISR} for each incoming beam. The scale is set to $Q = p_0 \cos \theta$ as given above. As in the fixed order method, both runs can be combined for integration and event simulation.

5.4 Difference to fixed order method

5.4.1 Negative weights

The resummation approach does eliminate the problem of negative weights: shifting the energy cutoff below the experimental resolution, such that photons are explicitly generated whenever they can be resolved, the subtracted effective squared $2 \rightarrow 2$ matrix element is still positive semidefinite in the whole phase space. After resummation, the only potentially remaining source of negative event weights is the soft-noncollinear region. Negative weights are absent as long as

$$\mathcal{O}(1) \times \frac{\alpha}{\pi} \ln \frac{(\Delta E_\gamma)^2}{s} \ln(\Delta\theta_\gamma) < 1,$$

where the $\mathcal{O}(1)$ prefactor depends on the specific process. For the cutoff and parameter ranges we are considering here, this condition is fulfilled.

Figure 5.3 shows $|\widetilde{\mathcal{M}}_{eff}|^2$ for two different ΔE_γ cuts. We see that the positivity condition is fulfilled. Since neither the inclusion of the ISR structure function nor the addition of the $2 \rightarrow 3$ part introduces further sources of negative weights, unweighting of generated events is now possible, so this method allows for realistic simulation at NLO.

5.4.2 Higher-order photon contributions

As the fixed order method discussed in Chapter 4 does not include higher-order contributions, the resummation method differs in all higher-order terms discussed in Section 5.2. Below, we give the analytic expression for these differences. In addition, we discuss the difference between the resummation method and the inclusion of ISR as discussed in Section 3.7. Throughout the section, we neglect the contributions coming from the respective $2 \rightarrow 3$ integrations, i.e. processes where the last photon is hard and non-collinear. Here, differences between the methods are obvious from Section 5.2.

Radiation off one particle

In this case, we again consider $\widetilde{\mathcal{M}}_{eff}^{(1)}$ (5.3) and $\sigma_{v+s,ISR}^{(1)}$ (5.4), i.e. only subtract one factor of $f_{soft,ISR}$. We consider the soft and the hard region separately and again assume that, in the matrix element, x can be set to 1 in the soft region (5.21).

In the soft sector, we obtain

$$\begin{aligned} \Delta_{\text{soft}} &= \int_{x_0}^1 dx f_{\text{ISR}}(x) |\widetilde{\mathcal{M}}_{\text{eff}}^{(1)}|^2(x, s) - (1 + f_{\text{soft}}) |\mathcal{M}_{\text{Born}}|^2(s) - 2 \text{Re}(\mathcal{M}_{\text{Born}} \mathcal{M}_{1\text{-loop}}^*)(s) \\ &= \left(f_{\text{soft,ISR}} (f_{\text{soft}} - f_{\text{soft,ISR}}) + F^{(2)} \right) |\mathcal{M}_{\text{Born}}|^2(s) + 2 \text{Re}(\mathcal{M}_{\text{Born}} \mathcal{M}_{1\text{-loop}}^*)(s) f_{\text{soft,ISR}} \\ &\quad + \mathcal{O}(\alpha^3). \end{aligned} \tag{5.25}$$

In the hard sector, we obtain

$$\begin{aligned} \Delta_{\text{hard}} &= \int_{x_0}^1 dx f_{\text{ISR}}(x) |\widetilde{\mathcal{M}}_{\text{eff}}^{(1)}|^2(x, s) - \sum_{\sigma=\pm} \int_0^{x_0} dx f^{\sigma}(x) |\mathcal{M}_{\text{Born}}^{\sigma}|^2(x, s) \\ &= \int_0^{x_0} dx \left\{ ((f^+(x) (f_{\text{soft}} - f_{\text{soft,ISR}}) + F_2(x)) |\mathcal{M}_{\text{Born}}|^2(x, s) \right. \\ &\quad \left. + f^+(x) 2 \text{Re}(\mathcal{M}_{\text{Born}} \mathcal{M}_{1\text{-loop}}^*)(x, s)) \right\} - \int_0^{x_0} dx f^-(x) |\mathcal{M}_{\text{Born}}^-|^2(x, s) \\ &\quad + \mathcal{O}(\alpha^3). \end{aligned} \tag{5.26}$$

These results correspond exactly to the $\mathcal{O}(\alpha^2)$ contributions discussed in Section 5.2.

Radiation off two particles

We integrate now over $|\widetilde{\mathcal{M}}_{eff}|^2$ (5.1) according to (5.2).

In the soft-soft sector, we obtain

$$\begin{aligned}
\Delta_{ss} &= \int_{x_0}^1 dx_1 \int_{x_0}^1 dx_2 f_{ISR}(x_1) f_{ISR}(x_2) |\widetilde{\mathcal{M}}_{eff}|^2(x_1, x_2, s) \\
&\quad - (1 + f_{soft} |\mathcal{M}_{Born}|^2(s) - 2 \operatorname{Re}(\mathcal{M}_{Born} \mathcal{M}_{1-loop}^*)(s)) \\
&= \left\{ 2 \left(f_{soft, ISR} (f_{soft} - f_{soft, ISR}) + F^{(2)} \right) - f_{soft, ISR} \right\} |\mathcal{M}_{Born}|^2(s) \\
&\quad + 4 f_{soft, ISR} \operatorname{Re}(\mathcal{M}_{Born} \mathcal{M}_{1-loop}^*)(s) + \mathcal{O}(\alpha^3) \\
&= 2 \Delta_{soft} - f_{soft, ISR}^2 |\mathcal{M}_{Born}|^2(s) + \mathcal{O}(\alpha^3). \tag{5.27}
\end{aligned}$$

In the hard-soft section, we have

$$\begin{aligned}
\Delta_{sh} &= \int_{x_0}^1 dx_1 \int_0^{x_0} dx_2 f_{ISR}(x_1) f_{ISR}(x_2) |\widetilde{\mathcal{M}}_{eff}|^2(x_1, x_2, s) \\
&\quad - \int_0^{x_0} dx_2 \sum_{\sigma=\pm} f^\sigma(x_2) |\mathcal{M}_{Born}^\sigma|^2(x_2, s) \\
&= \int_0^{x_0} dx_2 \left\{ [f^+(x_2) (f_{soft} - 2 f_{soft, ISR}) + F_2(x_2)] |\mathcal{M}_{Born}|^2(x_2, s) \right. \\
&\quad \left. + f^+(x_2) 2 \operatorname{Re}(\mathcal{M}_{Born} \mathcal{M}_{1-loop}^*)(x_2, s) \right\} - \int_0^{x_0} dx_2 f^-(x_2) |\mathcal{M}_{Born}|^2(x_2, s) + \mathcal{O}(\alpha^3) \\
&= \Delta_{hard} + \mathcal{O}(\alpha^3). \tag{5.28}
\end{aligned}$$

In the hard-hard sector,

$$\begin{aligned}
\Delta_{hh} &= \int_0^{x_0} dx_1 \int_0^{x_0} dx_2 f_{ISR}(x_1) f_{ISR}(x_2) |\widetilde{\mathcal{M}}_{eff}|^2(x_1, x_2, s) \\
&= \int_0^{x_0} dx_1 \int_0^{x_0} dx_2 F_1(x_1) F_1(x_2) |\widetilde{\mathcal{M}}_{Born}|^2(x_1, x_2, s) + \mathcal{O}(\alpha^3). \tag{5.29}
\end{aligned}$$

We see that, in general, nearly all second order contributions for the simultaneous photon radiation of e^+ and e^- can already be obtained from the second order terms for only one radiating particle. This only works in the approximation (5.21), as this approximation does not distinguish the emitting particles for soft photons. We will make use of this for a rough higher-order estimation in Section 6.2.2.

Resumming only the Born matrix element

We now consider the difference between $\sigma_{tot, ISR+}$ (5.19) and $\sigma_{tot, ISR(b)}$ (3.16); in the latter, only the Born cross section is convoluted with f_{ISR} . The leading and first order terms, which are already contained in the NLO corrected matrix element, are then subtracted to avoid double counting (cf. Eq. (3.16)). Up to $\mathcal{O}(\alpha)$, $\sigma_{tot, ISR(b)}$ corresponds

to the fixed order result σ_{tot} (3.11). As in the last section, we only consider $\mathcal{O}(\alpha^2)$ contributions.

In the soft-soft region, the second order effects from convoluting the Born cross section are given by

$$(f_{soft,ISR}^2 + 2F^{(2)}) |\mathcal{M}_{Born}|^2(s)$$

and Δ_{ss} (5.27) becomes

$$\begin{aligned} \Delta'_{ss} &= 2 (f_{soft,ISR} (f_{soft} - 2 f_{soft,ISR})) |\mathcal{M}_{Born}|^2(s) + 4 f_{soft,ISR} \text{Re} (M_{\text{Born}} M_{1\text{-loop}}^*)(s) \\ &+ \mathcal{O}(\alpha^3). \end{aligned}$$

In order to understand this expression, we again have to decompose $f_{soft,ISR}$ and f_{soft} into parts radiating from the same or two different particles and include a decomposition as (5.11), obtaining

$$\begin{aligned} 2 (f_{soft,ISR} (f_{soft} - 2 f_{soft,ISR})) &\hat{=} \\ &\left(F^{(1)} \Delta F^{(1)} \right) (x_1) + \left(F^{(1)} \Delta F^{(1)} \right) (x_2) + F^{(1)}(x_1) \Delta F^{(1)}(x_2) + F^{(1)}(x_2) \Delta F^{(1)}(x_1) \end{aligned}$$

This corresponds to the substitution of the $f_{ISR,soft}$ by f_{soft} for the last soft-collinear photons in $\sigma_{tot,ISR+}$ and the substitution of the interference term description for virtual collinear last photons. In addition, $4 f_{soft,ISR} \text{Re} (\mathcal{M}_{\text{Born}} \mathcal{M}_{1\text{-loop}}^*)(s)$ gives all contributions of $\hat{\sigma}_{rest}$, i.e. virtual contributions untouched by the subtraction, combined with the radiation of a soft-collinear photon from either incoming particle.

In the hard-soft region, the $\mathcal{O}(\alpha^2)$ contributions to $\sigma_{tot,ISR(b)}$ are given by

$$\int_0^{x_0} dx_2 [f^+(x_2) f_{soft,ISR} + F_2(x_2)] |\mathcal{M}_{Born}|^2(x_2, s)$$

and Δ_{sh} (5.28) becomes

$$\begin{aligned} \Delta'_{sh} &= \int_0^{x_0} dx_2 f^+(x_2) (f_{soft} - 2 f_{soft,ISR}) |\mathcal{M}_{Born}|^2(x_2, s) \\ &+ f^+(x_2) 2 \text{Re} (M_{\text{Born}} M_{1\text{-loop}}^*)(x_2, s) \} - \int_0^{x_0} dx_2 f^-(x_2) |\mathcal{M}_{Born}|^2(x_2, s) + \mathcal{O}(\alpha^3). \end{aligned}$$

The hard-soft part of this is equivalent to

$$F_2(x_2) \left((\Delta F^{(1)}(x_1) + \Delta F^{(1)}(x_2)) \right).$$

This corresponds again to the substitution of the $f_{ISR,soft}$ by f_{soft} for the last soft-collinear photon (virtual last photon and interference term).

In the hard-hard sector, the contribution to $\sigma_{tot,ISR(b)}$ up to $\mathcal{O}(\alpha^2)$ is given by Δ_{hh} (5.29).

In summary, we can say that the difference between the $2 \rightarrow 2$ integration regions of $\sigma_{tot,ISR(+)}$ and $\sigma_{tot,ISR(b)}$ are the substitution of the $f_{ISR,soft}$ by f_{soft} for soft-collinear and the interference term description for virtual collinear photons in $\sigma_{tot,ISR(+)}$. In addition, terms of the form

$$\int_0^1 dx_1 \int_0^1 dx_2 f_{ISR}(x_1) f_{ISR}(x_2) \hat{\sigma}_{rest}(x_1, x_2, s) - \hat{\sigma}_{rest}(s) \quad (5.30)$$

are included, where $\hat{\sigma}_{rest}$ is defined as in Eq. (5.16). These are the dominant contributions, as all other differences between $\sigma_{tot,ISR}$ and $\sigma_{tot,ISR(b)}$ are proportional to $\Delta F^{(1)}$ and therefore subleading. The $\mathcal{O}(\alpha^2)$ contribution to (5.30) is given by

$$2 \left(\int_0^{x_0} dx f_h^+(x) \hat{\sigma}_{rest}(x, s) + f_{ISR,soft} \hat{\sigma}_{rest}(s) \right). \quad (5.31)$$

For $e^+e^- \rightarrow \tilde{\chi}_1^+ \tilde{\chi}_1^-$, these contributions are in the % regime; cf. Section 6.2. The sign of the correction term depends on the specific process (note that $f_{soft,ISR} < 0$, while $f^+(x) \geq 0$).

6 Results

6.1 Cut dependencies

6.1.1 Energy cutoff dependence

In Fig. 6.1 we compare the numerical results obtained using the semianalytic fixed-order calculation with our Monte-Carlo integration in the fixed-order and in the resummation schemes, respectively. Throughout this section, we set the process energy to $\sqrt{s} = 1$ TeV and refer to the SUSY parameter point SPS1a'. All $2 \rightarrow 2$ and $2 \rightarrow 3$ contributions are included, so the results would be cutoff-independent if there were no approximations involved. For the discussion of the ΔE_γ dependence of σ_{tot} , we refer to Section 4.6.1.

The fully resummed result $\sigma_{tot,ISR+}$ shows an increase of about 5‰ of the total cross section with respect to the fixed-order result which stays roughly constant until $\Delta E_\gamma > 10$ GeV where the soft approximation breaks down. This increase is a real effect; it is due to higher-order photon radiation that is absent from the fixed-order calculation.

We now discuss the reshuffling of contributions in the overlap region of the soft-collinear and hard-collinear (ISR) descriptions for second order contributions. If we raise ΔE_γ , photons that have been hard now become soft. In the case of photons radiated from two different external particles, a soft-collinear photon which has been described by f_{ISR} is now described by f_{soft} according to the soft approximation (3.6). For the case of two photons radiated off the same particle, we have to distinguish whether the two photons are k_\perp -ordered or not. If they are, the description again changes from f_{ISR} to f_{soft} . If there is no k_\perp -ordering, either the first or the second radiated photon can change from hard to soft (or both). For the first photon, it is a smooth transition where only the last two terms of Eq. (5.20) are involved. If the second photon changes to soft, new contributions of the form $\Delta F^{(1)}$ (5.17) appear.

The effects of reshuffling the photon descriptions are, up to $\Delta E_\gamma = 10$ GeV, smaller than 2‰. If we only consider the dominant k_\perp contributions, it would be preferable to raise ΔE_γ as long as the $\mathcal{O}(\alpha)$ effects from the soft approximation are negligible. In our case, these effects reach the 2‰ level for $\Delta E_\gamma = 1$ GeV (cf. Section 4.6.1).

Finally, we compare the difference between $\sigma_{tot,ISR}$ and $\sigma_{tot,ISR+}$. For the latter, the emission of a last hard non-collinear photon is also combined with multiple photon radiation described by f_{ISR} . We observe that for $\Delta E_\gamma > 1$ GeV these higher-order contributions are caught by ISR resummation of the $2 \rightarrow 2$ part. For a lower cutoff, they have to be explicitly included in the $2 \rightarrow 3$ part.

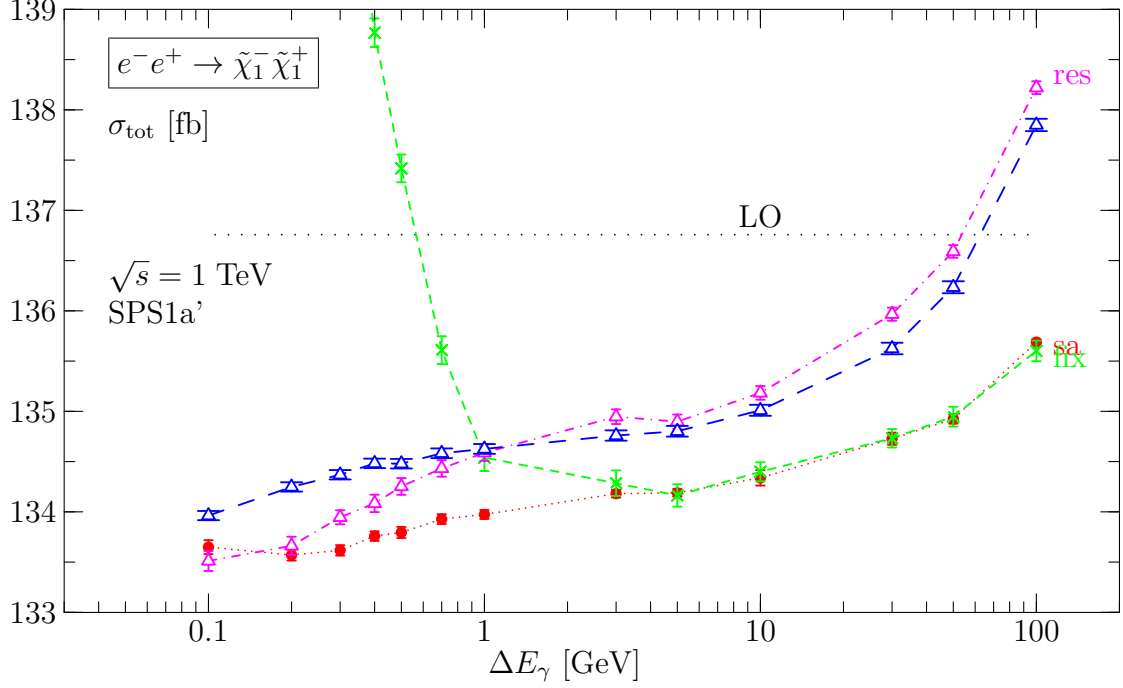


Figure 6.1: Total cross section dependence on the energy cutoff ΔE_γ using different calculational methods: ‘sa’ (red, dotted) = fixed-order semianalytic result using **FeynArts/FormCalc**; ‘fix’ (green, dashed) = fixed-order Monte-Carlo result σ_{tot} (3.11) using **WHIZARD**; ‘res’ (blue, long-dashed) = ISR-resummed Monte-Carlo result $\sigma_{tot,ISR+}$ (5.19) using **WHIZARD**; (magenta, dash-dots) = same but resummation applied only to the $2 \rightarrow 2$ part (5.18). Statistical Monte-Carlo integration errors are shown. For the Monte-Carlo results, the collinear cutoff has been fixed to $\Delta\theta_\gamma = 1^\circ$. The Born cross section is indicated by the dotted horizontal line.

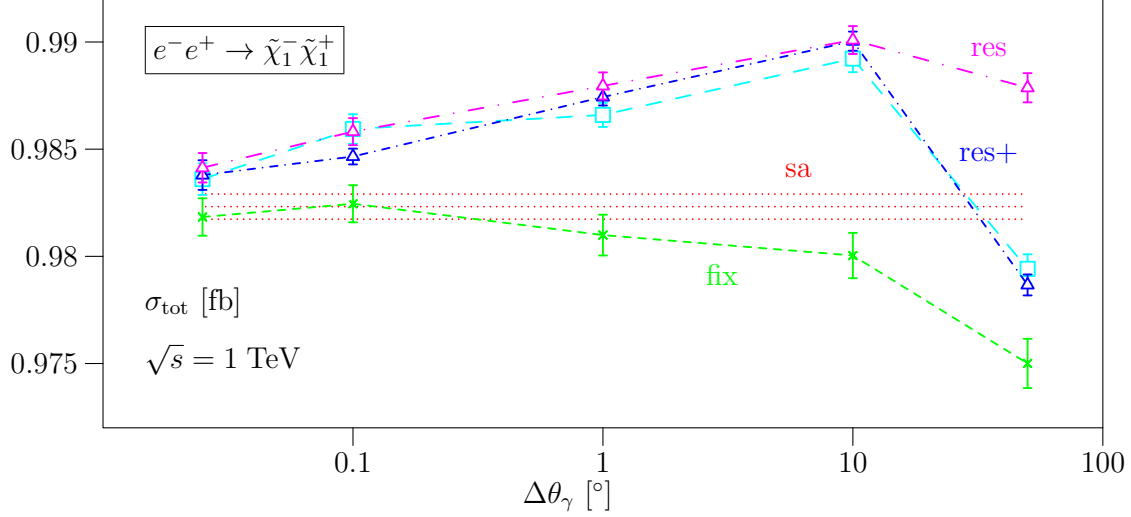


Figure 6.2: Relative dependence of the cross section on the collinear cutoff $\Delta\theta_\gamma$ using different calculational methods: sa (red, dotted) = fixed-order semianalytic result using **FeynArts**/**FormCalc** with respective integration errors; fix (green, dashed) = fixed-order Monte-Carlo result σ_{tot} (3.11) using **WHIZARD**; res+ (blue, dash-dots) = third-order completely resummed Monte-Carlo result $\sigma_{tot,ISR+}$ (5.19) using **WHIZARD**; (magenta, long dash-dotted) = third-order resummed Monte-Carlo result $\sigma_{tot,ISR}$ (5.18) using **WHIZARD**; Statistical Monte-Carlo integration errors are shown. The soft cutoff has been fixed to $\Delta E_\gamma = 10$ GeV. All results are scaled to $\sigma_{Born} = 1$.

6.1.2 Collinear cutoff dependence

In $\mathcal{O}(\alpha)$, the collinear angle dependence tests the validity regime of the collinear approximation used in Eq. (3.9). This was already discussed in Section 4.6.1, where we found the approximation is valid for $\Delta\theta_\gamma \leq 1^\circ$. The difference between the fixed order result σ_{tot} and the fully resummed result $\sigma_{ISR,+}$ are again the higher-order contributions discussed in Section 5.2.

Figure 6.2 shows the higher-order effects associated with raising the collinear cutoff $\Delta\theta_\gamma$. For $\Delta\theta_\gamma = 0.1^\circ$ (1°), the difference between σ_{tot} and $\sigma_{tot,ISR+}$ is 4‰ (7‰). Raising $\Delta\theta_\gamma$ shuffles photons from a non-collinear to a collinear description. First, this opens up phase space for all photons described by f_{ISR} . For the radiation off the same particle, raising the collinear cutoff also improves the description of k_\perp ordered photons if the sum of their transverse momenta is now lower than the new transverse cutoff associated with $\Delta\theta_\gamma$. They are contained in the second order ISR contributions $F^{(2)}$, F_2 and switch from a description $\propto \Delta F^{(1)}$ to terms of the form (5.20), where the second soft (virtual) collinear photon is given by f_{soft} (the interference term).

Unfortunately, raising the collinear cutoff also enhances the phase space of contributions $\propto \Delta F^{(1)}$ which can appear when multiple (collinear) photons which are not k_\perp ordered

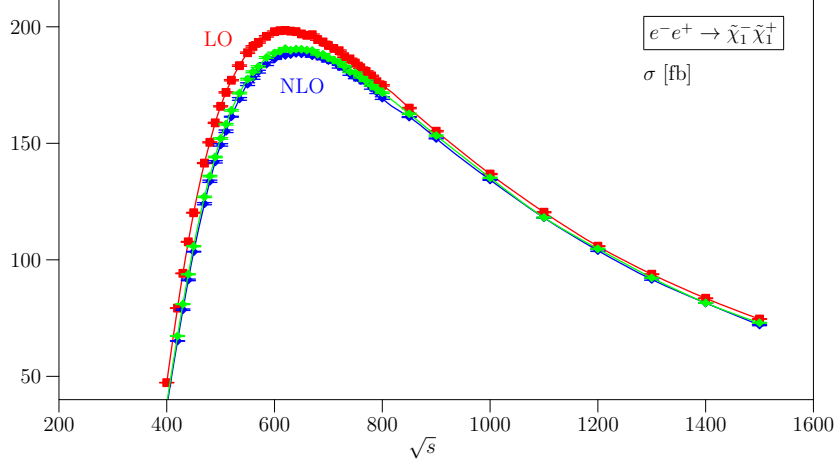


Figure 6.3: σ_{Born} , σ_{tot} , $\sigma_{ISR,+}$ as a function of \sqrt{s} . All results in fb

are emitted from the same particle; cf. Section 5.2. Similarly, raising the cutoff can worsen the description for photons that lie in the soft regime near the limit of the soft-collinear regime and change into the latter. For non- k_\perp -ordered photons, the description switches from f_{soft} (interference term) to contributions $\propto \Delta F^{(1)}$. However, these effects are subleading.

For the leading-log contributions, raising the cutoffs gives a better description as long as the collinear approximation is valid. From Figure 6.2, we see that this is a 3–4 % effect. The difference between $\sigma_{tot,ISR}$ and $\sigma_{tot,ISR+}$ is similarly small (about 1 %) in the validity regime of the soft approximation. The size of these contributions therefore mainly depends on the choice of the soft cut ΔE_γ (cf. Section 6.1.1). For the $\Delta E_\gamma = 10$ GeV as above, all leading contributions are already summed up in the ISR part of the $2 \rightarrow 2$ integration.

6.2 Total cross section

6.2.1 Leading and first order results

In leading and next-to-leading order, the fixed order result σ_{tot} (3.11) and the resummation result $\sigma_{tot,ISR(+)}$ (5.18), (5.19) agree. All differences between the results are therefore due to higher-order effects. For the discussion of first order behavior of the total cross section, we therefore refer to the Sections 3.6 and 4.6.

In Figures 6.3 and 6.4 we display the LO result together with the NLO results for the fixed-order and resummed approach. Near the cross-section maximum, the relative correction in the resummed approach is about –5.5 %, approaching –2 % at $\sqrt{s} = 1$ TeV. Near threshold and at asymptotic energies, the relative NLO correction gets up to –20 %.

A short remark concerns the neglected helicity-flipping terms $f^-(x)$ (F.5) in the hard part of f_{ISR} which are in principle $\mathcal{O}(\alpha)$, but do not contain collinear logarithms; cf.

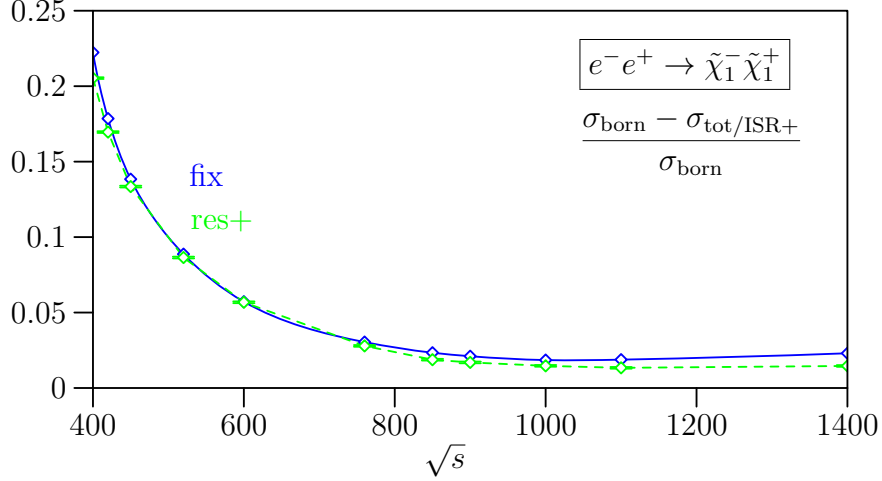


Figure 6.4: relative difference of σ_{tot} (and σ_{ISR+}) to σ_{Born} , resulting from NLO (NLO and higher-order) corrections

Section F.3. Figure 6.5 shows the relative magnitude of these terms for unpolarized initial particles with respect to the Born cross section. The contribution is in the per mille regime.

6.2.2 Higher-order effects

Figure 6.6 shows the differences between $\sigma_{tot,ISR}$, $\sigma_{tot,ISR+}$, $\sigma_{tot,ISR(b)}$ and the fixed order result σ_{tot} (3.11). $\sigma_{tot,ISR}$, $\sigma_{tot,ISR+}$, and $\sigma_{tot,ISR(b)}$ all contain different kinds of higher-order contributions (cf. Section 5.4.2), which we will now consider in more detail. The largest effects clearly result from the higher-order contributions in the transition from the fixed order result σ_{tot} (3.11) to the resummation result $\sigma_{tot,ISR}$ (5.18) discussed in Section 5.4.2, i.e. the inclusion of multiple photon radiation off the Born as well as the interference term in the $2 \rightarrow 2$ integration region. They are up to a few percent for small center of mass energies. Including the convoluting of the $2 \rightarrow 3$ integration region of $\sigma_{tot,ISR}$ with f_{ISR} , i.e. including also diagrams where the last radiated photon is hard and non-collinear as in $\sigma_{tot,ISR+}$ (5.19), significantly reduces these effects. These extra terms cannot be neglected. However, it was shown in Section 6.1 that the magnitude of these corrections strongly depends on the soft cut ΔE_γ . If the energy cutoff is high enough, the dominant contributions are included in the convolution of the effective matrix element in the $2 \rightarrow 2$ region with f_{ISR} ; cf. Figure 6.1. Apparently, the cut value $\Delta E_\gamma/\sqrt{s} = 5 \cdot 10^{-3}$ chosen for Figure 6.6 is not sufficiently high for low \sqrt{s} values to include all dominant contributions.

Finally, we see that the difference between $\sigma_{tot,ISR(b)}$ and $\sigma_{tot,ISR+}$, which is mainly given by the terms $\propto \int \hat{\sigma}_{rest}$ (5.30), is similarly in the % range. Shuffling photon descriptions, in contrast, is a ‰ effect; cf. Section 6.1. The change of ISR order in the resummation method only concerns the hard regime and clearly shows no significant effect.

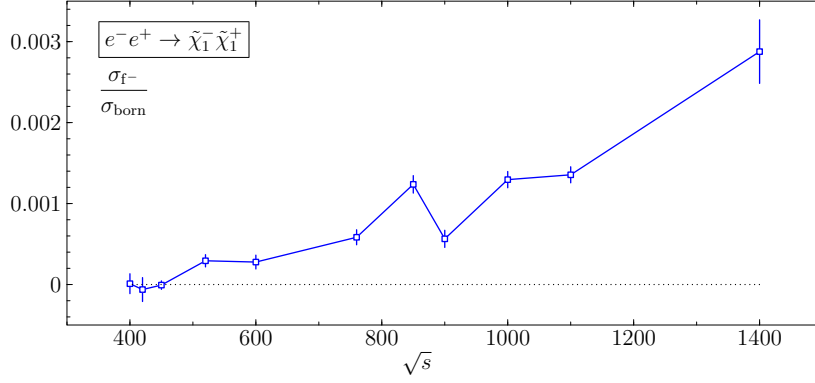


Figure 6.5: Contribution of the part of σ_{tot} resulting from the helicity-flipping part f^- (F.5) of the hard-collinear approximation with respect to σ_{Born} . 1σ errors from WHIZARD integration are shown

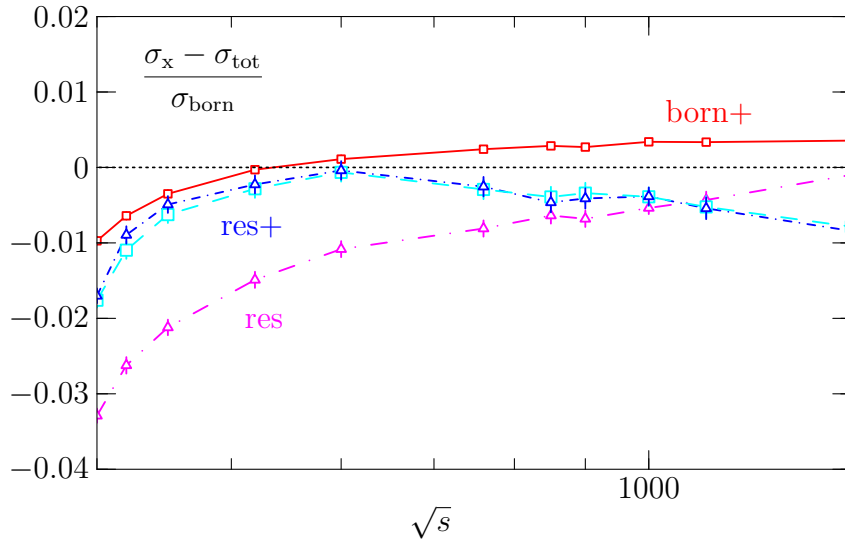


Figure 6.6: Relative higher-order effects for different methods: (magenta, long dash dot-dotted) = $\sigma_{tot,ISR}$ (5.18), (blue/ cyan and dash-dotted/ dashed) = $\sigma_{tot,ISR+}$ (5.19), and (red, solid) = $\sigma_{tot,ISR(b)}$ (3.16) vs σ_{tot} (3.11). $\Delta\theta_\gamma = 1^\circ$, $\Delta E_\gamma/\sqrt{s} = 5 \cdot 10^{-3}$.

Third (and higher) order estimation

Eqs. (5.27), (5.28), and (5.29), show that we can in principle do a $\mathcal{O}(\alpha^3)$ and higher-order estimation when using the results from radiation off one particle Δ_s (5.25), Δ_h (5.26) to predict the $\mathcal{O}(\alpha^2)$ effects for the radiation off two particles. Analytically, we have

$$\Delta_{ss} + 2\Delta_{sh} = 2(\Delta_s + \Delta_h) - f_{soft,ISR}^2 |\mathcal{M}_{Born}|^2 + \mathcal{O}(\alpha^3). \quad (6.1)$$

Deviations from the “estimate” on the right hand side can give us an idea of the order of magnitude of the higher-order corrections. Note, however, that numerically the calculation of these terms are very involved and limited by computer precision; similarly, errors resulting from setting $x = 1$ in the matrix element the soft regime are neglected. This estimate also does not predict the actual sign of the higher-order corrections. It tests the numerical difference between expressions which are analytically equivalent up to $\mathcal{O}(\alpha^2)$.

Figure 6.7 shows the estimated and actual $\mathcal{O}(\alpha^2)$ contributions, here for the convolution of $|\mathcal{M}_{Born}|^2$ as in $\sigma_{tot,ISR(b)}$ (3.16) only where similar considerations can be done. We see that the deviation from the prediction is already in the 0.5 – 1% regime. Note that for a comparison we also added points where

$$\Delta_{hh}^{Born} = \int_0^{x_0} dx_1 \int_0^{x_0} dx_2 f_{ISR}(x_1) f_{ISR}(x_2) |\mathcal{M}_{Born}|^2$$

was replaced by Δ_{hh} (5.29). These two expressions differ in third and higher-order terms involving the radiation of two and more hard-collinear photons off the virtual (+ soft-collinear) NLO term. They are of similar magnitude.

Figure 6.8 shows the magnitude of the $\mathcal{O}(\alpha^3)$ errors in Eq. (6.1) relative to the Born cross section and the equivalent contribution from $\sigma_{tot,ISR(b)}$ in Figure 6.7. We see that, for $\sqrt{s} \leq 600$ GeV, the third order effects are of similar order for both methods. For larger cm energies, however, the estimate from $\sigma_{tot,ISR}$ deviates from the Born-related estimate and goes up to nearly 2%. This is related to second and higher-order effects resulting from the convoluting of the virtual part with f_{ISR} for both beams. The importance of these contributions was already shown in $\mathcal{O}(\alpha^2)$ in Figure 6.6 as well as the difference between Δ_{hh}^{Born} and Δ_{hh} in Figure 6.7. Summarizing, we can say that according to the estimation done in Eq. (6.1), even third and higher-orders are important if the ILC precision of a few ‰ is reached.

6.3 Event Generation

As for the total cross section, events generated using \mathcal{M}_{eff} (4.4) and $\widetilde{\mathcal{M}}_{eff}$ (5.1) are equivalent up to and including $\mathcal{O}(\alpha)$. For the discussion of the NLO effects, we therefore refer to Section 4.6. Differences between the two methods originate from higher-order contributions.

Figure 6.9 shows the binned distribution of the chargino production angle as in Figures 4.8 and 4.9, together with the events generated using the resummation method. For a

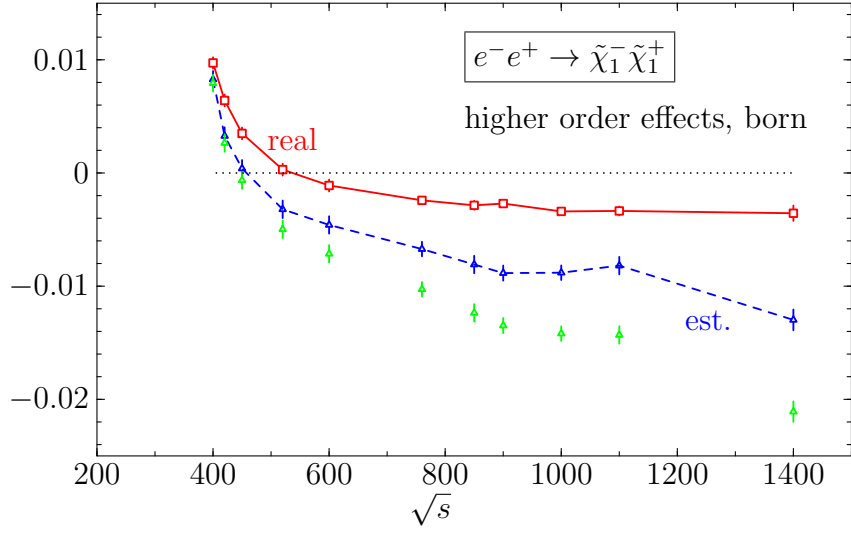


Figure 6.7: Second and higher-order effects; estimate from 1 photon (blue, dashed) compared to actual result (red, solid) . Born only

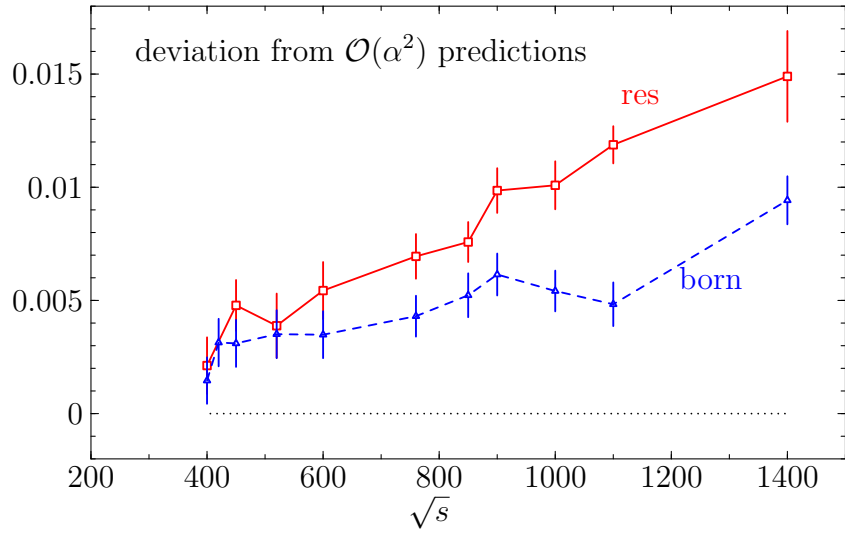


Figure 6.8: third order effects from (6.1), Born (blue, dashed) only vs completely convoluted (red, solid) version

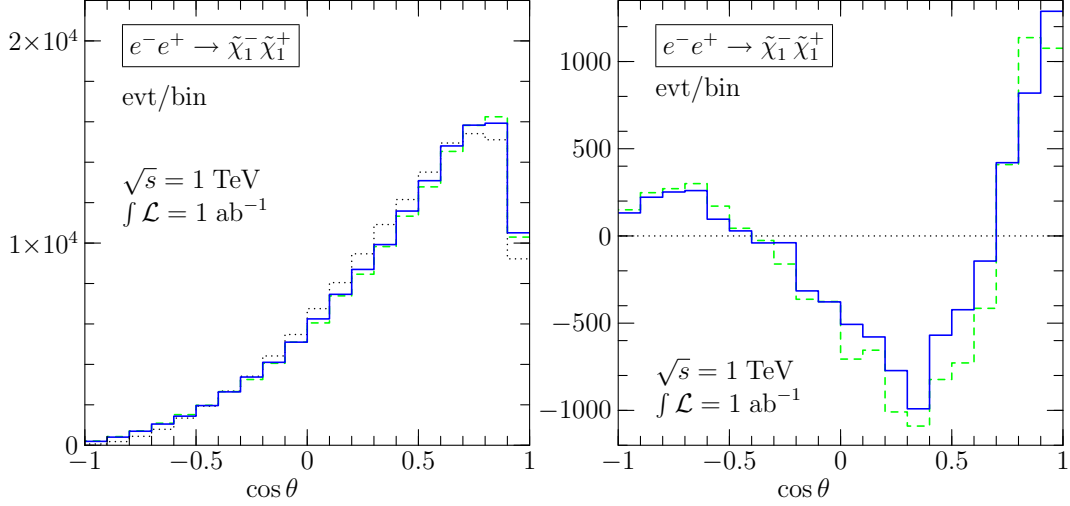


Figure 6.9: Polar scattering angle distribution for an integrated luminosity of 1 ab^{-1} at $\sqrt{s} = 1 \text{ TeV}$. Left: total number of events per bin; right: difference w.r.t. the Born distribution. LO (black, dotted) = Born cross section without ISR; fix (green, dashed) = fixed-order approach; res (blue, full) = resummation approach. Cutoffs: $\Delta E_\gamma = 3 \text{ GeV}$ and $\Delta\theta_\gamma = 1^\circ$.

kinematically more accurate description of the NLO contributions, decreasing the cutoffs would be preferred, but choosing lower values would invalidate the fixed-order approach for the comparison.

Figures 6.10 and 6.11 show the difference in the number of events between the angular distribution for fixed order and the resummation method as well as a 1σ effect from the Born cross section. The higher-order effects are not as striking. They are visible mostly in the central-to-forward region. For $\cos\theta \geq 0.5$, they are statistically significant. Going to higher luminosities would of course improve the significance for even lower values of $\cos\theta$. From Figure 6.11, we can see that the integration over $\cos\theta$ reproduces the $\sim 6\%$ effect shown in Figure 6.1 (compare also to Figure 6.6 with $\Delta E_\gamma = 5 \text{ GeV}$; from Figure 6.1, we know that the difference between the resummation and the fixed order result stays roughly the same up to $\Delta E_\gamma = 10 \text{ GeV}$).

Finally, we can test the effect of lowering ΔE_γ such that we get into the critical soft cut region discussed in Section 4.5. Figure 6.12 shows the difference between the two methods of adding photons for $\Delta E_\gamma = 0.5 \text{ GeV}$, $\Delta\theta = 0.5^\circ$. We clearly see the effects of setting the negative effective squared matrix elements to zero where it becomes negative. The behaviour of $|\mathcal{M}_{eff}|^2$ for the (sub)dominant helicity combination was shown in Figures 4.2 and 4.3. For $\cos\theta > 0$, the differences between the resummation method and the fixed-order method have a behaviour as in the higher energy cut case, cf. Figure 6.10. They are smaller in magnitude. As in this region of phase space, $|\mathcal{M}_{eff}|^2 \geq 0$ for the

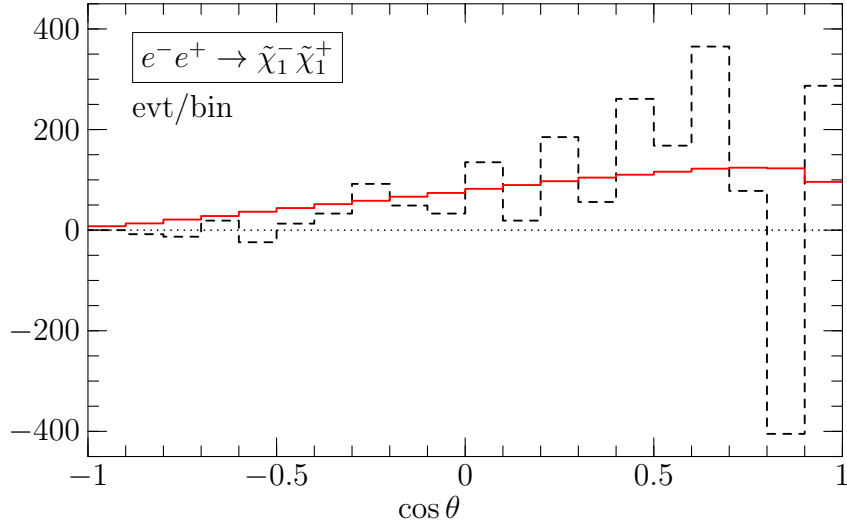


Figure 6.10: Polar scattering angle dependence of difference between events resulting from completely resummed and fixed order method: $N_{res} - N_{ex}$. Standard deviation from Born (solid, red) is shown

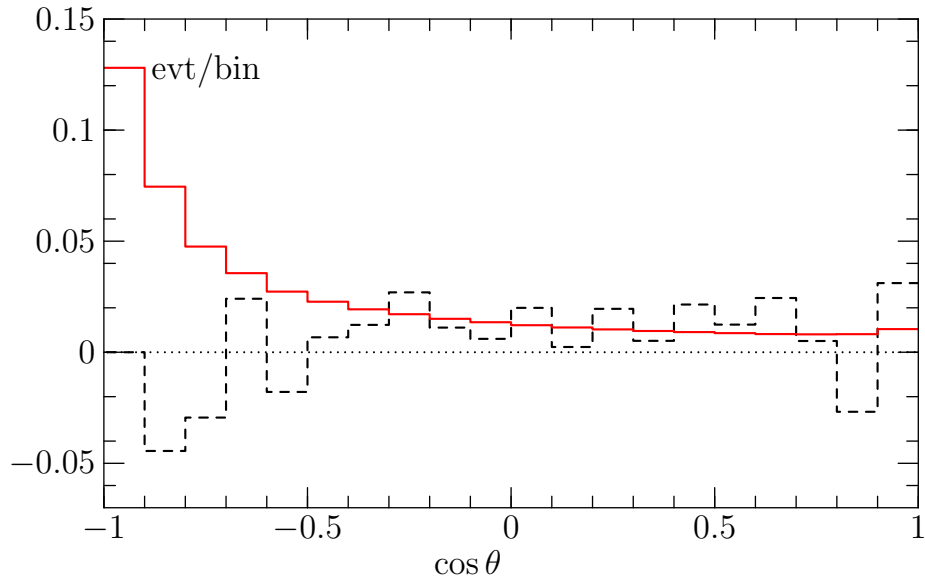


Figure 6.11: Same as Figure 6.10, normalized to Born results

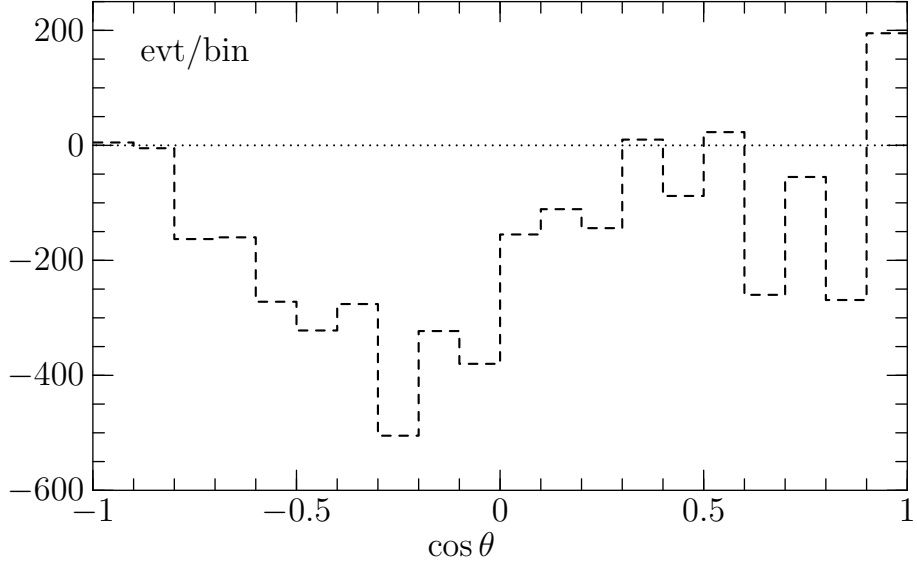


Figure 6.12: Difference between complete resummation and fixed order method for $\sqrt{s} = 1 \text{ TeV}$ with $\Delta E_\gamma = 0.5 \text{ GeV}$, $\Delta\theta_\gamma = 0.5^\circ$. With the energy cut in the critical region (cf. Section 4.5), effects of setting $|\mathcal{M}_{eff}|^2$ to zero become apparent for $\cos \theta < 0$.

dominant helicity combination, this difference can be attributed to the lower angular cuts which decrease the difference between σ_{tot} and $\sigma_{tot,ISR+}$ (cf. Section 6.1.2).

7 Summary and Outlook

As an e^+e^- collider with a cm energy of 500 GeV (1 TeV), the ILC will provide a clean environment for precision tests of physics in and beyond the Standard Model. In the chargino and neutralino sector of the MSSM, a small number of measurements already determines the supersymmetric parameters at the electroweak scale. The parameters at the SUSY breaking scale can be derived from renormalization group equations and eventually give information about the SUSY breaking mechanism. The clean experimental environment of the ILC leads to small experimental errors which calls for matching accuracy of theoretical NLO and higher-order predictions. These effects need to be included in Monte Carlo event generators, the simulation tools that are actually used in the experimental analyses.

Inclusion of NLO corrections in WHIZARD

We have presented results obtained from implementing the NLO corrections for chargino pair production at the ILC into the Monte-Carlo event generator **WHIZARD**. On top of the genuine SUSY/electroweak corrections, we have considered several approaches of including photon radiation, where a strict fixed-order approach allows for comparison and consistency checks with published semianalytic results in the literature. However, this approach suffers from negative event weights in certain points of phase space. Extending approaches used in Monte Carlo generators for LEP analyses, we developed a method for including virtual-, soft- and hard-collinear resummation of photon radiation. It not just improves the numerical result, but actually is more straightforward to implement and does not suffer from negative event weights in or near the experimentally accessible part of phase space. The generator accounts for all yet known higher-order effects, allows for small cutoffs, and explicitly generates photons where they can be resolved experimentally. In addition, the generated event samples allow for quick analyses of NLO effects in angular distributions, correlations, and other quantities. We also interfaced **WHIZARD** with a (modified) **FormCalc** code which in principle allows for the inclusion of any other (NLO) process.

Magnitude of next-to-leading and higher-order corrections

For the mSugra point SPS1a', the NLO corrections for chargino production and decay cross sections at the ILC are in the percent range. Convolution of the virtual non-collinear part with the ISR structure function leads to additional percent effects for

large \sqrt{s} . These contributions are not included in the standard treatment of ISR resummation, where multiple photon emissions are combined with the Born process only.

Minor next-to-leading and higher-order uncertainties for the cross sections stem from the use of approximations in the soft and collinear regime, reshuffling of photon descriptions, enhancement of phase space for higher-order photons, and neglecting of the non-logarithmic $\mathcal{O}(\alpha)$ photon radiation from the helicity flipping term in the hard-collinear approximation. A rough estimate shows that even higher-order contributions described by the resummed structure functions can become $\mathcal{O}(\%)$ and are therefore important in a thorough analysis of the process and dominant with respect to the non-leading helicity flip contribution. The latter is $\mathcal{O}(\%)$ for unpolarized cross sections; it can in principle be easily implemented in the resummation method.

Cutoff dependencies

In general, a careful analysis of the dependence on the technical cutoffs on photon energy and angle is necessary, as it reveals uncertainties related to higher-order radiation and breakdown of the soft or collinear approximation. The soft approximation leads to a deviation from the exact solution of $\approx 5\%$ for a ratio of the soft photon cut to the center of mass energy $\Delta E_\gamma/\sqrt{s} = 10^{-2}$. The collinear approximation breaks down for the collinear cutoff $\Delta\theta = 1^\circ$. We compared the corrections resulting from the use of the approximations to the magnitude of the NLO effects as well as higher-order corrections. For the precision reached at the ILC, both the soft and collinear approximations imply the use of low cuts. On the other hand, raising the cutoffs in principle enhances phase space for multiple photon emissions and reshuffles photon description from the leading log initial state radiation description to the soft approximation for soft and the exact virtual description for virtual photons at leading order. These reshuffling effects are in the $\%$ regime, but smaller than the errors arising from raising the cutoffs for the first order approximations. This implies the use of low cutoffs for a more exact NLO description. The $2 \rightarrow 3$ process describing the $\mathcal{O}(\alpha)$ emission of hard non-collinear photons also needs to be convoluted with the ISR structure function, as these contributions also are in the $\%$ regime.

Cross sections and event generation

With both the fixed order and the resummation method implemented in WHIZARD, we reproduce the semianalytic literature results for chargino production at NLO. The angular event distributions reflect the size of the corrections for total cross sections discussed above. For a center of mass energy of 1 TeV and an integrated luminosity of 1 ab^{-1} , simulation results derived from both the NLO fixed order and the resummation method differ significantly from the Born distribution and each other. The corrections cannot be described by a constant proportionality factor K between the Born and the NLO result. The fixed and resummed distributions differ in higher-orders. This is most obvious in

the forward-scattering region, where the distributions differ by more than three (Born) standard deviations.

Outlook

The constructed generator should be regarded as a step towards a complete NLO simulation of SUSY processes at the ILC. If charginos happen to be metastable, it already provides all necessary ingredients. Beam effects (beamstrahlung, beam energy spread, polarization) are available for simulation and can easily be included. However, charginos are metastable only for peculiar SUSY parameter points. If the theoretical prediction should match the experimental accuracy, a full description of the end products seen in experiment needs to include the chargino decay at NLO as well as non-factorizing contributions to the $2 \rightarrow n$ process, e.g. in the double-pole approximation. These we have to match with off-shell and background effects, already available for simulation in **WHIZARD**. Furthermore, in the threshold region the Coulomb singularity calls for resummation, not yet accounted for in the program. These lines of improvement will be pursued in future work.

A Conventions, SUSY overview, MSSM Lagrangian

There are various introductions to the formal construction of a $N = 1$ SUSY Lagrangian, cf. [30, 32, 20, 139, 33, 34]. We just cite the main results and refer to the literature for further details.

A.1 Conventions

In the following, we define $g_{\mu\nu}$ by

$$g_{\mu\nu} = g^{\mu\nu} = \text{diag}(1, -1, -1, -1).$$

The Dirac matrices γ^μ obey

$$\{\gamma_\mu, \gamma_\nu\} = 2 g_{\mu\nu} \mathbb{1}_{4 \times 4}.$$

In the Weyl representation, they read

$$\gamma^\mu = \begin{pmatrix} 0 & \sigma^\mu \\ \bar{\sigma}^\mu & 0 \end{pmatrix}, \quad (\text{A.1})$$

with

$$\sigma^\mu = (\mathbb{1}_2, \sigma^i), \quad \bar{\sigma}^\mu = (\mathbb{1}_2, -\sigma^i), \quad (\text{A.2})$$

and the σ^i being the Pauli matrices. In addition, we define

$$\sigma^{\mu\nu} = \frac{1}{4} (\sigma^\mu \bar{\sigma}^\nu - \sigma^\nu \bar{\sigma}^\mu), \quad \bar{\sigma}^{\mu\nu} = \frac{1}{4} (\bar{\sigma}^\mu \sigma^\nu - \bar{\sigma}^\nu \sigma^\mu), \quad (\text{A.3})$$

and

$$\Sigma_{\mu\nu} = \frac{i}{2} [\gamma_\mu, \gamma_\nu].$$

The two-component Weyl spinors transforming under the $(\frac{1}{2}, 0)$ and $(0, \frac{1}{2})$ representation of the Lorentz-group are given by

$$\psi_\alpha \quad (\frac{1}{2}, 0), \quad \bar{\psi}^{\dot{\alpha}} \quad (0, \frac{1}{2}).$$

The index-raising and lowering matrices are given by

$$\begin{aligned} \epsilon^{\alpha\beta} &= \epsilon_{\dot{\alpha}\dot{\beta}} = \begin{pmatrix} 0 & -1 \\ 1 & 0 \end{pmatrix}, \\ \epsilon_{\alpha\beta} &= \epsilon^{\dot{\alpha}\dot{\beta}} = \begin{pmatrix} 0 & 1 \\ -1 & 0 \end{pmatrix}. \end{aligned} \quad (\text{A.4})$$

A four-component spinor is then given by

$$\Psi = \begin{pmatrix} \psi_\alpha \\ \bar{\chi}^{\dot{\alpha}} \end{pmatrix}. \quad (\text{A.5})$$

The index structure of the σ matrices (A.2), (A.3) is

$$(\sigma^\mu)_{\alpha\dot{\alpha}}, (\bar{\sigma}^\mu)^{\dot{\alpha}\alpha}, (\sigma^{\mu\nu})_\alpha{}^\beta, (\bar{\sigma}^{\mu\nu})^{\dot{\alpha}}{}_{\dot{\beta}},$$

in accordance with Eqs. (A.1) and (A.5).

Multiplication of Weyl spinors (as well as any Grassmann numbers) is defined by

$$\chi\psi = \chi^\alpha\psi_\alpha, \quad \bar{\chi}\bar{\psi} = \bar{\chi}_{\dot{\alpha}}\bar{\psi}^{\dot{\alpha}}.$$

Together with Eq. (A.4), this leads to

$$\begin{aligned} \chi\psi &= \psi\chi = -\chi_\alpha\psi^\alpha, \\ \bar{\chi}\bar{\psi} &= \bar{\psi}\bar{\chi} = -\bar{\chi}^{\dot{\alpha}}\bar{\psi}_{\dot{\alpha}}. \end{aligned}$$

A.2 Poincaré and SUSY algebra

We define the generators P_μ of the translation group and $\mathcal{M}_{\mu\nu}$ of the Lorentz group such that the infinitesimal transformations are

$$\begin{aligned} x'_\mu &= x_\mu + a_\mu = x_\mu - i a_\lambda (P^\lambda)_\mu & (\text{translation}), \\ x'^\rho &= x^\rho + \omega^\rho_\sigma x^\sigma = x^\rho - \frac{i}{2} \omega_{\mu\nu} (M^{\mu\nu})^\rho_\sigma x^\sigma & (\text{Lorentz transformation}). \end{aligned}$$

The generators $P_\mu, M_{\mu\nu}$ then obey the Poincaré algebra

$$\begin{aligned} [P^\lambda, P^\mu] &= 0, \\ [M^{\mu\nu}, P^\lambda] &= i(g^{\nu\lambda}P^\mu - g^{\mu\lambda}P^\nu), \\ [M^{\mu\nu}, M^{\rho\sigma}] &= i(g^{\nu\rho}M^{\mu\sigma} + g^{\mu\sigma}M^{\nu\rho} - g^{\mu\rho}M^{\nu\sigma} - g^{\nu\sigma}M^{\mu\rho}). \end{aligned}$$

A supersymmetry transformation is an extension of the Poincaré Algebra relating bosonic and fermionic degrees of freedom. We define $Q_\alpha, \bar{Q}^{\dot{\alpha}}$ to be the supersymmetry generators in the two-dimensional $(\frac{1}{2}, 0), (0, \frac{1}{2})$ representations of the Lorentz group. The properties under transformations and closure of the algebra require (anti-)commutation rules which in four-component notation read

$$[M^{\mu\nu}, Q] = 0, \quad \{Q, \bar{Q}\} = 0, \quad [M^{\mu\nu}, Q] = -\frac{1}{2}\Sigma^{\mu\nu}Q,$$

where

$$Q = \begin{pmatrix} Q_\alpha \\ \bar{Q}^{\dot{\alpha}} \end{pmatrix}.$$

In two-component notation, this reads

$$\begin{aligned}
[Q_\alpha, P_\mu] &= [\bar{Q}_{\dot{\alpha}}, P_\mu] = 0, \quad [Q_\alpha, M_{\mu\nu}] = -i(\sigma_{\mu\nu})_\alpha{}^\beta Q_\beta, \\
[\bar{Q}^{\dot{\alpha}}, M_{\mu\nu}] &= -i(\bar{\sigma}_{\mu\nu})^{\dot{\alpha}}{}_{\dot{\beta}} \bar{Q}^{\dot{\beta}}, \quad \{Q_\alpha, \bar{Q}^{\dot{\beta}}\} = 2(\sigma^\mu)_\alpha{}^{\dot{\beta}} P_\mu, \\
\{Q_\alpha, Q_\beta\} &= \{\bar{Q}^{\dot{\alpha}}, \bar{Q}^{\dot{\beta}}\} = 0.
\end{aligned} \tag{A.6}$$

A.3 Expansion in component fields

A SUSY transformation for a field operator $\phi(x)$ is given by

$$\exp\left(i(\xi^\alpha Q_\alpha + \bar{\xi}_{\dot{\alpha}} \bar{Q}^{\dot{\alpha}})\right) \phi(x) \exp\left(-i(\xi^\alpha Q_\alpha + \bar{\xi}_{\dot{\alpha}} \bar{Q}^{\dot{\alpha}})\right),$$

where ξ are Grassmann-valued variables. Infinitesimally, this becomes

$$\phi(x) \rightarrow \phi(x) + \delta_\xi \phi(x), \quad \delta_\xi \phi(x) = [i(\xi Q + \bar{\xi} \bar{Q}), \phi(x)].$$

Starting with a scalar field $\phi(x)$ and requiring the closure of the algebra, we obtain the transformation rules

$$\begin{aligned}
\delta_\xi \phi &= \sqrt{2} \xi \psi, \\
\delta_\xi \psi &= i\sqrt{2} \sigma^\mu \bar{\xi} \partial_\mu \phi + \sqrt{2} \xi F, \\
\delta_\xi F &= i\sqrt{2} \bar{\xi} \bar{\sigma}^\mu \partial_\mu \psi,
\end{aligned} \tag{A.7}$$

where ψ and F are a spinor/ auxiliary field with the dimensions $\frac{3}{2}/2$ respectively.

From (A.6), we can determine the action of a SUSY transformation generator

$$G(a^\mu, \xi, \bar{\xi}) = \exp(i(\xi Q + \bar{\xi} \bar{Q} - a^\mu P_\mu))$$

on a superfield $S(x^\mu, \theta, \bar{\theta})$:

$$S(x^\mu, \theta, \bar{\theta}) \rightarrow \exp(i(\xi Q + \bar{\xi} \bar{Q} - a^\mu P_\mu)) S(x^\mu, \theta, \bar{\theta}).$$

$S(x^\mu, \theta, \bar{\theta})$ can be expanded in components proportional to $\theta, \bar{\theta}, \theta\theta, \dots$; the generators are then given by

$$\begin{aligned}
P_\mu &= i\partial_\mu, \\
iQ_\alpha &= \frac{\partial}{\partial\theta^\alpha} - i\sigma^\mu_{\alpha\dot{\beta}} \bar{\theta} \partial_\mu, \\
i\bar{Q}_{\dot{\alpha}} &= -\frac{\partial}{\partial\bar{\theta}^{\dot{\alpha}}} + i\theta \sigma^\mu_{\dot{\alpha}\beta} \partial_\mu.
\end{aligned}$$

Fermionic derivatives which anticommute with the Q, \bar{Q} are then given by

$$D_\alpha = \frac{\partial}{\partial\theta^\alpha} + i\sigma^\mu_{\alpha\dot{\beta}} \bar{\theta} \partial_\mu, \quad \bar{D}_{\dot{\alpha}} = -\frac{\partial}{\partial\bar{\theta}^{\dot{\alpha}}} - i\theta \sigma^\mu_{\dot{\alpha}\beta} \partial_\mu,$$

which obey

$$\{D_\alpha, \bar{D}_{\dot{\alpha}}\} = 2i\sigma_{\alpha\dot{\alpha}}^\mu \partial_\mu.$$

All other anticommutators vanish.

Defining a **chiral superfield** Φ by requiring

$$\bar{D}_{\dot{\alpha}} \Phi = 0,$$

we obtain

$$\Phi(x^\mu, \theta, \bar{\theta}) = \phi + \sqrt{2}\theta\psi + \theta\theta F + i\partial_\mu \phi \theta \sigma^\mu \bar{\theta} - \frac{i}{\sqrt{2}} \theta\theta \partial_\mu \psi \sigma^\mu \bar{\theta} - \frac{1}{4} \partial_\mu \partial^\mu \phi \theta\theta \bar{\theta}\bar{\theta},$$

with the component fields and their transformation rules given by Eq. (A.7).

The antichiral field Φ^\dagger is given by

$$\Phi^\dagger = \phi^\dagger + \sqrt{2}\bar{\theta}\bar{\psi} + \bar{\theta}\bar{\theta} F^\dagger - i\partial_\mu \phi^\dagger \theta \sigma^\mu \bar{\theta} + \frac{i}{\sqrt{2}} \bar{\theta}\bar{\theta} \sigma^\mu \partial_\mu \bar{\psi} - \frac{1}{4} \partial_\mu \partial^\mu \phi^\dagger \theta\theta \bar{\theta}\bar{\theta},$$

which obeys

$$D_\alpha \Phi^\dagger = 0.$$

A **vector superfield** V is defined by requiring

$$V = V^\dagger.$$

This leads to

$$\begin{aligned} V(x, \theta, \bar{\theta}) = & C(x) + i\theta\chi - i\bar{\theta}\bar{\chi} + \frac{1}{2}i\theta\theta[M(x) + N(x)] - \frac{1}{2}i\bar{\theta}\bar{\theta}[M(x) - iN(x)] \\ & + \theta\sigma^\mu\bar{\theta}V_\mu(x) + i\theta\theta\bar{\theta}\left[\bar{\lambda}(x) + \frac{i}{2}\bar{\sigma}^\mu\partial_\mu\chi(x)\right] - i\bar{\theta}\bar{\theta}\theta\left[\lambda(x) + \frac{i}{2}\sigma^\mu\partial_\mu\bar{\chi}(x)\right] \\ & + \frac{1}{2}\theta\theta\bar{\theta}\bar{\theta}\left[D - \frac{1}{2}\partial_\mu\partial^\mu C\right], \end{aligned}$$

with C, M, N, D being real scalar fields, χ, λ Weyl spinor fields, and V_μ a real vector field. Note that there is a gauge invariance with respect to

$$V \rightarrow V + i[\Phi - \Phi^\dagger],$$

which helps to reduce V to

$$V_{WZ}(x, \theta, \bar{\theta}) = \theta\sigma^\mu\bar{\theta}V_\mu(x) + i\theta\theta\bar{\theta}\bar{\lambda}(x) - i\bar{\theta}\bar{\theta}\theta\lambda(x) + \frac{1}{2}\theta\theta\bar{\theta}\bar{\theta}D$$

$(\Phi_1\Phi_2), (\Phi_1\Phi_2\Phi_3), (\bar{D}^2 D_\alpha V)$	chiral fields
$(\Phi_1^\dagger\Phi_1), i[\Phi_1 - \Phi_1^\dagger]$	vector fields

Table A.1: superfield character of different superfield combinations

in the Wess Zumino (WZ) gauge. The fields V_μ, λ, D transform under SUSY transformation as

$$\begin{aligned}\delta\lambda_\alpha &= -iD\xi_\alpha - \frac{1}{2}(\sigma^\mu\bar{\sigma}^\nu)\xi V_{\mu\nu}, \\ \delta V^\mu &= i(\xi\sigma^\mu\bar{\lambda} - \lambda\sigma^\mu\bar{\xi}) - \partial^\mu(\xi\chi + \bar{\chi}\bar{\xi}), \\ \delta D &= \partial_\mu(-\xi\sigma^\mu\bar{\lambda} + \lambda\sigma^\mu\bar{\xi}),\end{aligned}$$

with the field strength $V_{\mu\nu} = \partial_\mu V_\nu - \partial_\nu V_\mu$. We see that supersymmetry is explicitly broken in the WZ gauge; however, it can be restored by a proper gauge transformation.

Combinations of (anti)chiral and vector superfields which are again (anti-)chiral and vector superfields are given in table A.1. A more extensive list can be found in [32].

A.4 General gauge-invariant Lagrangian and superpotential

For the construction of a Lagrangian, we have to find components of superfields which are supersymmetric. It is easy to see that these are given by the $\theta\theta(\bar{\theta}\bar{\theta})$ components of the $\Phi(\Phi^\dagger)$ (F-terms) and the $\theta\theta\bar{\theta}\bar{\theta}$ components of V (D-term) respectively, as all of these transform up to a total derivative. Lagrangians are therefore constructed using the F-terms of chiral and the D-terms of vector superfields and the field combinations as given in table A.1.

Gauge invariance

For a general $U(1)$ invariant Lagrangian, we define the field-strength superfield

$$W_\alpha(y, \theta) = 4i\lambda_\alpha(y) - [4\delta_\alpha{}^\beta D(y) + 2i(\sigma^\mu\bar{\sigma}^\nu)_\alpha{}^\beta V_{\mu\nu}(y)]\theta_\beta + 4\theta\theta\sigma_{\alpha\dot{\alpha}}^\mu\partial_\mu\bar{\lambda}^{\dot{\alpha}},$$

where $y^\mu = x^\mu + i\theta\sigma^\mu\bar{\theta}$. This contains a spinor λ_α with the dimension $\frac{3}{2}$ and the field strength $V_{\mu\nu}$ with dimension 2 as well as the auxiliary field D . The pure gauge term is then given by the F-term of $(W_\alpha W^\alpha + hc)$:

$$\mathcal{L}_V = \frac{1}{64}(W^\alpha W_\alpha + \bar{W}_{\dot{\alpha}}\bar{W}^{\dot{\alpha}})_F = -\frac{1}{4}V^{\mu\nu}V_{\mu\nu} + i\lambda\sigma^\mu\partial_\mu\bar{\lambda} + \frac{1}{2}D^2. \quad (\text{A.8})$$

The interaction between matter and gauge bosons is then given by the D-term of the vector superfield $\Phi^\dagger e^V \Phi$:

$$\mathcal{L}_\Phi = [\Phi^\dagger e^V \Phi]_D = (D_\mu\phi)^\dagger(D^\mu\phi) + i\psi\sigma^\mu D_\mu^\dagger\bar{\psi} + F^\dagger F + i\sqrt{2}g(\phi^\dagger\lambda\psi - \bar{\psi}\bar{\lambda}\phi) + g\phi^\dagger D\phi, \quad (\text{A.9})$$

where $D_\mu = \partial_\mu + i g V_\mu$. Then, the total gauge-invariant Lagrangian is

$$\mathcal{L}_{inv} = \mathcal{L}_V + \mathcal{L}_\Phi.$$

For the construction of QED with massive fermions, we have to include left- and righthanded component fields; this can be done by defining the combinations

$$\Phi_+ = \frac{1}{\sqrt{2}}(\Phi_1 + i\Phi_2), \quad \Phi_- = \frac{1}{\sqrt{2}}(\Phi_1 - i\Phi_2).$$

Their transformations are then given by

$$\Phi_+ \rightarrow \exp(-2i\Lambda)\Phi_+, \quad \Phi_- \rightarrow \exp(2i\Lambda)\Phi_-, \quad V \rightarrow V + i(\Lambda - \Lambda^\dagger).$$

In addition to $\mathcal{L}_{\Phi_+}, \mathcal{L}_{\Phi_-}$, this allows the inclusion of mass generating terms of the form

$$\mathcal{L}_{\text{mass}} = m \left((\Phi_+\Phi_-)_{\theta\theta} + (\Phi_+^\dagger\Phi_-^\dagger)_{\bar{\theta}\bar{\theta}} \right),$$

so the total gauge-invariant Lagrangian including the coupling of massive particles to the gauge bosons is

$$\mathcal{L}_{inv} = \mathcal{L}_V + \mathcal{L}_{\Phi_+} + \mathcal{L}_{\Phi_-} + \mathcal{L}_{\text{mass}}.$$

This procedure can be extended to any (non)abelian gauge group. We have to add terms in the form of Eqs. (A.8), (A.9) for every new gauge group and modify D_μ accordingly. In the non-abelian case, the vector superfield is given by

$$V_{\mu\nu}^a = \partial_\mu V_\nu^a - \partial_\nu V_\mu^a - g f^{abc} V_\mu^b V_\nu^c,$$

where f^{abc} are the structure constants of the non-abelian gauge group. Its transformation is given by

$$V^a \rightarrow V^a + i(\Lambda^a - \Lambda^{a,\dagger}) - g f^{abc} V^b (\Lambda^c + \Lambda^{\dagger,c}) + \mathcal{O}(g^2).$$

Superpotential

The superpotential defines the possible self-interactions terms of chiral fields. Renormalizability requirements determine the most general SUSY-preserving potential

$$f(\Phi_i) = \sum_i a_i (\Phi_i)_{\theta\theta} + \frac{1}{2} \sum_{i,j} m_{i,j} (\Phi_i \Phi_j)_{\theta\theta} + \frac{1}{3} \sum_{i,j,k} g_{ijk} (\Phi_i \Phi_j \Phi_k)_{\theta\theta}.$$

Elimination of auxiliary fields

The unphysical auxiliary fields F_i, D are generally eliminated by requiring

$$\frac{\partial \mathcal{L}}{\partial D} = \frac{\partial \mathcal{L}}{\partial F_i} = 0,$$

which leads to

$$F_i^\dagger = -\frac{\partial f}{\partial \phi_i}, \quad D = -\sum_i \phi_i^\dagger g \phi_i. \quad (\text{A.10})$$

gauge group	non-singlet SM matter fields
$U(1) (Y)$	$u_L, d_L (\frac{1}{6}), \nu_{l,L}, l_L (-\frac{1}{2}), u_R (-\frac{2}{3}), d_R (\frac{1}{3}), l_R (1), H (\frac{1}{2})$
$SU(2)$	$\begin{pmatrix} u_L \\ d_L \end{pmatrix}, \begin{pmatrix} \nu_{l,L} \\ l_L \end{pmatrix}, H$
$SU(3)$	$u_{L,c}, d_{L,c}, u_{R,c}, d_{R,c}$

Table A.2: Standard Model matter content and gauge-group transformation properties. $u = (u, c, t)$, $d = (d, s, b)$, $l = (e, \mu, \tau)$ run over the respective families and c is the color index. Y is the hypercharge. Transformation properties of gauge fields are not listed.

A.5 MSSM field content and superpotential

As the MSSM is the minimal supersymmetric extension of the Standard Model, it is designed to reproduce the SM particle content including as few extra fields as possible. We therefore need

- Vector fields as in (A.8) for the $SU(2) \times U(1)$ electroweak as well as the $SU(3)$ strong gauge groups
- gauge-particle interactions as in (A.9) for the Standard Model matter content as listed in table A.2.
- a superpotential f_{MSSM} giving masses to the (s)fermions. This requires a modified Higgs sector: instead of the SM Higgs, the two Higgs doublets given by Eq. (A.12) are introduced. They carry the hypercharges $Y = \frac{1}{2} (H_u)$ and $Y = -\frac{1}{2} (H_d)$.

The minimal superpotential reproducing the Yukawa-terms of the Standard Model and preserving supersymmetry is

$$f_{MSSM}(\phi) = \bar{u}y_uQH_u - \bar{d}y_dQH_d - \bar{e}y_eLH_d + \mu H_uH_d, \quad (\text{A.11})$$

with

$$H_u = \begin{pmatrix} H_u^+ \\ H_u^0 \end{pmatrix}, H_d = \begin{pmatrix} H_d^0 \\ H_d^- \end{pmatrix}, \quad (\text{A.12})$$

and $\bar{u}, \bar{d}, \bar{e}$ denote the righthanded $SU(2)$ quark and lepton singlets and Q, L the left-handed $SU(2)$ quark doublets. y_i are the respective Yukawa matrices.

A.6 Symmetry breaking and Lagrangian of the MSSM

SUSY and gauge breaking

Supersymmetry breaking terms need to preserve the cancellation of the quadratic divergences of the corrections to the Higgs mass. The most general terms fulfilling this

requirement are

$$\begin{aligned}
\mathcal{L}_{SUSY-breaking} = & m_{\tilde{q}}^2 |\tilde{q}_L|^2 + m_{\tilde{u}}^2 |\tilde{u}_R|^2 + m_{\tilde{d}}^2 |\tilde{d}_R|^2 + m_{\tilde{l}}^2 |\tilde{l}_L|^2 + m_{\tilde{e}}^2 |\tilde{e}_R|^2 \\
& + \left(\lambda_E A_E H_d \tilde{l}_L \tilde{e}_R + \lambda_D A_D H_d \tilde{q}_L \tilde{u}_R + \lambda_U A_U H_u \tilde{q}_L \tilde{d}_R + B \mu H_u H_d + h.c. \right) \\
& + m_{H_u}^2 |H_u|^2 + m_{H_d}^2 |H_d|^2 + \frac{1}{2} \left(M_1 \tilde{B} \tilde{B} + M_2 \tilde{W} \tilde{W} + M_3 \tilde{g} \tilde{g} + h.c. \right).
\end{aligned} \tag{A.13}$$

Here, $m_{\tilde{q}}^2$, $m_{\tilde{u}}^2$, $m_{\tilde{d}}^2$, $m_{\tilde{l}}^2$, $m_{\tilde{e}}^2$ are general hermitian 3×3 matrices and $\lambda_E A_E$, $\lambda_D A_D$, $\lambda_U A_U$ general 3×3 matrices, $|\tilde{q}_L|^2 = (u_L^\dagger u_L + d_L^\dagger d_L)$ (same for \tilde{l}_L) and the multiplication of two $SU(2)$ doublets is given by

$$D_1 D_2 = \epsilon^{ij} D_{1,i} D_{2,j} = D_{1,1} D_{2,2} - D_{2,1} D_{1,2}. \tag{A.14}$$

As in the SM, the electroweak gauge symmetry is broken because the Higgs doublet acquire non-zero VEVs. However, the specific form of the MSSM Higgs potential requires both μ in f_{MSSM} and $B\mu$ in $\mathcal{L}_{SUSY-breaking}$ to be non-zero.

MSSM Lagrangian

The complete MSSM Lagrangian is then given by

$$\begin{aligned}
\mathcal{L}_{MSSM} = & -\frac{1}{4} V_{g'}^{\mu\nu} V_{g',\mu\nu} + i \lambda_{g'} \sigma^\mu \partial_\mu \bar{\lambda}_{g'} + \frac{1}{2} D_{g'}^2 - \frac{1}{4} V_g^{i,\mu\nu} V_{g,\mu\nu}^i + i T^i \lambda_g^i \sigma^\mu \partial_\mu \bar{\lambda}_g^i + \frac{1}{2} (D_g^i)^2 \\
& - \frac{1}{4} V_{g_s}^{a,\mu\nu} V_{g_s,\mu\nu}^a + i T^a \lambda_{g_s}^a \sigma^\mu \partial_\mu \bar{\lambda}_{g_s}^a + \frac{1}{2} (D_{g_s}^a)^2 \\
& + (D_\mu \phi_I)^\dagger (D^\mu \phi_I) + i \psi_I \sigma^\mu D_\mu^\dagger \bar{\psi}_I + F_I^\dagger F_I + i \sqrt{2} g_k (\phi_I^\dagger T^k \lambda^k \psi_I - \bar{\psi}_I \bar{\lambda}^k T^k \phi_I) + g_k \phi_I^\dagger D_I \phi_I \\
& + m_{\tilde{q}}^2 |\tilde{q}_L|^2 + m_{\tilde{u}}^2 |\tilde{u}_R|^2 + m_{\tilde{d}}^2 |\tilde{d}_R|^2 + m_{\tilde{l}}^2 |\tilde{l}_L|^2 + m_{\tilde{e}}^2 |\tilde{e}_R|^2 \\
& + \left(\lambda_E A_E H_d \tilde{l}_L \tilde{e}_R + \lambda_D A_D H_d \tilde{q}_L \tilde{u}_R + \lambda_U A_U H_u \tilde{q}_L \tilde{d}_R + B \mu H_u H_d + h.c. \right) \\
& + m_{H_u}^2 |H_u|^2 + m_{H_d}^2 |H_d|^2 + \frac{1}{2} \left(M_1 \tilde{B} \tilde{B} + M_2 \tilde{W} \tilde{W} + M_3 \tilde{g} \tilde{g} + h.c. \right) \\
& + (\bar{u} y_u Q H_u - \bar{d} y_d Q H_d - \bar{e} y_e L H_d + \mu H_u H_d)_{\theta\theta},
\end{aligned}$$

where $i = 1, 2, 3$ is the $SU(2)$ and $a = 1, 2, \dots, 8$ the $SU(3)$ group index; the index I in the gauge-matter interaction part (A.9) runs over all superfields corresponding to the SM particles listed in Table A.2 and the Higgs fields (A.12), where the index k symbolizes that all respective gauge-groups as given in Table A.2 have to be taken into account. The field content from the superpotential is given by its $(\theta\theta)$ component and can be derived using Eq. (A.14) and

$$\begin{aligned}
\Phi_i \Phi_j|_{(\theta\theta)} &= -\psi_i \psi_j, \\
\Phi_i \Phi_j \Phi_k|_{(\theta\theta)} &= -(\psi_i \psi_j \phi_k + \text{cyclic terms}).
\end{aligned}$$

bosonic		fermionic, spin = $\frac{1}{2}$	
$\tilde{e}_{L,R}, \tilde{\mu}_{L,R}, \tilde{\tau}_{L,R}$	(sleptons, spin = 0)	$e_{L,R}, \mu_{L,R}, \tau_{L,R}$	(leptons)
$\tilde{u}_{L,R}, \tilde{d}_{L,R}, \tilde{c}_{L,R}, \tilde{s}_{L,R}, \tilde{t}_{L,R}, \tilde{b}_{L,R}$	(squarks, spin = 0)	$u_{L,R}, d_{L,R}, c_{L,R}, s_{L,R}, t_{L,R}, b_{L,R}$	(quarks)
B, W^i, g^a	(gauge bosons, spin = 1)	$\tilde{B}, \tilde{W}^i, \tilde{g}^a$	(gauginos)
$H_u^+, H_u^0, H_d^-, H_d^0$	(Higgs bosons, spin = 0)	$\tilde{H}_u^+, \tilde{H}_u^0, \tilde{H}_d^-, \tilde{H}_d^0$	(Higgsinos)

Table A.3: field content in the MSSM

Finally, D and F terms are eliminated using Eq. (A.10).

The field content of the MSSM is then given in Table A.3. Physically observed particles correspond to superpositions of these fields carrying the same quantum numbers which are rotated into mass-eigenstates. In addition, the two-component Weyl-spinors λ, ψ have to be combined to obtain four-component Dirac- or Majorana spinors. For the gaugino/ Higgsino sector, this is done in Appendix B. For a more complete treatment, we refer to e.g. [30, 33, 34].

B Chargino and Neutralino Sector of the MSSM

Here, we sketch the derivation of the Feynman rules for any vertices including charginos and neutralinos. We hereby closely follow [30]. We point to differences in conventions if necessary.

B.1 Chargino mass eigenstates

In the MSSM, the EW symmetry is spontaneously broken by non-zero VEVs of the two neutral components of the Higgs doublets:

$$\langle H_d^0 \rangle = v_1, \quad \langle H_u^0 \rangle = v_2.$$

$\tan \beta$ is defined as the ratio of these VEVs¹:

$$\tan \beta = \frac{v_2}{v_1}$$

Taking this into account in the chargino-chargino-Higgs couplings and using

$$\mu H_u^+ H_d^- |_{\theta\theta,\psi} = -\mu \tilde{H}_u^+ \tilde{H}_d^-,$$

we obtain the following mass terms in the Lagrangian:

$$(M_2 \tilde{W}^+ \tilde{W}^- - \mu \tilde{H}_u^+ \tilde{H}_d^-) + h.c. - \overline{\imath g \tilde{H}_d^- \tilde{W}^-} v_1 + \imath g v_1^* \tilde{H}_d^- \tilde{W}^- - \overline{\imath g \tilde{H}_u^+ \tilde{W}^+} v_2 + \imath g v_2^* \tilde{H}_u^+ \tilde{W}^-.$$

We now define Ψ^- and Ψ^+ by

$$\Psi^- = \begin{pmatrix} -\imath \tilde{W}^- \\ \tilde{H}_d^- \end{pmatrix}, \quad \Psi^+ = \begin{pmatrix} -\imath \tilde{W}^+ \\ \tilde{H}_u^+ \end{pmatrix}, \quad (\text{B.1})$$

and obtain

$$-\Psi^{-\top} X \Psi^+ - (\overline{\Psi^+})^\top X^\dagger \overline{\Psi^-},$$

as mass terms of the Lagrangian with

$$X = \begin{pmatrix} M_2 & g v_2 \\ g v_1 & \mu \end{pmatrix}.$$

¹Note that the definition of $\tan \theta_v$ in [30] is given by $\tan \theta_v = (\tan \beta)^{-1}$.

Using the relation

$$m_w^2 = \frac{1}{2} g^2 (v_1^2 + v_2^2),$$

we can rewrite this as

$$X = \begin{pmatrix} M_2 & \sqrt{2} m_w \sin \beta \\ \sqrt{2} m_w \cos \beta & \mu \end{pmatrix}. \quad (\text{B.2})$$

This matrix can now be diagonalized using

$$U_- X U_+^{-1} = M_{\text{diag}},$$

with

$$U_{\pm} = \begin{pmatrix} \cos \Phi_{\pm} & \sin \Phi_{\pm} \\ -\sin \Phi_{\pm} & \cos \Phi_{\pm} \end{pmatrix}.$$

The angles $\cos \Phi_{\pm}$ and $\sin \Phi_{\pm}$ obey [76, 78]:

$$\begin{aligned} \cos 2\Phi_{\pm} &= -[M_2^2 - |\mu|^2 \pm 2m_W^2 \cos 2\beta] / \Delta_C, \\ \sin 2\Phi_{\pm} &= -2m_W \sqrt{M_2^2 + |\mu|^2 \mp (M_2^2 - |\mu|^2) \cos 2\beta + 2M_2|\mu| \sin 2\beta} / \Delta_C, \\ \Delta_C &= \sqrt{(M_2^2 - |\mu|^2)^2 + 4m_W^2 \cos^2 2\beta + 4m_W^2 (M_2^2 + |\mu|^2) + 8m_W^2 M_2|\mu| \sin 2\beta}. \end{aligned}$$

The two-component charged mass-eigenstates χ^{\pm} are then given by

$$\chi^+ = U_+ \Psi^+, \quad \chi^- = U_-^* \Psi^-,$$

and the four-component Dirac spinors $\tilde{\chi}_i^{\pm}$ by

$$\tilde{\chi}_i^+ = \begin{pmatrix} \chi_i^+ \\ \bar{\chi}_i^- \end{pmatrix} \quad \text{or} \quad \tilde{\chi}_i^- = \begin{pmatrix} \chi_i^- \\ \bar{\chi}_i^+ \end{pmatrix},$$

depending on the particle/ antiparticle choice.

Note that there are different notations for these matrices in the literature which have to be taken into account when comparing results. We here give a short overview:

We start with the form

$$(\Psi^+ \ \Psi^-) \begin{pmatrix} 0 & X^{\top} \\ X & 0 \end{pmatrix} \begin{pmatrix} \Psi^+ \\ \Psi^- \end{pmatrix}$$

with Ψ^{\pm} as by Eq. (B.1) and X as by Eq. (B.2). We now define the matrices U, V such that

$$\chi^- = U \Psi^-; \quad \chi^+ = V \Psi^+$$

and see that X is diagonalized using

$$U^* X V^{\dagger}.$$

Depending on the parameterization of U and V , $m_{\tilde{\chi}_1^{\pm}}$ can be larger or smaller than $m_{\tilde{\chi}_2^{\pm}}$. Table B.1 gives an overview of the different conventions used in the literature.

Source			diag.
HK[30]	V	U	$U^* X V^\dagger$
here	U_+	U_-^*	$U_- X U_+^\dagger$
LH[129]	V	U	$U^* X V^\dagger$
Choi[78]	U_R	U_L	$U_L^* X U_R^\dagger$
FC[80]	V	U	$U^* X V^\dagger$

Table B.1: Different conventions for chargino-diagonalization matrices in the literature

B.2 Neutralino Mass Eigenstates

From \mathcal{L}_{MSSM} , the neutralino mass terms are given by

$$\begin{aligned} & \left(\frac{1}{2} M_1 \tilde{B} \tilde{B} + \frac{1}{2} M_2 \tilde{W}^0 \tilde{W}^0 + \mu \tilde{H}_d^0 \tilde{H}_u^0 - \frac{i g}{\sqrt{2}} v_2 \tilde{H}_u^0 \tilde{W}^0 + \frac{i g'}{\sqrt{2}} v_2 \tilde{H}_u^0 \tilde{B} \right. \\ & \left. + \frac{i g}{\sqrt{2}} v_1 \tilde{H}_d^0 \tilde{W}^0 - \frac{i g'}{\sqrt{2}} v_2 \tilde{H}_d^0 \tilde{B} \right) + h.c. \end{aligned}$$

We define Ψ_L^0 by

$$\Psi_L^0 = \begin{pmatrix} -i \tilde{B} \\ -i \tilde{W}^0 \\ \tilde{H}_d^0 \\ \tilde{H}_u^0 \end{pmatrix} = \begin{pmatrix} \tilde{B}_L \\ \tilde{W}_L^0 \\ (\tilde{H}^d)_L \\ (\tilde{H}^u)_L \end{pmatrix},$$

with the four-component Majorana-spinors

$$\tilde{B} = \begin{pmatrix} -i \tilde{B} \\ i \tilde{B} \end{pmatrix}, \quad \tilde{W}^0 = \begin{pmatrix} -i \tilde{W}^0 \\ i \tilde{W}^0 \end{pmatrix}, \quad \tilde{H}^u = \begin{pmatrix} H_u^0 \\ H_u^0 \end{pmatrix}, \quad \tilde{H}^d = \begin{pmatrix} H_d^0 \\ H_d^0 \end{pmatrix}.$$

We can then rewrite the mass part of the Lagrangian as

$$-\frac{1}{2} \Psi_L^{0\top} M \Psi_L^0 + h.c.,$$

with

$$M = \begin{pmatrix} M_1 & 0 & -\frac{g'}{\sqrt{2}} v_1 & \frac{g'}{\sqrt{2}} v_2 \\ 0 & M_2 & \frac{g}{\sqrt{2}} v_1 & -\frac{g}{\sqrt{2}} v_2 \\ -\frac{g'}{\sqrt{2}} v_1 & \frac{g}{\sqrt{2}} v_1 & 0 & -\mu \\ \frac{g'}{\sqrt{2}} v_2 & -\frac{g}{\sqrt{2}} v_2 & -\mu & 0 \end{pmatrix}.$$

Using

$$m_z^2 = \frac{1}{2} (g^2 + g'^2) v^2; \quad \frac{s_w}{c_w} = \frac{g'}{g}; \quad \frac{s_\beta}{c_\beta} = \frac{v_2}{v_1}; \quad v^2 = v_1^2 + v_2^2,$$

we obtain

$$M = \begin{pmatrix} M_1 & 0 & -m_Z c_\beta s_w & m_Z s_\beta s_w \\ 0 & M_2 & m_Z c_\beta c_w & -m_Z s_\beta c_w \\ -m_Z c_\beta s_w & m_Z c_\beta c_w & 0 & -\mu \\ m_Z s_\beta s_w & -m_Z s_\beta c_w & -\mu & 0 \end{pmatrix}.$$

This can be diagonalized using a unitary matrix such that

$$M_{diag} = N^* M N^\dagger.$$

We obtain N from the diagonalization of $M M^\dagger$:

$$M_{diag} M_{diag}^\dagger = N^* M M^\dagger N^\top.$$

The two-component mass eigenstates are then given by

$$\chi_i^0 = N_{ij} \Psi_{L,j}^0,$$

and the four-component spinors by

$$\tilde{\chi}_i^0 = \begin{pmatrix} \chi_i^0 \\ \frac{\chi_i^0}{\chi_i^0} \end{pmatrix}.$$

When taking N purely real, neutralino masses can come out negative. In this case, the physical field is given by $\gamma_5 \tilde{\chi}^0$. Note that this has to be taken into account when deriving the Feynman rules for the physical particles from \mathcal{L} .

An analytic expression for the diagonalization matrix N can be found in the literature, cf. e.g. [140] and [141].

B.3 Chargino-Gauge-boson couplings

We will here and in the following switch between two-component Weyl spinors and four-component Dirac- and Majorana-spinors; a good introduction can e.g. be found in [139]. The part of \mathcal{L}_{MSSM} describing chargino-chargino-gauge boson coupling is given by

$$\begin{aligned} & \frac{1}{2} g \overline{\tilde{H}_d^-} \bar{\sigma}^\mu W_\mu^0 \tilde{H}_d^- + \frac{1}{2} g' \overline{\tilde{H}_d^-} \bar{\sigma}^\mu B_\mu \tilde{H}_d^- - \frac{1}{2} g \overline{\tilde{H}_u^+} \bar{\sigma}^\mu W_\mu^0 \tilde{H}_u^+ \\ & - \frac{1}{2} g' \overline{\tilde{H}_u^+} \bar{\sigma}^\mu B_\mu \tilde{H}_u^+ - g \overline{\tilde{W}^+} \bar{\sigma}^\mu W_\mu^0 \tilde{W}^+ + g \overline{\tilde{W}^-} \bar{\sigma}^\mu W_\mu^0 \tilde{W}^- \end{aligned}$$

Let us define the $\tilde{\chi}^+$ as the particle. If we use

$$\tilde{W} = \begin{pmatrix} -i\tilde{W}^+ \\ (-i\tilde{W}^-) \end{pmatrix}, \quad \tilde{H} = \begin{pmatrix} \tilde{H}_u^+ \\ \tilde{H}_d^- \end{pmatrix},$$

the Lagrangian is given by

$$- g \overline{\tilde{W}} \gamma^\mu W_\mu^0 \tilde{W} - \frac{1}{2} g \overline{\tilde{H}} \gamma^\mu W_\mu^0 \tilde{H} - \frac{1}{2} g' \overline{\tilde{H}} \gamma^\mu B_\mu \tilde{H}. \quad (\text{B.3})$$

We can now split both \widetilde{W} and \widetilde{H} into left- and right-handed parts as

$$\overline{\widetilde{W}}\gamma^\mu W_\mu^0\widetilde{W} = \overline{\widetilde{W}_L}\gamma^\mu W_\mu^0\widetilde{W}_L + \overline{\widetilde{W}_R}\gamma^\mu W_\mu^0\widetilde{W}_R$$

and same with B_μ and \widetilde{H} . We then obtain the following respective relations between the left- and righthanded parts of $\widetilde{\chi}_{1,2}$ and $\widetilde{H}, \widetilde{W}^0$:

$$\begin{pmatrix} \widetilde{\chi}_{1L} \\ \widetilde{\chi}_{2L} \end{pmatrix} = U^+ \begin{pmatrix} \widetilde{W}_L \\ \widetilde{H}_L \end{pmatrix}, \quad \begin{pmatrix} \widetilde{\chi}_{1R} \\ \widetilde{\chi}_{2R} \end{pmatrix} = U^- \begin{pmatrix} \widetilde{W}_R \\ \widetilde{H}_R \end{pmatrix}.$$

The whole coupling term of the Lagrangian containing left-handed parts now reads

$$\begin{aligned} & -g\overline{\widetilde{W}_L}\gamma^\mu W_\mu^0\widetilde{W}_L - \frac{1}{2}g\overline{\widetilde{H}_L}\gamma^\mu W_\mu^0\widetilde{H}_L - \frac{1}{2}g'\overline{\widetilde{H}_L}\gamma^\mu B_\mu\widetilde{H}_L \\ & = -\overline{\begin{pmatrix} \widetilde{W}_L \\ \widetilde{H}_L \end{pmatrix}}^\top \begin{pmatrix} g\gamma^\mu W_\mu^0 & 0 \\ 0 & \frac{1}{2}(g\gamma^\mu W_\mu^0 + g'\gamma^\mu B_\mu) \end{pmatrix} \begin{pmatrix} \widetilde{W}_L \\ \widetilde{H}_L \end{pmatrix}. \end{aligned}$$

The same relation (with $L \leftrightarrow R$) holds for the right-handed part.

If we define the negatively charged charginos to be the particles, the derivation is similar; however, we then have to define

$$\widetilde{W}' = \begin{pmatrix} -i\widetilde{W}^- \\ (-i\widetilde{W}^+) \end{pmatrix}, \quad \widetilde{H}' = \begin{pmatrix} \widetilde{H}_d^- \\ \widetilde{H}_u^+ \end{pmatrix}.$$

The terms in the Lagrangian describing the gauge-boson couplings are the same up to a sign change. The transformation rules for the right- and left-handed parts are given by

$$\begin{pmatrix} \widetilde{\chi}_{1L} \\ \widetilde{\chi}_{2L} \end{pmatrix} = (U^-)^* \begin{pmatrix} \widetilde{W}_L \\ \widetilde{H}_L \end{pmatrix}, \quad \begin{pmatrix} \widetilde{\chi}_{1R} \\ \widetilde{\chi}_{2R} \end{pmatrix} = (U^+)^* \begin{pmatrix} \widetilde{W}_R \\ \widetilde{H}_R \end{pmatrix}$$

and $\widetilde{\chi}^-$ is defined as

$$\widetilde{\chi}_i^- = \begin{pmatrix} \chi_i^- \\ \chi_i^+ \end{pmatrix},$$

i.e. the charge-conjugate of $\widetilde{\chi}^+$ (as required).

Using the definition of the physical fields Z_μ and A_μ ,

$$\begin{pmatrix} Z_\mu \\ A_\mu \end{pmatrix} = \begin{pmatrix} \cos\theta_w & -\sin\theta_w \\ \sin\theta_w & \cos\theta_w \end{pmatrix} \begin{pmatrix} W_\mu^0 \\ B_\mu \end{pmatrix},$$

with θ_w being the weak mixing angle, we obtain from Eq. (B.3) for the left-handed parts of the $\widetilde{\chi}^+$:

$$-\overline{\widetilde{\chi}_L^+}^\top \widetilde{A}_L\gamma^\mu Z_\mu\widetilde{\chi}_L^+ = -\overline{\begin{pmatrix} \widetilde{W}_L \\ \widetilde{H}_L \end{pmatrix}}^\top \begin{pmatrix} g\cos\theta_w & 0 \\ 0 & \frac{1}{2}(g\cos\theta_w - g'\sin\theta_w) \end{pmatrix} \gamma^\mu Z_\mu \begin{pmatrix} \widetilde{W}_L \\ \widetilde{H}_L \end{pmatrix},$$

coupling	Feynman rule
$\tilde{\chi}_{i,L}^+ \tilde{\chi}_{j,L}^+ Z_\mu$	$-i c_{ij} \gamma_\mu$
$\tilde{\chi}_{i,R}^+ \tilde{\chi}_{j,R}^+ Z_\mu$	$-i c'_{ij} \gamma_\mu$
$\tilde{\chi}_i^+ \tilde{\chi}_j^+ A_\mu$	$-i e \delta_{ij} \gamma_\mu$

Table B.2: Feynman rules for $\tilde{\chi}^+ \tilde{\chi}^+$ gauge boson couplings for an incoming $\tilde{\chi}_j$

with

$$\widetilde{A}_L = U^{+-1} \begin{pmatrix} g \cos \theta_w & 0 \\ 0 & \frac{1}{2}(g \cos \theta_w - g' \sin \theta_w) \end{pmatrix} U^+ = \begin{pmatrix} c_{11} & c_{12} \\ c_{12} & c_{22} \end{pmatrix}.$$

The c_{ij} are given by [76]:

$$c_{11} = -\frac{g_W}{c_W} \left[s_W^2 - \frac{3}{4} - \frac{1}{4} \cos 2\Phi_+ \right], c_{12} = \frac{g_W}{4 c_W} \sin 2\Phi_+,$$

$$c_{22} = -\frac{g_W}{c_W} \left[s_W^2 - \frac{3}{4} + \frac{1}{4} \cos 2\Phi_+ \right].$$

For the coupling to the right-handed $\tilde{\chi}^+$, we obtain

$$-\overline{\tilde{\chi}_R^+}^\top \begin{pmatrix} c'_{11} & c'_{12} \\ c'_{12} & c'_{22} \end{pmatrix} \gamma^\mu Z_\mu \tilde{\chi}_R^+,$$

with

$$c'_{11} = -\frac{g_W}{c_W} \left[s_W^2 - \frac{3}{4} - \frac{1}{4} \cos 2\Phi_- \right], c'_{12} = \frac{g_W}{4 c_W} \sin 2\Phi_-,$$

$$c'_{22} = -\frac{g_W}{c_W} \left[s_W^2 - \frac{3}{4} + \frac{1}{4} \cos 2\Phi_- \right].$$

Similarly, the coupling of both left- and righthanded parts of $\tilde{\chi}^+$ are given by

$$\langle \tilde{\chi}_i^+ | A | \tilde{\chi}_i^+ \rangle = e$$

with the term in \mathcal{L}_{MSSM} given by

$$-\delta_{ij} e \overline{\tilde{\chi}}^+ \gamma^\mu A_\mu \tilde{\chi}^+.$$

If we choose the $\tilde{\chi}^-$ to be the particle, we have to substitute

$$\overline{\tilde{\chi}_{L/R}^+} \gamma^\mu X_\mu \tilde{\chi}_{L/R}^+ \rightarrow -\overline{\tilde{\chi}_{R/L}^-} \gamma^\mu X_\mu \tilde{\chi}_{R/L}^-.$$

The Feynman rules for $\tilde{\chi} \tilde{\chi}$ gauge-boson couplings are given in Table B.2.

B.4 Lepton-slepton and quark-squark chargino couplings

We will now derive the general Feynman rules for the coupling of a sample $SU(2)$ doublet to charginos. Feynman rules for MSSM particles can then be obtained by putting in the respective quantum numbers and the MSSM form of the superpotential.

For a sample doublet

$$\phi = \begin{pmatrix} \widetilde{u} \\ \widetilde{d} \end{pmatrix}, \psi = \begin{pmatrix} u \\ d \end{pmatrix},$$

the following couplings to charged gauginos and Higgsinos appear:

- gauginos

$$ig(\widetilde{u}_L^* \widetilde{W}^+ d_L + \widetilde{d}_L^* \widetilde{W}^- u_L) + h.c.$$

(all $SU(2)$ doublets)

- Higgsinos

terms of the form

$$\widetilde{u}_R y_U d_L \widetilde{H}_u^+ + u_R y_U \widetilde{d}_L \widetilde{H}_u^+ + \widetilde{d}_R y_D u_L \widetilde{H}_d^- + d_R y_D \widetilde{u}_L \widetilde{H}_d^- + h.c.$$

Rewriting these terms using

$$\bar{\Psi}_1 P_L \Psi_2 = \eta_1 \chi_2, \quad \bar{\Psi}_1 P_R \Psi_2 = \bar{\eta}_2 \bar{\chi}_1,$$

with Ψ defined by [30]

$$\Psi = \begin{pmatrix} \chi_\alpha \\ \bar{\eta}^{\dot{\alpha}} \end{pmatrix},$$

we end up with

$$\begin{aligned} & -g \left(\bar{\psi}_u P_R \widetilde{W} \widetilde{d}_L + \bar{\psi}_d P_R \widetilde{W}^c \widetilde{u}_L \right) + y_{U,ij} \left(\bar{\psi}_{d,j} P_R \widetilde{H}^c \widetilde{u}_{R,i}^* + \widetilde{d}_{L,j} \bar{\psi}_{u,i} P_L \widetilde{H} \right) \\ & + y_{D,ij} \left(\bar{\psi}_{u,j} P_R \widetilde{H} \widetilde{d}_{R,i}^* + \widetilde{u}_{L,j} \bar{\psi}_{d,i} P_L \widetilde{H}^c \right) + h.c. \end{aligned}$$

We use

$$\begin{aligned} \begin{pmatrix} P_L \widetilde{W} \\ P_L \widetilde{H} \end{pmatrix} &= (U^+)^{-1} \begin{pmatrix} \widetilde{\chi}_{1L} \\ \widetilde{\chi}_{2L} \end{pmatrix}, & \begin{pmatrix} P_R \widetilde{W} \\ P_R \widetilde{H} \end{pmatrix} &= (U^-)^{-1} \begin{pmatrix} \widetilde{\chi}_{1R} \\ \widetilde{\chi}_{2R} \end{pmatrix}, \\ \begin{pmatrix} P_L \widetilde{W}^c \\ P_L \widetilde{H}^c \end{pmatrix} &= (U^-)^\top \begin{pmatrix} \widetilde{\chi}_{1L}^c \\ \widetilde{\chi}_{2L}^c \end{pmatrix}, & \begin{pmatrix} P_R \widetilde{W}^c \\ P_R \widetilde{H}^c \end{pmatrix} &= (U^+)^\top \begin{pmatrix} \widetilde{\chi}_{1R}^c \\ \widetilde{\chi}_{2R}^c \end{pmatrix}, \end{aligned}$$

with

$$\widetilde{W}^c = \begin{pmatrix} -i\widetilde{W}^- \\ (-i\widetilde{W}^+) \end{pmatrix}, \quad \widetilde{H}^c = \begin{pmatrix} \widetilde{H}_d^- \\ \widetilde{H}_u^+ \end{pmatrix}, \quad \widetilde{\chi}_i^c = \begin{pmatrix} \chi_i^- \\ \chi_i^+ \end{pmatrix}.$$

This yields

(a) coupling to left-handed charginos

$$\bar{\psi}_u y_U \tilde{d}_L (U_{i2}^+)^* \tilde{\chi}_{iL}$$

(b) coupling to right-handed charginos

$$(-g \tilde{d}_L \bar{\psi}_u (U_{i1}^-)^* + \tilde{d}_R^* y_D \bar{\psi}_u (U_{i2}^-)^*) \tilde{\chi}_{iR}$$

(c) coupling to left-handed charge-conjugated charginos

$$\bar{\psi}_d y_D \tilde{u}_L U_{i2}^- \tilde{\chi}_{iL}^c$$

(d) coupling to right-handed charge-conjugated charginos

$$(-g \tilde{u}_L \bar{\psi}_d U_{i1}^+ + \tilde{u}_R^* \bar{\psi}_d y_U U_{i2}^+) \tilde{\chi}_{iR}^c$$

(+ *h.c.* for all terms).

They describe the following in- and outgoing charginos

- incoming +, outgoing −

$$(a), (b), (c)^\dagger, (d)^\dagger$$

- incoming −, outgoing +

$$(a)^\dagger, (b)^\dagger, (c), (d)$$

independent of the particle/ antiparticle choice.

From the explicit form of the MSSM potential (A.11)

$$f_{MSSM} = \bar{u} y_u Q H_u - \bar{d} y_d Q H_d - \bar{e} y_e L H_d + \mu H_u H_d,$$

we assign the following values to the sample matrices y_D, y_U used above:

	y_U	y_D
quarks	y_u	y_d
leptons	0	y_e
Higgs	0	0

In the calculation, we assumed y_U and y_D to be real (neglecting CP violating phases). In the high-energy limit, they are usually taken to be nonzero only for the third generations:

$$y_U \propto \delta_{33}, \quad y_D \propto \delta_{33}.$$

The Feynman rules for an incoming $\tilde{\chi}_i^+$ are given in Table B.3.

(s)quarks	(s)leptons	$\tilde{\chi}_i^+$ pol.	Feynman rule
$(t \tilde{b}_L)$		L	$\imath y_t (U_{i2}^+)^*$ (a)
$(u \tilde{d}_L), (c \tilde{s}_L), (t \tilde{b}_L)$	$(\nu_i \tilde{l}_{i,L})$	R	$-\imath g (U_{i1}^-)^*$ (b)
$(t \tilde{b}_R)$	$(\nu_\tau \tilde{\tau}_R)$	R	$\imath y_{b/\tau} (U_{i2}^-)^*$ (b)
$(b \tilde{t}_L)$	$(\tau \tilde{\nu}_{\tau,L})$	R	$\imath y_{b/\tau} (U_{i2}^-)^*$ (c)
$(d \tilde{u}_L), (s \tilde{c}_L), (b \tilde{t}_L)$	$(L_i \tilde{\nu}_{i,L})$	L	$-\imath g (U_{i1}^+)^*$ (d)
$(b \tilde{t}_R)$		L	$\imath y_t (U_{i2}^+)^*$ (d)

Table B.3: quark-squark and lepton-slepton couplings to $\tilde{\chi}_i^+$. $y_{t/b/\tau}$ are the (3,3) indices of the respective CKM matrices, $l_i = e, \mu, \tau$.

B.5 Chargino-Neutralino-Gauge boson and Chargino-Neutralino-Higgs couplings

The part of \mathcal{L}_{MSSM} describing the chargino-neutralino-gauge boson couplings is given by

$$\widetilde{W}^+ \bar{\sigma}^\mu W_\mu^+ \widetilde{W}^0 - \widetilde{W}^0 \bar{\sigma}^\mu W_\mu^+ \widetilde{W}^- - \widetilde{W}^- \bar{\sigma}^\mu W_\mu^- \widetilde{W}^0 + \widetilde{W}^0 \bar{\sigma}^\mu W_\mu^- \widetilde{W}^+$$

from the gaugino sector and

$$-\frac{g}{\sqrt{2}} \left(\widetilde{H}_d^0 \bar{\sigma}^\mu W_\mu^+ \widetilde{H}_d^- + \widetilde{H}_u^+ \bar{\sigma}^\mu W_\mu^+ \widetilde{H}_u^0 + \widetilde{H}_d^- \bar{\sigma}^\mu W_\mu^- \widetilde{H}_d^0 + \widetilde{H}_u^0 \bar{\sigma}^\mu W_\mu^- \widetilde{H}_u^+ \right)$$

from the Higgsino sector.

Rewriting this in four-component notation using the notations of the previous sections, we obtain ²

$$g \left(\widetilde{W}^0 \gamma^\mu W_\mu^- \widetilde{W} + \frac{1}{\sqrt{2}} (\widetilde{H}_d \gamma^\mu W_\mu^- P_R \widetilde{H} - \widetilde{H}_u \gamma^\mu W_\mu^- P_L \widetilde{H}) \right) + h.c.$$

The chargino-neutralino-Higgs coupling terms arise from the gauge part of the Lagrangian

$$-\sqrt{2} \imath g (\bar{\psi} T^a \bar{\lambda}^a \phi - \phi^* T^a \lambda^a \psi).$$

Taking the quantum numbers of the Higgs doublets into account, they are given explicitly by

²We use

$$(\bar{\psi}_1 \gamma^\mu W_\mu^- P_{L/R} \psi_2)^\dagger = \bar{\psi}_2 \gamma^\mu W_\mu^+ P_{R/L} \psi_1$$

and

$$(\psi_1 \gamma^\mu W_\mu^- \psi_2)^\dagger = \bar{\psi}_2 \gamma^\mu W_\mu^+ \psi_1.$$

- H_u terms:

$$\begin{aligned} & \imath \left(g \left[(H_u^+)^* \widetilde{W}^+ \widetilde{H}_u^0 + (H_u^0)^* \widetilde{W}^- \widetilde{H}_u^+ \right] \right. \\ & + \frac{g}{\sqrt{2}} \left[(H_u^+)^* \widetilde{W}^0 \widetilde{H}_u^+ - (H_u^0)^* \widetilde{W}^0 \widetilde{H}_u^0 \right] \\ & \left. + \frac{g'}{\sqrt{2}} \left[(H_u^+)^* \widetilde{B} \widetilde{H}_u^+ + (H_u^0)^* \widetilde{B} \widetilde{H}_u^0 \right] \right) + h.c. \end{aligned}$$

- H_d terms:

$$\begin{aligned} & \imath \left(g \left[(H_d^0)^* \widetilde{W}^+ \widetilde{H}_d^- + (H_d^-)^* \widetilde{W}^- \widetilde{H}_d^0 \right] \right. \\ & + \frac{g}{\sqrt{2}} \left[(H_d^0)^* \widetilde{W}^0 \widetilde{H}_d^0 - (H_d^-)^* \widetilde{W}^0 \widetilde{H}_d^- \right] \\ & \left. - \frac{g'}{\sqrt{2}} \left[(H_d^0)^* \widetilde{B} \widetilde{H}_d^0 + (H_d^-)^* \widetilde{B} \widetilde{H}_d^- \right] \right) + h.c. \end{aligned}$$

We can split this up into chargino-chargino-Higgs, neutralino-neutralino-Higgs, and chargino-neutralino-Higgs couplings. For actual calculations, we need to transform the Higgs bosons into Higgs mass eigenstates. We postpone this and here only sketch the coupling structure coming from the chargino/ neutralino sector. More details can be found in [142].

Chargino-Chargino-Higgs couplings

The respective terms in the Lagrangian are given by

$$\imath g ((H_u^0)^* \widetilde{W}^- \widetilde{H}_u^+ + (H_d^0)^* \widetilde{W}^+ \widetilde{H}_d^-) + h.c.$$

In four-component notation, this reads

$$-g (\widetilde{W}_R (H_u^0)^* \widetilde{H}_L + \widetilde{H}_R (H_d^0)^* \widetilde{W}_L) + h.c.$$

Transforming this into the chargino eigenstates, we obtain

$$-g \left(\widetilde{\chi}_{i,R}^+ \left[U_{i1}^- (H_u^0)^* (U_{j2}^+)^* + U_{i2}^- (H_d^0)^* (U_{j1}^+)^* \right] \widetilde{\chi}_{j,L}^+ \right) + h.c.$$

for the couplings of left- and right-handed charginos to Higgs bosons. Apart from the rotation into the Higgs mass eigenstates, these couplings agree with the ones given in [142].

Chargino-neutralino-Higgs couplings

Chargino-neutralino-Higgs couplings are given by

$$\begin{aligned} & \imath \left((H_u^+)^* \left(g \widetilde{W}^+ \widetilde{H}_u^0 + \frac{g}{\sqrt{2}} \widetilde{W}^0 \widetilde{H}_u^+ + \frac{g'}{\sqrt{2}} \widetilde{B} \widetilde{H}_u^+ \right) \right. \\ & \left. + (H_d^-)^* \left(g \widetilde{W}^- \widetilde{H}_d^0 - \frac{g}{\sqrt{2}} \widetilde{W}^0 \widetilde{H}_d^- - \frac{g'}{\sqrt{2}} \widetilde{B} \widetilde{H}_d^- \right) \right) + h.c. \end{aligned}$$

coupling	Feynman rule
$\tilde{\chi}_{i,R}^+ \tilde{\chi}_{j,L}^- H_u^0$	$i g (U_{i1}^-)^* U_{j2}^+$
$\tilde{\chi}_{i,R}^+ \tilde{\chi}_{j,L}^- H_d^0$	$i g (U_{i2}^-)^* U_{j1}^+$
$\tilde{\chi}_{i,L}^+ \tilde{\chi}_{j,R}^0 H_u^+$	$-i \left(\frac{g'}{\sqrt{2}} N_{j1}^* (U_{i2}^+)^* + \frac{g}{\sqrt{2}} N_{j2}^* (U_{i2}^+)^* + g N_{j4}^* (U_{i1}^+)^* \right)$
$\tilde{\chi}_{i,R}^+ \tilde{\chi}_{j,L}^0 H_d^-$	$i \left(\frac{g'}{\sqrt{2}} N_{j1} (U_{i2}^-)^* + \frac{g}{\sqrt{2}} N_{j2} (U_{i2}^-)^* - g N_{j3} (U_{i1}^-)^* \right)$

Table B.4: Feynman rules for an incoming $\tilde{\chi}^+$

In four-component notation, we obtain

$$\begin{aligned} & \left((H_u^+)^* (-g \tilde{H}_{u,R} \tilde{W}_L - \frac{g}{\sqrt{2}} \tilde{W}_R \tilde{H}_L - \frac{g'}{\sqrt{2}} \tilde{B}_R \tilde{H}_L) \right. \\ & \left. + (H_d^-) (-g \tilde{H}_{d,L} \tilde{W}_R + \frac{g}{\sqrt{2}} \tilde{W}_L \tilde{H}_R + \frac{g'}{\sqrt{2}} \tilde{B}_L \tilde{H}_R) \right) + h.c. \end{aligned}$$

Rotating this into the mass eigenstate basis, we obtain

- Coupling of right-handed neutralinos to left-handed charginos

$$\left[-(H_u^+)^* \tilde{\chi}_{R,i}^0 \left(\frac{g'}{\sqrt{2}} N_{i1}^* (U_{j2}^+)^* + \frac{g}{\sqrt{2}} N_{i2}^* (U_{j2}^+)^* + g N_{i4}^* (U_{j1}^+)^* \right) \tilde{\chi}_{L,j}^+ \right] + h.c.$$

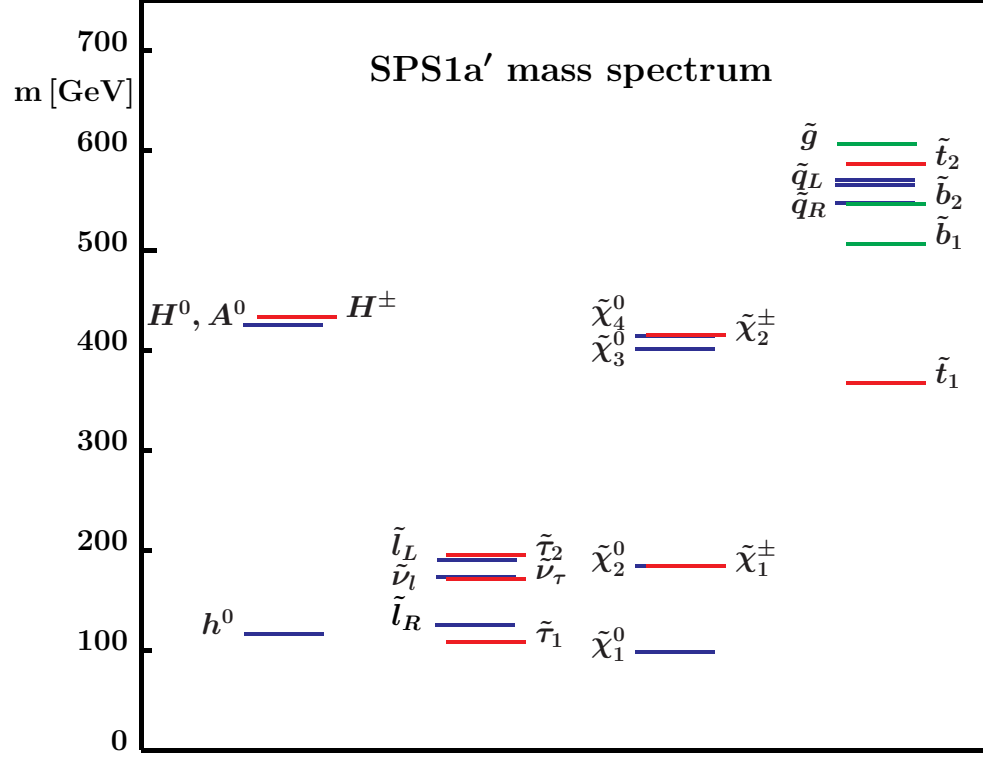
- Coupling of left-handed neutralinos to right-handed charginos

$$\left[-H_d^- \tilde{\chi}_{L,i}^0 \left(-\frac{g'}{\sqrt{2}} N_{i1} (U_{j2}^-)^* - \frac{g}{\sqrt{2}} N_{i2} (U_{j2}^-)^* + g N_{i3} (U_{j1}^-)^* \right) \tilde{\chi}_{R,j}^+ \right] + h.c.$$

Apart from the rotation into Higgs mass eigenstates, this again agrees with the couplings as given in [142].

The Feynman rules for an incoming $\tilde{\chi}^+$ are given in Table B.4

C Point SPS1a'



The mSugra point SPS1a' used in this analysis is defined in [46, 37]. It corresponds to a “typical” mSugra scenario. The respective mSugra parameters are

$$M_{1/2} = 250 \text{ GeV}, M_0 = 70 \text{ GeV}, A_0 = -300 \text{ GeV}, \text{sign}(\mu) = +1, \tan \beta = 10.$$

All particles masses in the point SPS1a' are smaller than 1 TeV and therefore within the reach of future high energy colliders (LHC/ ILC). Branching ratios for decays can be found in [37].

D Helicity eigenstates for massive fermions

In the Dirac formalism, the helicity operator is given by

$$h = \Sigma^k \hat{e}_k, \quad \Sigma^k = \begin{pmatrix} \sigma^k & 0 \\ 0 & \sigma^k \end{pmatrix}$$

for the projection of the spin along the \hat{e}_k direction (see e.g. [143]). Choosing the direction of flight along the z-axis, we can therefore define a spin up/ down projector by

$$P_{u/d} = \frac{1 \pm \sigma \hat{e}_z}{2}.$$

As the helicity operator and the Hamiltonian commute, the Dirac spinors in the Dirac theory can be chosen to be eigenstates of the helicity operator and the Hamilton operator simultaneously; however, the helicity operator is not Lorentz-invariant¹ and therefore frame-dependent. Samples of eigenstates can be found in [143] or [144].

The projector can be brought into a covariant form

$$\Sigma(s) = \frac{1 + \gamma_5 \not{s}}{2}$$

for a spin vector s obeying

$$p^\mu s_\mu = 0$$

(see [144] or [145] for more details).

It can easily be shown that

$$\Sigma(\pm s)\Sigma(\pm s) = \Sigma(\pm s) \quad \text{while} \quad \Sigma(\pm s)\Sigma(\mp s) = 0.$$

The helicity projection operator as well as the energy projection operator then determine the eigenstates $u_\pm(p)$, $v_\mp(p)$ which solve the Dirac equation. For massless states ($p^2 = 0$), the helicity projector reduces to the chirality projector $P_{R/L} = \frac{1 \pm \gamma_5}{2}$.

There are different approaches in the literature to deal with helicity states for massive fermions (see e.g. [146] for an original work or [147] and [127] for reviews on massive fermion treatment/ spinor techniques in general). However, we stick to the formalism introduced in [77]. Here, the authors construct $u_\pm(p)$, $v_\pm(p)$ which satisfy the Dirac equation and are eigenstates of the helicity operator. They then reformulate the 4-component S-matrix elements into spinor-matrix elements using Fierz identities, which they evaluate explicitly in dependence of the respective momenta in a given lab frame.

¹This only holds for massive particles; for massless particles, the helicity projector coincides with the chirality projector which is of course Lorentz-invariant.

Here, we just repeat the formulas used in the calculation of the helicity amplitudes and refer to the original work for further details.

A four component matrix element can be reduced to a two component one using

$$\bar{\psi}_1 \gamma^\mu P_{R/L} \psi_2 = \bar{\psi}_1 \pm \sigma_\pm^\mu \psi_2 \pm.$$

Here,

$$\psi_i = \begin{pmatrix} \psi_{i-} \\ \psi_{i+} \end{pmatrix}.$$

Fierz identities give

$$\begin{aligned} (\psi_1^\dagger)_\alpha \sigma_\pm^\mu (\psi_2)_\beta (\psi_3^\dagger)_\gamma \sigma_{\mu\pm} (\psi_4)_\delta &= 2(\psi_1^\dagger)_\alpha (\psi_4)_\delta (\psi_3^\dagger)_\gamma (\psi_2)_\beta, \\ (\psi_1^\dagger)_\alpha \sigma_\pm^\mu (\psi_2)_\beta (\psi_3^\dagger)_\gamma \sigma_{\mu\mp} (\psi_4)_\delta &= 2(\psi_1^\dagger)_\alpha (\psi_2)_\beta (\psi_3^\dagger)_\gamma (\psi_4)_\delta \\ &\quad - 2(\psi_1^\dagger)_\alpha (\psi_4)_\delta (\psi_3^\dagger)_\gamma (\psi_2)_\beta \end{aligned}$$

where $\alpha, \beta, \gamma, \delta = +, -$. The product of two two-component spinors is given by

$$(\psi_i^\dagger)_\alpha (\psi_j)_\beta = C_i C_j w_{\alpha\lambda_i} w_{\beta\lambda_j} S(p_i, p_j)_{\lambda_i \lambda_j},$$

where

$$\begin{aligned} C_k &= 1 \text{ for } (\psi_k)_\tau = (u_k)_\tau, \\ C_k &= \tau \text{ for } (\psi_k)_\tau = (v_k)_\tau, \\ w_\pm(p) &= \sqrt{E \pm |\vec{p}|}. \end{aligned}$$

If S only depends on the momenta of the external particles, it reduces to the scalar quantity T :

$$S(p_i p_j)_{\lambda_i \lambda_j} = T(p_i p_j)_{\lambda_i \lambda_j} = \chi_\alpha^\dagger(p_i) \chi_\beta(p_j)$$

where χ_\pm are helicity eigenstate spinors. $\lambda_{i,j}$ denote the helicities of the resulting massive particles in the given frame while α, β denote the chiralities². $T(p_i p_j)$ are given as

$$\begin{aligned} T(p_1 p_2)_{++} &= \frac{(|\vec{p}_1| + p_{1,z})(|\vec{p}_2| + p_{2,z}) + (p_{1,x} - ip_{1,y})(p_{2,x} - ip_{2,y})}{2\sqrt{|\vec{p}_1|(|\vec{p}_1| + p_{1,z})|\vec{p}_2|(|\vec{p}_2| + p_{2,z})}}, \\ T(p_1 p_2)_{+-} &= \frac{- (|\vec{p}_1| + p_{1,z})(p_{2,x} - ip_{2,y}) + (|\vec{p}_2| + p_{2,z})(p_{1,x} - ip_{1,y})}{2\sqrt{|\vec{p}_1|(|\vec{p}_1| + p_{1,z})|\vec{p}_2|(|\vec{p}_2| + p_{2,z})}}, \\ T(p_1 p_2)_{-+} &= -T^*(p_1 p_2)_{+-}, \\ T(p_1 p_2)_{--} &= T^*(p_1 p_2)_{++}. \end{aligned}$$

If for example $p_{1,z} = -|\vec{p}_1|$

$$\begin{aligned} T(p_1 p_2)_{++} &= \frac{p_{2,x} + ip_{2,y}}{\sqrt{2|\vec{p}_2|(|\vec{p}_2| + p_{2,z})}}, \\ T(p_1 p_2)_{+-} &= \frac{|\vec{p}_2| + p_{2,z}}{\sqrt{2|\vec{p}_2|(|\vec{p}_2| + p_{2,z})}}. \end{aligned}$$

² $w_{\alpha\lambda_i}$ should be read as $w_{\alpha \times \lambda_i}$, i.e. w_+ for $\alpha = \lambda$ and w_- for $\alpha \neq \lambda$. $w_- = 0$ for massless particles.

Furthermore, it holds that

$$T(p_1 p_2)_{\alpha\beta} = T^*(p_2 p_1)_{\beta\alpha},$$

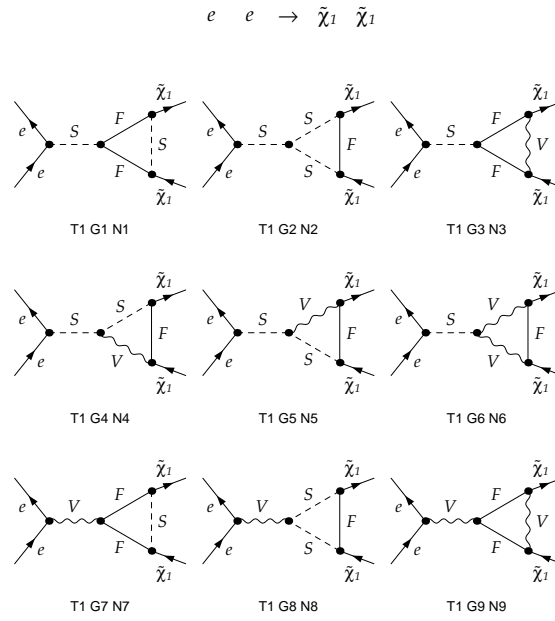
which gives a complete determination of all possible $T_{\alpha\beta}$.

The definition of the eigenstates given here always guarantees that the helicity eigenstates projected in an arbitrary frame correspond to eigenstates of the spin polarization in the rest frame of the respective particle; see [77] and [145] for further details³.

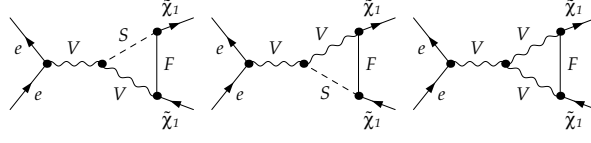
³You just have to identify the χ_{\pm} in [77] (3.19) with the Λ_{\pm} in [145] (Eqn (2-50)).

E Generic diagrams contributing to NLO Chargino production

In the following, we give the generic Feynman diagrams contributing to the process $e^+e^- \rightarrow \tilde{\chi}_1^+ \tilde{\chi}_1^-$ at NLO. S denotes scalar, V vector particles, and F fermions. All diagrams including tadpoles are omitted. The output was generated using **FeynArts**.



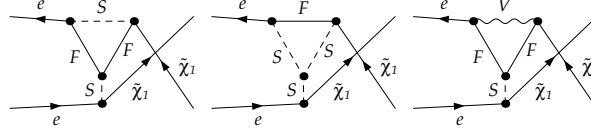
$$e \quad e \rightarrow \tilde{\chi}_1 \quad \tilde{\chi}_1$$



T1 G10 N10

T1 G11 N11

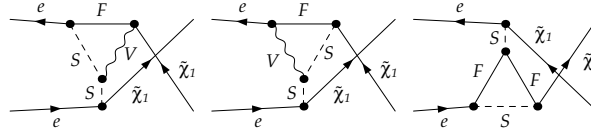
T1 G12 N12



T2 G1 N13

T2 G2 N14

T2 G3 N15

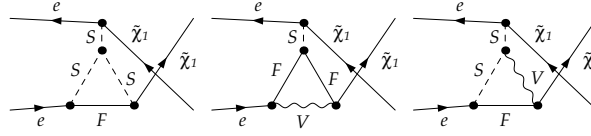


T2 G4 N16

T2 G5 N17

T3 G1 N18

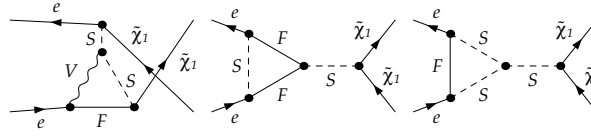
$$e \quad e \rightarrow \tilde{\chi}_1 \quad \tilde{\chi}_1$$



T3 G2 N19

T3 G3 N20

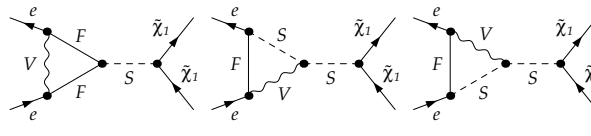
T3 G4 N21



T3 G5 N22

T4 G1 N23

T4 G2 N24

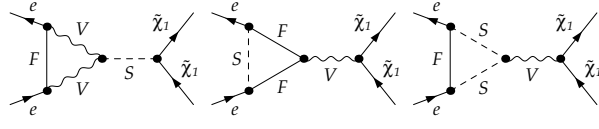


T4 G3 N25

T4 G4 N26

T4 G5 N27

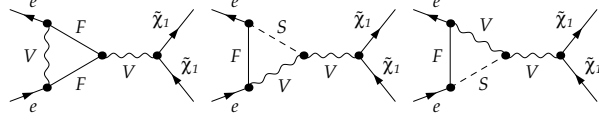
$$e \quad e \rightarrow \tilde{\chi}_1 \quad \tilde{\chi}_1$$



T4 G6 N28

T4 G7 N29

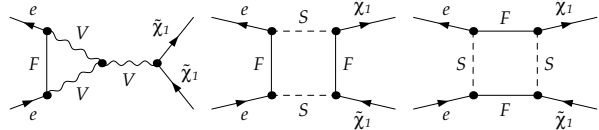
T4 G8 N30



T4 G9 N31

T4 G10 N32

T4 G11 N33

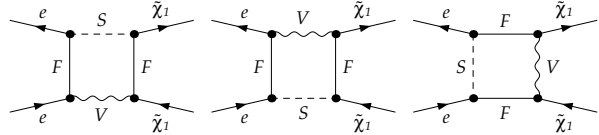


T4 G12 N34

T5 G1 N35

T5 G2 N36

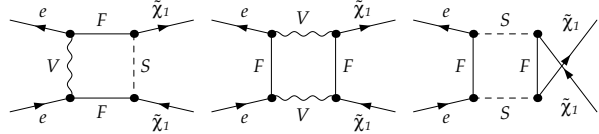
$$e \quad e \rightarrow \tilde{\chi}_1 \quad \tilde{\chi}_1$$



T5 G3 N37

T5 G4 N38

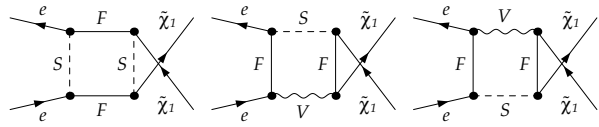
T5 G5 N39



T5 G6 N40

T5 G7 N41

T6 G1 N42

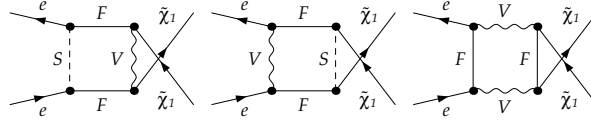


T6 G2 N43

T6 G3 N44

T6 G4 N45

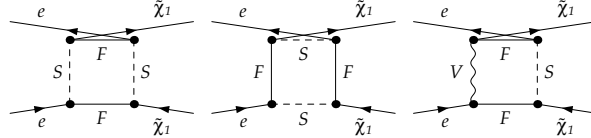
$$e \quad e \rightarrow \tilde{\chi}_1 \quad \tilde{\chi}_1$$



T6 G5 N46

T6 G6 N47

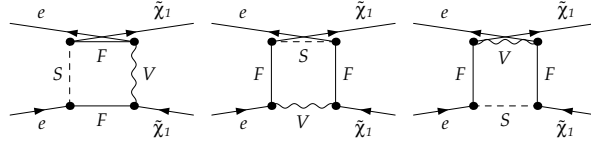
T6 G7 N48



T7 G1 N49

T7 G2 N50

T7 G3 N51

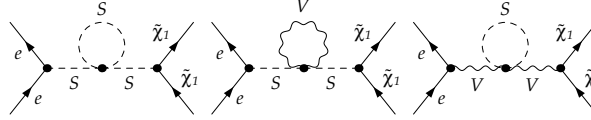


T7 G4 N52

T7 G5 N53

T7 G6 N54

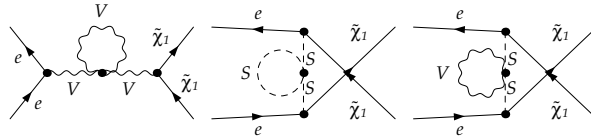
$$e \quad e \rightarrow \tilde{\chi}_1 \quad \tilde{\chi}_1$$



T8 G1 N55

T8 G2 N56

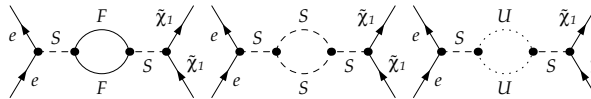
T8 G3 N57



T8 G4 N58

T9 G1 N59

T9 G2 N60

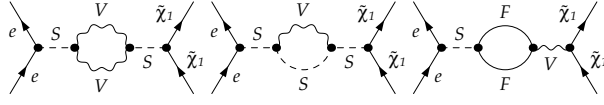


T10 G1 N61

T10 G2 N62

T10 G3 N63

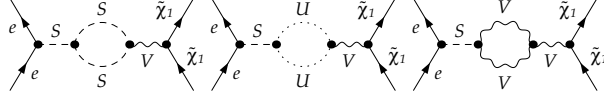
$$e \quad e \rightarrow \tilde{\chi}_1 \quad \tilde{\chi}_1$$



T10 G4 N64

T10 G5 N65

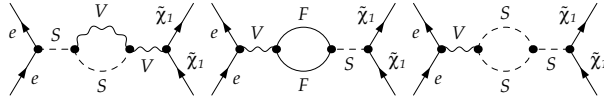
T10 G6 N66



T10 G7 N67

T10 G8 N68

T10 G9 N69

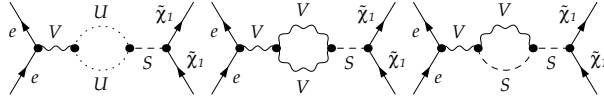


T10 G10 N70

T10 G11 N71

T10 G12 N72

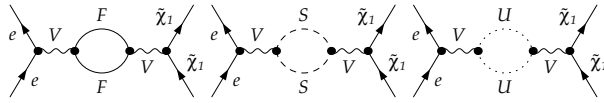
$$e \quad e \rightarrow \tilde{\chi}_1 \quad \tilde{\chi}_1$$



T10 G13 N73

T10 G14 N74

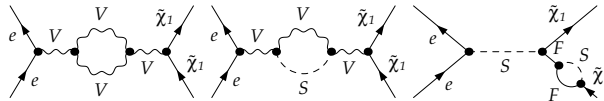
T10 G15 N75



T10 G16 N76

T10 G17 N77

T10 G18 N78

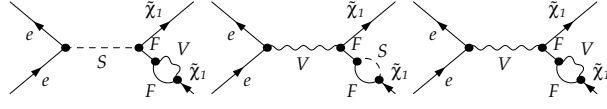


T10 G19 N79

T10 G20 N80

T11 G1 N81

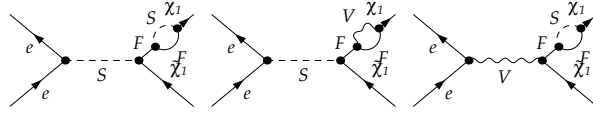
$$e \quad e \rightarrow \tilde{\chi}_1 \quad \tilde{\chi}_1$$



T11 G2 N82

T11 G3 N83

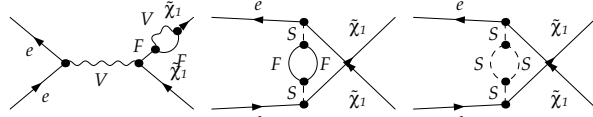
T11 G4 N84



T12 G1 N85

T12 G2 N86

T12 G3 N87

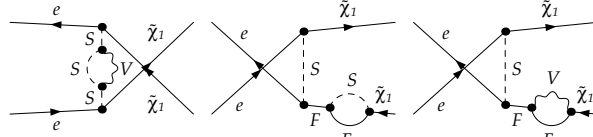


T12 G4 N88

T13 G1 N89

T13 G2 N90

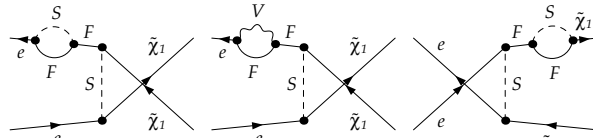
$$e \quad e \rightarrow \tilde{\chi}_1 \quad \tilde{\chi}_1$$



T13 G3 N91

T14 G1 N92

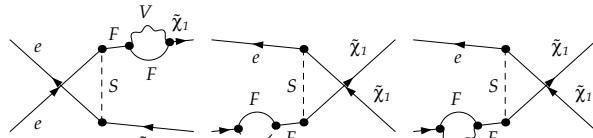
T14 G2 N93



T15 G1 N94

T15 G2 N95

T16 G1 N96

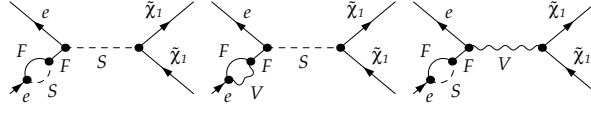


T16 G2 N97

T17 G1 N98

T17 G2 N99

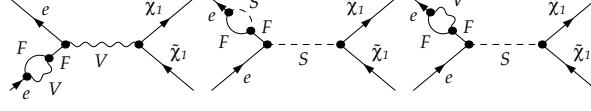
$$e \quad e \rightarrow \tilde{\chi}_1 \quad \tilde{\chi}_1$$



T18 G1 N100

T18 G2 N101

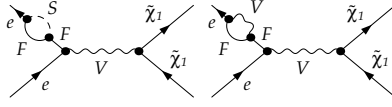
T18 G3 N102



T18 G4 N103

T19 G1 N104

T19 G2 N105



T19 G3 N106

T19 G4 N107

F Soft and collinear approximation; ISR structure function

F.1 Soft Photon Factor

The soft photon factor is given by Eq.(3.6), the integral appearing therein has been calculated in [87] and is given by

$$\int_{|\mathbf{k}| \leq \Delta \mathbf{E}_\gamma} \frac{d^3 k}{2\omega_k} \frac{2p_i p_j}{(p_i k)(p_j k)} = 4\pi \frac{\alpha p_i p_j}{(\alpha p_i)^2 - p_j^2} \left\{ \frac{1}{2} \log \frac{(\alpha p_i)^2}{p_j^2} \log \frac{4\Delta E_\gamma^2}{\lambda^2} \right. \\ \left. + \left[\frac{1}{4} \log^2 \frac{u_0 - |\mathbf{u}|}{u_0 + |\mathbf{u}|} Li_2 \left(1 - \frac{u_0 + |\mathbf{u}|}{v} \right) + Li_2 \left(1 - \frac{u_0 - |\mathbf{u}|}{v} \right) \right]_{u=p_j}^{u=\alpha p_i} \right\},$$

where

$$v = \frac{(\alpha p_i)^2 - p_j^2}{2(\alpha p_{i0} - p_{j0})},$$

and α defined by

$$\alpha^2 p_i^2 - 2\alpha p_i p_j + p_j^2 = 0, \quad \frac{\alpha p_{i0} - p_{j0}}{p_{j0}} > 0.$$

Li_2 are dilogarithms. The integral is regulated by the photon mass λ .

F.2 Hard-collinear approximation

F.2.1 Finite mass effects in collinear radiation

If photons are radiated off a charged particle under a very small angle θ , in the integration over this region of phase space logarithms $\propto \log m$ of the particle appear. The effects can be estimated by the collinear approximation, where in the squared matrix element only terms $\propto \frac{1}{m^2}$ are kept and higher-order terms in θ are neglected. Work along these lines has been done in [148]; we just sketch the derivation and point to this work for further reference. We will deal with the case of unpolarized initial state particles and initial particles in a well-defined helicity eigenstate.

Unpolarized initial particle

We start with the general description of an amplitude where one of the incoming particles radiates off a photon. Without the radiation, the amplitude is given by

$$\mathcal{M} = A(q_i) u(p),$$

where q_i denote the momenta of the other particles involved in the process. If we include radiation, this cross section is modified to

$$\mathcal{M}' = -\frac{e}{2pk} A(q_i) (\not{p} - \not{k} + m) \not{\varepsilon}(k) u(p),$$

where k denotes the momentum of the photon and ε its polarization vector. Squaring the amplitude and summing over the photon polarizations, we obtain

$$|\mathcal{M}|^2 = \sum_{\lambda} \frac{e^2}{4(pk)^2} A(q_i) (\not{p} - \not{k} + m) \gamma^{\mu} (\not{p} + m) \gamma^{\nu} (\not{p} - \not{k} + m) \overline{A}(q_i) \varepsilon_{\lambda}^{\mu} \varepsilon_{\lambda}^{\nu}$$

For the photon polarization sum, we take advantage of the gauge freedom and choose

$$\sum \varepsilon^{\mu} \varepsilon^{\nu} = -g^{\mu\nu} + \frac{k^{\mu} q^{\nu} + q^{\mu} k^{\nu}}{qk},$$

where q is a general lightlike fourvector. We consider the $g^{\mu\nu}$ and the $\frac{k^{\mu} q^{\nu} + q^{\mu} k^{\nu}}{qk}$ part separately.

From the $g^{\mu\nu}$ term, we obtain

$$\begin{aligned} |\mathcal{M}|^2 &= -\frac{e^2}{4(pk)^2} A(q_i) (\not{p} - \not{k} + m) \gamma^{\mu} (\not{p} - m) \gamma_{\mu} (\not{p} - \not{k} + m) \overline{A}(q_i) \\ &= -\frac{e^2}{(pk)^2} A(q_i) (m^3 + (\not{p} - \not{k})m^2 - kp(\not{k} + m)) \overline{A}(q_i), \end{aligned}$$

and for the second part

$$\begin{aligned} |\mathcal{M}|^2 &= \frac{e^2}{4(pk)^2} A(q_i) (\not{p} - \not{k} + m) \gamma_{\mu} (\not{p} - m) \gamma_{\nu} (\not{p} - \not{k} + m) \overline{A}(q_i) \frac{k^{\mu} q^{\nu} + q^{\mu} k^{\nu}}{qk} \\ &= \frac{e^2}{pk} A(q_i) \left(\frac{\not{q} kp - \not{k} pq + 2(m + \not{p})pq}{qk} - (m + \not{p}) \right) \overline{A}(q_i). \end{aligned}$$

In the collinear approximation, we assume that

$$\vec{k} \approx \frac{|\vec{k}|}{|\vec{p}|} \vec{p},$$

i.e. the angle θ between \vec{k} and \vec{p} is small. We then obtain

$$k^{\mu} = x \begin{pmatrix} p^0 \\ |\vec{p}|(\theta + \mathcal{O}(\theta^3)) \\ 0 \\ |\vec{p}|(1 + \mathcal{O}(\theta^2)) \end{pmatrix} \approx x p^{\mu} (1 + \mathcal{O}(\theta)),$$

where

$$x \equiv \frac{k^0}{p^0}.$$

Therefore,

$$pk = p^\mu k_\mu = xm^2(1 + \mathcal{O}(\theta)).$$

Now, we consider the terms pq and kq . In [148], it is assumed that the angles α' between \vec{k} and \vec{q} , and β' between \vec{p} and \vec{q} are very large such that

$$\begin{aligned} \vec{k} \cdot \vec{q} &= |\vec{k}| |\vec{q}| (\alpha + \mathcal{O}(\alpha^3)), \\ \vec{p} \cdot \vec{q} &= |\vec{p}| |\vec{q}| (\beta + \mathcal{O}(\beta^3)), \end{aligned}$$

with

$$\alpha = \frac{\pi}{2} - \alpha', \quad \beta = \frac{\pi}{2} - \beta',$$

and therefore

$$\frac{kq}{pq} = x \left(1 + \mathcal{O}(\alpha) + \mathcal{O}(\beta) + \mathcal{O}\left(\frac{m_e^2}{(p^0)^2}\right) \right).$$

Note that this analysis also holds if \vec{q} is nearly parallel to \vec{k} and \vec{p} as for

$$q^\mu = \frac{1}{\sqrt{2}} \begin{pmatrix} 1 \\ -\hat{k} \end{pmatrix}.$$

Then, one has

$$\vec{k} \cdot \vec{q} = -\frac{1}{\sqrt{2}} |\vec{k}|, \quad \vec{p} \cdot \vec{q} = -\frac{1}{\sqrt{2}} |\vec{p}| \cos \theta$$

and therefore

$$\frac{kq}{pq} = \frac{2k^0}{p^0 + p^0 \sqrt{(1 - \frac{m^2}{(p^0)^2})(1 - \sin^2 \theta)}} = x \left(1 + \mathcal{O}(\theta) + \mathcal{O}\left(\frac{m^2}{(p^0)^2}\right) \right).$$

We can then continue as before and replace $\mathcal{O}(\alpha) + \mathcal{O}(\beta)$ by $\mathcal{O}(\theta)$ in the error considerations.

Now we look at the single contributions, where we only keep terms of $\mathcal{O}(m^{-2})$ and equally ignore higher-order terms in θ, α, β . We obtain from the $-g^{\mu\nu}$ term:

$$\begin{aligned} \frac{m^3}{(pk)^2} &\longrightarrow \frac{1}{x^2} \mathcal{O}(m^{-1})(1 + \mathcal{O}(\theta)); \\ \frac{m^2}{(pk)^2} k &\longrightarrow x \frac{m^2}{(pk)^2} \not{p} + \frac{1}{x} \mathcal{O}(m^{-2}) \mathcal{O}(\theta) \not{p}; \\ \frac{1}{kp} k &\longrightarrow \frac{1}{kp} x \not{p} + \mathcal{O}(\theta) \mathcal{O}(m^{-2}) \not{p}; \\ \frac{m}{pk} &\longrightarrow \frac{1}{x} \mathcal{O}(m^{-1})(1 + \mathcal{O}(\theta)) \end{aligned}$$

and therefore

$$\frac{1}{(pk)^2} (m^3 + (\not{p} - \not{k})m^2 - kp(\not{k} + m)) = \left(\frac{m^2(1-x)}{(pk)^2} - \frac{x}{pk} \right) \not{p} + \mathcal{O}\left(\frac{1}{m}, \frac{\theta}{m^2}\right).$$

For the $\frac{k^\mu q^\nu + q^\mu k^\nu}{qk}$ part, one has

$$\begin{aligned} \frac{1}{qk} &\longrightarrow \mathcal{O}(1), \\ \not{k} \frac{pq}{kq pk} &\longrightarrow \frac{1}{pk} \not{p} + \frac{1}{x} \mathcal{O}(m^{-2}) (\mathcal{O}(\theta, \alpha \beta)) \not{p}, \\ \frac{m pq}{pk kq} &\longrightarrow \frac{1}{x^2} \mathcal{O}(m^{-1}) (1 + \mathcal{O}(\theta, \alpha, \beta)), \\ \not{p} \frac{pq}{kq pk} &\longrightarrow \not{p} \frac{1}{x} \frac{1}{pk} + \frac{1}{x^2} \mathcal{O}(m^{-2}) \mathcal{O}(\alpha, \beta) \not{p}, \end{aligned}$$

and therefore

$$\frac{1}{pk} \left(\frac{\not{q} kp - \not{k} pq + 2(m + \not{p}) pq}{qk} - (m + \not{p}) \right) = \frac{1}{x pk} (-2x + 2) \not{p} + \mathcal{O}\left(\frac{1}{m}, \frac{\theta}{m^2}, \frac{\alpha}{m^2}, \frac{\beta}{m^2}\right).$$

Summing up everything, we arrive at

$$|\mathcal{M}|^2 = \frac{e^2}{pk} A(q_i) \left(\frac{2 - 2x + x^2}{x} - \frac{m^2(1-x)}{pk} \right) \not{p} \bar{A}(q_i) \quad (\text{F.1})$$

as given in [148].

Initial particle in definite helicity state

If the radiating particle is in a definite helicity state, \mathcal{M}' is given by

$$\mathcal{M}' = -\frac{e}{2pk} A(q_i) (\not{p} - \not{k} + m) \not{\epsilon}(k) \frac{1}{2} (1 \pm \gamma^5 \not{s}) u(p),$$

where $\vec{s} \parallel \vec{k}$ and $\frac{1}{2}(1 \pm \gamma^5 \not{s})$ projects out the positive/ negative helicity eigenstate. We parameterize s according to

$$s^\mu = P_\parallel \left(\frac{p^\mu}{m} - m \frac{q^\mu}{pq} \right) + P_\perp s_\perp^\mu. \quad (\text{F.2})$$

For the helicity eigenstates, $P_\perp = 0$, and we choose $P_\parallel \geq 0$ and define positive/ negative helicity by the \pm sign.

We now have to calculate

$$|\mathcal{M}|^2 = \sum_\lambda \frac{e^2}{4(pk)^2} A(q_i) (\not{p} - \not{k} + m) \gamma_\mu (\not{p} + m) \frac{1}{2} (1 \pm \gamma^5 \not{s}) \gamma_\nu (\not{p} - \not{k} + m) \bar{A}(q_i) \varepsilon_\lambda^\mu \varepsilon_\lambda^\nu$$

with the same gauge choice as for the unpolarized case. We first consider the $g^{\mu\nu}$ contribution and the p^μ and q^μ part of s^μ , separately. Furthermore, we only calculate the part depending on P_\parallel (the part proportional to 1 in the helicity projector corresponds to the unpolarized case multiplied by $\frac{1}{2}$). In the following, we use Z defined by

$$|\mathcal{M}'|^2 \equiv e^2 A(q_i) Z \overline{A}(q_i).$$

We consider the contributions coming from the combination of two terms in the polarization sum and two terms in s separately. In the following, the first term in the brackets denotes the term coming from the polarization sum $\sum \varepsilon^{\mu\nu}$, the second the term stemming from s^ρ .

$$\left(-g^{\mu\nu}, \frac{p^\rho}{m}\right)$$

For the $\frac{p^\mu}{m}$ part, we obtain

$$Z = -\frac{1}{4(pk)^2} \left(-2 \not{k} \cdot \gamma^5 (m^2 - kp) + m (\not{k} \cdot \not{p} \cdot \gamma^5 - \not{p} \cdot \not{k} \cdot \gamma^5 + 4 \gamma^5 kp)\right).$$

We first look at the $\mathcal{O}(m^2)$ terms in the numerator; they are given by

$$-\frac{1}{2} \frac{m^2 - kp}{(pk)^2} \gamma^5 \not{k} \longrightarrow -\frac{1}{2} \gamma^5 \frac{m^2 - kp}{(pk)^2} x \not{p} + \left(1 + \frac{1}{x}\right) \mathcal{O}(m^{-2}) \mathcal{O}(\theta).$$

The leftover terms are of order $\frac{1}{x} \mathcal{O}(m^{-1})$.

$$\left(-g^{\mu\nu}, -m \frac{q^\rho}{pq}\right)$$

From the $-m \frac{q^\mu}{pq}$ part, we obtain

$$\begin{aligned} Z &= \frac{m}{4(pk)^2(pq)} (m^2 \not{k} \cdot \not{q} \cdot \gamma^5 - m^2 \not{p} \cdot \not{q} \cdot \gamma^5 - m^2 \not{q} \cdot \not{k} \cdot \gamma^5 + m^2 \not{q} \cdot \not{p} \cdot \gamma^5 \\ &\quad - 2 \not{q} \cdot \gamma^5 (m^3 - m(kp)) + 2m \not{k} \cdot \gamma^5(kq) - 2m \not{p} \cdot \gamma^5(kq) - 2m \not{k} \cdot \gamma^5(pq) \\ &\quad + 2m \not{p} \cdot \gamma^5(pq) + 4 \gamma^5(kp)(pq)). \end{aligned}$$

Here, the terms relevant for the approximation are given by

$$-\frac{m^2}{2(pk)^2} \gamma^5 \left(1 - \frac{kq}{pq}\right) (\not{p} - \not{k}) \longrightarrow -\frac{m^2}{2(pk)^2} \gamma^5 (x^2 - 2x + 1) \not{p} + \left(1 + \frac{1}{x}\right) \mathcal{O}(m^{-2}) \mathcal{O}(\theta, \alpha, \beta) \not{p}.$$

$$\left(\frac{\not{k}^\mu \not{q}^\nu + \not{q}^\mu \not{k}^\nu}{kq}, \frac{p^\rho}{m}\right)$$

The $\frac{k^\mu q^\nu + q^\mu k^\nu}{kq}$ part of the polarization sum is given by

$$\begin{aligned}
Z &= \frac{1}{4(pk)^2 qk} (m \not{p} \cdot \not{q} \cdot \gamma^5 (kp) + 2m \not{q} \cdot \not{k} \cdot \gamma^5 (kp) - m \not{q} \cdot \not{p} \cdot \gamma^5 (kp) \\
&+ 2 \not{q} \cdot \gamma^5 (m^2 - (kp)) (kp) - 2m^2 \not{k} \cdot \gamma^5 (kq) - 2m \not{p} \cdot \not{k} \cdot \gamma^5 (kq) \\
&+ 2m \gamma^5 (kp) (kq) + 2 \not{p} \cdot \gamma^5 (kp) (kq) + 2m^2 \not{k} \cdot \gamma^5 (pq) - m \not{k} \cdot \not{p} \cdot \gamma^5 (pq) \\
&+ m \not{p} \cdot \not{k} \cdot \gamma^5 (pq) + 2 \not{k} \cdot \gamma^5 (kp) (pq) - 4 \not{p} \cdot \gamma^5 (kp) (pq)).
\end{aligned}$$

The $\mathcal{O}(m^2)$ terms in the numerator are given by

$$\begin{aligned}
& -\frac{1}{2(pk)^2} \gamma^5 \left(m^2 \left(\frac{pq}{kq} - 1 \right) \not{k} + (pk) \left(\not{p} + \frac{pq}{kq} (\not{k} - 2\not{p}) \right) \right) \\
\longrightarrow & -\gamma^5 \frac{1}{2} \left(\frac{m^2}{(pk)^2} (1-x) + \frac{2}{pk} \left(1 - \frac{1}{x} \right) \right) \not{p} + \left(\frac{1}{x} + \frac{1}{x^2} \right) \mathcal{O}(m^{-2}) (\mathcal{O}(\theta, \alpha, \beta)) \not{p}.
\end{aligned}$$

$$\left(\frac{k^\mu q^\nu + q^\mu k^\nu}{kq}, -\frac{m q^\rho}{pq} \right)$$

This part of Z_{tot} is given by

$$\begin{aligned}
Z &= -\frac{m}{4(pk)^2 kq} (m \not{p} \cdot \not{q} \cdot \not{k} \cdot \gamma^5 - m \not{q} \cdot \not{k} \cdot \not{p} \cdot \gamma^5 + 2 \not{q} \cdot \not{p} \cdot \gamma^5 (kp) - 2m \not{k} \cdot \gamma^5 (kq) \\
&+ 2 \not{k} \cdot \not{p} \cdot \gamma^5 (kq) - 2 \not{k} \cdot \not{p} \cdot \gamma^5 (pq)).
\end{aligned}$$

From this, we keep¹

$$-\frac{m^2}{2(pk)^2} \gamma^5 (x-1) (\not{p} - \not{k}) \longrightarrow -\frac{m^2}{2(pk)^2} \gamma^5 (x-1) \not{p} + \frac{1}{x} \mathcal{O}(m^{-2}) \mathcal{O}(\theta).$$

Summing up all terms, we end up with

$$|\mathcal{M}'|^2 = \frac{e^2}{2pk} A(q_i) \left(\frac{2-2x+x^2}{x} - \frac{m^2(1-x+x^2)}{pk} \right) \gamma^5 \not{p} \bar{A}(q_i) \quad (\text{F.3})$$

for the part proportional to P_{\parallel} as given in [148].

F.2.2 Helicity dependent structure functions

In [91, 92, 93], Eqs. (F.1) and (F.3) have been used to derive helicity-dependent structure functions which describe photon radiation integrated over the collinear region. Again,

¹Here we used that

$$\not{p} \not{q} \not{k} = 2qk \not{p} - \not{p} \not{k} \not{q} = 2qk \not{p} - m^2(1 + \mathcal{O}(\theta)) \not{q}.$$

we only sketch the result and refer to these works for further reference. Without photon radiation, the matrix element is given by

$$\mathcal{M} = A(q_i) \frac{1}{2} (1 + \gamma^5 \not{s}) u(p),$$

and the square by

$$|\mathcal{M}|^2 = A(q_i) \frac{1}{2} (1 + \gamma^5 \not{s}) (\not{p} + m) \bar{A}(q_i).$$

With s^μ given by Eq. (F.2), we obtain

$$\not{s}(\not{p} + m) = P_{\parallel} \not{p} + \mathcal{O}(m^2) \not{q}$$

and

$$|\mathcal{M}|^2 = A(q_i) \left(\frac{1}{2} (1 + \gamma^5 P_{\parallel}) \not{p} + \mathcal{O}(m) \right) \bar{A}(q_i).$$

We now have to equate this with

$$|\mathcal{M}'|^2 = \frac{e^2}{2pk} A(q_i) (A_1 + P_{\parallel} A_2 \gamma^5) \bar{A}(q_i),$$

where the A_i were derived in the previous sections. A short calculation then gives

$$|\mathcal{M}'|^2 = \frac{e^2}{2pk} A(q_i) \left(B \frac{1}{2} (1 + \gamma^5 P_{\parallel}) + C \frac{1}{2} (1 - \gamma^5 P_{\parallel}) \right) \not{p} \bar{A}(q_i),$$

with

$$\begin{aligned} B &= \left(\frac{2}{x} - \frac{m^2}{pk} \right) (2 - 2x + x^2), \\ C &= \frac{m^2}{pk} x^2. \end{aligned} \tag{F.4}$$

The next step is the approximation of $\frac{1}{pk}$ by

$$\frac{1}{pk} \approx \frac{2}{x (m^2 + 4(p^0)^2 \sin^2 \frac{\theta}{2})}.$$

This approximation uses

$$\vec{p} \vec{k} \approx p^0 k^0 \left(\cos \theta - \frac{1}{2} \frac{m^2}{(p^0)^2} \right) + \mathcal{O}(\theta^2) \mathcal{O} \left(\frac{m^2}{(p^0)^2} \right) + \mathcal{O} \left(\frac{m^4}{(p^0)^4} \right).$$

Next, we have to approximate the integrals

$$\int_0^{\Delta\theta} \frac{\sin \theta}{pk} d\theta, \int_0^{\Delta\theta} \frac{\sin \theta}{(pk)^2} d\theta$$

in the collinear limit. Here, we use

$$\begin{aligned}\frac{1}{m^2 + 4(p^0)^2 \sin^2 \frac{\theta}{2}} &\approx \frac{1}{m^2 + (p^0)^2 \theta^2} (1 + \mathcal{O}(\theta^2)), \\ \sin \theta &\approx \theta + \mathcal{O}(\theta^3), \\ \ln \left(\frac{m^2 + (p^0)^2 (\Delta\theta)^2}{m^2} \right) &\approx \ln \left(\frac{(p^0)^2 (\Delta\theta)^2}{m^2} \right) + \mathcal{O} \left(\frac{m^2}{(p^0)^2 (\Delta\theta)^2} \right), \\ \left(\frac{1}{m^2} - \frac{1}{m^2 + (p^0)^2 (\Delta\theta)^2} \right) &\approx \frac{1}{m^2} \left(1 + \mathcal{O} \left(\frac{m^2}{(p^0)^2 (\Delta\theta)^2} \right) \right).\end{aligned}$$

As a next step, we approximate the integral over $|\vec{k}_1|$:

$$\int dk_1^0 |\vec{k}_1| = \int (p^0)^2 x (1 + \mathcal{O}(\theta)) dx.$$

Similarly, we assume

$$\begin{aligned}\int d\Gamma_1 d\Gamma_2 d\Gamma_3 \delta^{(4)}(p_1 + p_2 - k_1 - k_2 - k_3) F(p_1, p_2, k_1, k_2, k_3) = \\ \int \frac{|\vec{k}_1| dk_1^0}{(2\pi)^3 2} d\Omega_1 \int d\Gamma_2 d\Gamma_3 \delta^{(4)}(p'_1 + p_2 - k_2 - k_3) F(p'_1, p_2, k_2, k_3),\end{aligned}$$

when

$$p'_1 = (p_1 - k_1) = (1 - x + \mathcal{O}(\theta)) p_1.$$

The differential phase space is given by

$$d\Gamma_i = \frac{d^3 k_i}{(2\pi)^3 2 k_i^0}.$$

The phase space integration approximation is exact for $\theta = 0$.

Taking all this into account, we then obtain for the integration over the factors B and C (Eq. (F.4)):

$$\begin{aligned}\int d\Gamma_1 \frac{e^2}{2pk} (2 - 2x + x^2) \left(\frac{2}{x} - \frac{m^2}{pk} \right) |\mathcal{M}^+|^2 = \\ = \frac{\alpha}{2\pi} \left(\ln \left(\frac{s(\Delta\theta)^2}{4m^2} \right) - 1 \right) \int_{x_{min}}^{x_{max}} \frac{2 - 2x + x^2}{x} |\mathcal{M}^+|^2 dx, \\ \int d\Gamma_1 \frac{e^2 m^2}{2(pk)^2} x^2 |\mathcal{M}^-|^2 = \frac{\alpha}{2\pi} \int_{x_{min}}^{x_{max}} x |\mathcal{M}^-|^2 dx.\end{aligned}$$

Here, \mathcal{M}^\pm denote the same/flipped radiating particle helicity amplitudes for the $2 \rightarrow 2$ particle process and x_{min} and x_{max} are given by

$$\begin{aligned}x_{min} &= \frac{2\Delta E_\gamma}{\sqrt{s}} && \Delta E_\gamma: \text{soft photon cut} \\ x_{max} &= 1 - \frac{(m_3 + m_4)^2}{s} && \text{kinematic limit for 3 body decay.}\end{aligned}$$

If we want to bring this now in the form of a structure function

$$\sigma^{hard,coll}(s) = \int (f^+(x') \sigma^+(x's) + f^-(x') \sigma^-(x's)) dx',$$

we have to substitute

$$x \rightarrow x' = 1 - x \quad , \quad \not{x} = \frac{x'}{x'} \not{x}$$

and obtain

$$\begin{aligned} f^+(x) &= \frac{\alpha}{2\pi} \frac{\Phi(sx)}{\Phi(s)} \frac{1+x^2}{x(1-x)} \left(\ln \left(\frac{s(\Delta\theta)^2}{4m^2} \right) - 1 \right), \\ f^-(x) &= \frac{\alpha}{2\pi} \frac{\Phi(sx)}{\Phi(s)} \frac{1-x}{x}. \end{aligned} \tag{F.5}$$

The factor

$$\frac{\Phi(sx)}{\Phi(s)} = x \left(1 + \mathcal{O} \left(\frac{m^2}{s} \right) \right)$$

takes the difference of fluxes in the calculation of the total cross sections into account.

F.2.3 Connection to leading log expressions

In structure functions, collinear logarithms of the form

$$\ln \left(\frac{Q^2}{m^2} \right)$$

appear, where Q is the scale of the respective process. In these processes, Q is often taken as an upper limit for k_\perp . We show that a change of variables from $\cos \theta$ to p_\perp exactly reproduces the results derived in section F.2.2 and we can substitute

$$\ln \left(\frac{Q^2}{m^2} \right) \longrightarrow \ln \left(\frac{(p^0)^2 (\Delta\theta)^2}{m^2} \right)$$

in the structure functions. With k being the photon four-momentum,

$$\begin{aligned} k_\perp &= k^0 \sin \theta, \\ \cos \theta &= \sqrt{1 - \sin^2 \theta} = 1 - \frac{1}{2} \frac{k_\perp^2}{(k^0)^2} + \mathcal{O} \left(\frac{k_\perp^4}{(k^0)^4} \right), \\ \frac{d \cos \theta}{dk_\perp} &= -\frac{k_\perp}{(k^0)^2}. \end{aligned}$$

Furthermore, one has

$$\frac{1}{pk} = \frac{1}{p^0 k^0} \frac{1}{\frac{1}{2} \frac{k_\perp^2}{(k^0)^2} + \frac{1}{2} \frac{m^2}{(p^0)^2}} \left(1 + \mathcal{O} \left(\frac{k_\perp^4}{(k^0)^4} \right) + \mathcal{O} \left(\frac{m^2}{(p^0)^2} \right) \right).$$

Integrating

$$I := \int_0^{(xp^0\Delta\theta)} \frac{e^2}{2pk} \left(\frac{2}{x} - \frac{m^2}{pk} \right) (2 - 2x + x^2) dk_{\perp},$$

we obtain

$$I = \frac{e^2}{(p^0)^2 x^2} \left(\ln \left(\frac{(\Delta\theta)^2 (p^0)^2}{m^2} \right) - 1 \right) (2 - 2x + x^2),$$

i.e. exactly the result as given in the previous section. We therefore see that an upper limit

$$k_{\perp}^{(max)} = k^0 \Delta\theta$$

exactly gives the usual structure function result integrated up to a scale

$$Q^2 = (k^0 \Delta\theta)^2.$$

F.3 ISR structure function

F.3.1 Exact first order and soft solution

In the following, we will consider the exact first order solution as well as the infinitely summed up soft solution for the electron structure function evolution equation (3.13)

$$\frac{\partial}{\partial \eta} D^{NS}(x, \eta) = \frac{1}{4} \int_x^1 \frac{dz}{z} P(z) D^{NS} \left(\frac{x}{z}, \eta \right)$$

with

$$P_{ee}(x) = \left(\frac{1+x^2}{1-x} \right)_+, \quad \eta = \frac{2\alpha}{\pi} \log \left(\frac{Q^2}{m^2} \right).$$

(cf. Eqs. (3.12),(3.14)). The $+$ -distribution $(h(x))_+$ is defined by

$$(h(x))_+ = \lim_{\varepsilon \rightarrow 0} \left[\theta(1-x-\varepsilon) h(x) - \delta(1-x) \int_0^{1-\varepsilon} h(y) dy \right] \quad (\text{F.6})$$

leading to

$$\int_0^1 dx f(x) (h(x))_+ = \int_0^1 dx (f(x) - f(1)) h(x).$$

D^{NS} denotes the non-singlet part of the structure function [138] describing photon radiation only. In the derivation of the soft regime solution, we will closely follow [95].

The first order solution is given by

$$\begin{aligned} D^{NS,\alpha} &= \delta(1-x) + \lim_{\varepsilon \rightarrow 0} \frac{\eta}{4} \left(\delta(1-x) \left(\frac{3}{2} + 2 \ln(\varepsilon) \right) + \theta(1-x-\varepsilon) \frac{1+x^2}{1-x} \right), \\ \int_{x_0}^1 D^{NS,\alpha}(x) dx &= 1 + \frac{\eta}{4} \left(2 \ln(1-x_0) + x_0 + \frac{1}{2} x_0^2 \right). \end{aligned} \quad (\text{F.7})$$

The soft integrated $\mathcal{O}(\eta)$ contribution (F.17) is negative because, when integrating from x_0 to 1, we do take all virtual, but not all real photon contributions into account. For $x_0 = 0$, the $\mathcal{O}(\eta)$ contribution vanishes and as expected, $\int_0^1 D^{NS,\alpha}(x) dx = 1$.

For the derivation of the solution in the soft regime, we perform a Mellin transform (cf. App G) leading to

$$D^{NS(\xi)}(\eta) = 1 + \frac{1}{4} \int_0^\eta d\beta D^{NS(\xi)}(\beta) P^{(\xi)}, \quad (\text{F.8})$$

where

$$P^{(\xi)} = \psi_0(1) + \psi_0(3) - \psi_0(\xi) - \psi_0(\xi + 2).$$

and $\psi_0(x)$ being the Digamma function defined in Appendix G.5. The formal solution to Eq. (F.8) is

$$D^{NS(\xi)}(\eta) = \exp\left(\frac{1}{4}\eta P^{(\xi)}\right).$$

Performing the inverse Mellin transform then leads to

$$D^{NS}(\eta, x) = \frac{1}{2\pi i} \exp\left(\frac{\eta}{2}\left(\frac{3}{4} - \gamma\right)\right) \int_{c-i\infty}^{c+i\infty} d\xi x^{-\xi} \exp\left(\frac{\eta}{4}(-\psi_0(\xi) - \psi_0(\xi + 2))\right). \quad (\text{F.9})$$

Note that the exponential in front of the integral corresponds to the virtual part solution (modulo some constant terms which disappear when the ξ dependent digamma functions are subtracted).

We then use

$$\psi_0(\xi) + \psi_0(\xi + 2) = 2 \left(\ln(\xi) - \sum_{n=1}^{\infty} \frac{B_{2n}}{2n \xi^{2n}} + \frac{1}{2(\xi + 1)} \right), \quad (\text{F.10})$$

where B_{2n} denote the Bernoulli numbers (cf. Appendix G.5). Only the logarithmic term of Eq. (F.10) is kept. This results in

$$D^{NS}(\eta, x) \simeq \frac{1}{2\pi i} \exp\left(\frac{\eta}{2}\left(\frac{3}{4} - \gamma\right)\right) \int_{c-i\infty}^{c+i\infty} d\xi \frac{x^{-\xi}}{\xi^{\frac{\eta}{2}}} = \exp\left(\frac{\eta}{2}\left(\frac{3}{4} - \gamma\right)\right) \frac{\log\left(\frac{1}{x}\right)^{\frac{\eta}{2}-1}}{\Gamma\left(\frac{\eta}{2}\right)}. \quad (\text{F.11})$$

Finally, we use

$$-\ln(y) = (1 - y) + \frac{1}{2}(1 - y)^2 + \mathcal{O}((1 - y)^3) \quad (\text{F.12})$$

and obtain

$$D^{NS}(\eta, x) = \exp\left(\frac{\eta}{2}\left(\frac{3}{4} - \gamma\right)\right) \frac{\eta}{2} \frac{(1 - x)^{\frac{\eta}{2}-1}}{\Gamma\left(\frac{\eta}{2} + 1\right)}. \quad (\text{F.13})$$

This is the solution to Eq. (3.13) in the soft regime; it contains all orders in η .

Finally, we can ask which splitting function would exactly lead to Eq. (F.13). We therefore look for a function $f(\xi)$ such that (cf. Eq. (F.9))

$$\frac{1}{2\pi i} \int_{c-i\infty}^{c+i\infty} d\xi x^{-\xi} \exp\left(\frac{\eta}{4}f(\xi)\right) = \frac{(1-x)^{\frac{\eta}{2}-1}}{\Gamma(\frac{\eta}{2})}.$$

This is given by

$$f(\xi) = \frac{1}{\Gamma(\frac{\eta}{2})} \int_0^\infty (1-e^{-x})^{\frac{\eta}{2}-1} e^{-\xi x} dx = \frac{\Gamma(\xi)}{\Gamma(\xi+\frac{\eta}{2})} = 1 - \frac{\eta}{2} \psi_0(\xi) + \mathcal{O}((\frac{\eta}{2})^2),$$

where for simplicity we used the Laplace instead of the Mellin transform. Therefore, we see that the approximation for $y \approx 1$ leads then to

$$\psi_0(\xi) + \psi_0(\xi+2) \longrightarrow 2\psi_0(\xi).$$

This corresponds to

$$\frac{1+y^2}{1-y} \longrightarrow \frac{2}{1-y}$$

for the real photon part in the splitting function. In making this substitution, we omitted the term

$$\int_{x_0}^1 \left(\frac{1+y^2}{1-y} - \frac{2}{1-y} \right) dy = -\frac{3}{2} + x_0 + \frac{1}{2}x_0^2 = \mathcal{O}(1-x_0)$$

in the integration of the splitting function in the soft regime. We see that the (dominant) logarithmic behavior is exactly reproduced when integrating the modified structure function in the soft region; the errors are $\mathcal{O}(1-y)$.

F.3.2 Exponentiation

The basic idea of exponentiation is to combine the $\mathcal{O}(\eta^n), n \rightarrow \infty$ emission of soft photons, described in a leading logarithmic approach, with explicit finite order contribution in the hard-collinear regime into structure functions [138, 57, 75, 96, 149, 150]. Then,

- $D(x)$ in the hard regime and
- $\int_{x_0}^1 D(x) dx$ in the soft regime

correspond to the exact solutions up to a certain order of η . Comparisons of different approaches can be found in [75]. Following these lines, Skrzypek and Jadach obtained the following ISR structure function

$$\begin{aligned}
f_{\text{ISR}}(x) = & \frac{\exp\left(-\frac{1}{2}\eta\gamma_E + \frac{3}{8}\eta\right)}{\Gamma\left(1 + \frac{\eta}{2}\right)} \frac{\eta}{2} (1-x)^{\left(\frac{\eta}{2}-1\right)} - \frac{\eta}{4} (1+x) \\
& + \frac{\eta^2}{16} \left(-2(1+x) \ln(1-x) - \frac{2 \ln x}{1-x} + \frac{3}{2}(1+x) \ln x - \frac{x}{2} - \frac{5}{2} \right) \\
& + \frac{\eta^3}{8} \left[-\frac{1+x}{2} \left(\frac{9}{32} - \frac{\pi^2}{12} + \frac{3}{4} \ln(1-x) + \frac{1}{2} \ln^2(1-x) - \frac{1}{4} \ln x \ln(1-x) \right. \right. \\
& \quad \left. \left. + \frac{1}{16} \ln^2 x - \frac{1}{4} \text{Li}_2(1-x) \right) \right. \\
& \quad \left. + \frac{1+x^2}{2(1-x)} \left(-\frac{3}{8} \ln x + \frac{1}{12} \ln^2 x - \frac{1}{2} \ln x \ln(1-x) \right) \right. \\
& \quad \left. - \frac{1}{4}(1-x) \left(\ln(1-x) + \frac{1}{4} \right) + \frac{1}{32}(5-3x) \ln x + \mathcal{O}(\eta^4) \right] \quad (\text{F.14})
\end{aligned}$$

Here,

$$\eta = \frac{2\alpha}{\pi} \left[\ln \left(\frac{Q^2}{m_e^2} \right) - 1 \right]. \quad (\text{F.15})$$

This includes Eq. (F.11) as well as the exact solution for photon radiation up to $\mathcal{O}(\eta^3)$. We see that the definitions of η in (3.14) and (F.15) differ by a non-logarithmic factor; this corresponds to taking finite mass effects in the collinear approximation into account (cf. Appendix F.2).

Checking the requirements for exponentiation, we find that up to $\mathcal{O}(\eta)$,

$$f_{\text{ISR}}(x) = \frac{\eta}{2} (1-x)^{\frac{\eta}{2}-1} \left(1 + \frac{3}{4} \eta \right) - \frac{\eta}{4} (1+x). \quad (\text{F.16})$$

For the hard photon regime, we can expand this in η and obtain

$$f_{\text{ISR}}(x) = \frac{\eta}{2} \left(\frac{1}{1-x} - \frac{1}{2} (1+x) \right) = \frac{\eta}{4} \frac{1+x^2}{1-x} + \mathcal{O}(\eta^2).$$

This reproduces f^+ (F.5). The term missing in the structure function expansion corresponds to the helicity flip contribution f^- which is subdominant. Integrating Eq. (F.16) over the soft region yields

$$\begin{aligned}
\int_{x_0}^1 f_{\text{ISR}} dx &= (1-x_0)^{\frac{\eta}{2}} \left(1 + \frac{3}{8} \eta \right) - \frac{\eta}{4} \left(\frac{3}{2} - x_0 - \frac{1}{2} x_0^2 \right) \\
&= 1 + \frac{\eta}{4} \left(2 \ln(1-x_0) + x_0 + \frac{1}{2} x_0^2 \right) + \mathcal{O}(\eta^2). \quad (\text{F.17})
\end{aligned}$$

We see that this exactly corresponds to the result (F.17) obtained from integrating the the $\mathcal{O}(\eta)$ splitting function P_{ee} . We define the $\mathcal{O}(\alpha)$ part of Eq. (F.17) $f_{\text{soft,ISR}}$:

$$f_{\text{soft,ISR}}(\Delta E_\gamma, \Delta \theta_\gamma, m_e^2) = \frac{\eta}{4} \left(2 \ln(1-x_0) + x_0 + \frac{1}{2} x_0^2 \right). \quad (\text{F.18})$$

G Transformations and (Di)Gamma functions

G.1 The Fourier Transform

The Fourier transform of a function $f(x)$ is given by

$$\hat{f}(p) = \int_{-\infty}^{\infty} e^{-\imath p x} f(x) dx.$$

Its inverse is given by

$$f(x) = \frac{1}{2\pi} \int_{-\infty}^{\infty} e^{\imath p x} \hat{f}(p) dp,$$

where the distribution of factors of $\frac{1}{\sqrt{2\pi}}$ is purely conventional. Note that we used

$$\delta(x) = \frac{1}{2\pi} \int_{-\infty}^{\infty} e^{\imath p x} dx.$$

G.2 The Laplace Transform

The Laplace transform can be derived from the Fourier transform by taking the Fourier transform of

$$g(x) = f(x) e^{-c x},$$

where we assume that

$$f(x) = 0 \text{ for } x < 0$$

and additionally making the change of variables

$$s = c + \imath p.$$

We end up with the Laplace transform

$$\mathcal{L}(s) = \int_0^{\infty} e^{-s x} f(x) dx$$

and its inverse

$$f(x) = \frac{1}{2\imath\pi} \int_{c-\imath\infty}^{c+\imath\infty} e^{s x} \mathcal{L}(s) ds.$$

Note that here the delta-function is given by

$$\delta(x) = \frac{1}{2\imath\pi} \int_{c-\imath\infty}^{c+\imath\infty} e^{s x} ds.$$

An exhaustive list of Laplace transforms and their inverses can be found in [151, 152, 153].

G.3 The Mellin Transform

The Mellin transform can be derived from the Laplace transform by substituting

$$y = e^{-x} ; g(y) = f(-\ln(y)).$$

We then obtain

$$\mathcal{M}(s) = \int_0^{UL} y^{s-1} g(y) dy$$

and

$$g(y) = \frac{1}{2\imath\pi} \int_{c-\imath\infty}^{c+\imath\infty} y^{-s} \mathcal{M}(s) ds.$$

Note that the upper limit of the Mellin transform integral UL depends on the value of $f(x)$ for $x < 0$:

$$UL = \begin{cases} 1 & \text{for } f(x) = 0 \text{ for } x < 0 \\ \infty & \text{for } f(x) \neq 0 \text{ for } x < 0. \end{cases}$$

In the first case, we can easily get the Mellin transform from the Laplace transform by performing the change of variables $x = -\ln(y)$. The delta function is here given by

$$\delta(x - x') = \frac{1}{2\imath\pi} \int_{c-\imath\infty}^{c+\imath\infty} x^{-s} x'^{s-1} ds.$$

An overview on Mellin transformations can be found in [154].

G.4 The Euler Gamma function $\Gamma(x)$

The Gamma function $\Gamma(x)$ is defined by

$$\Gamma(x) = \int_0^\infty t^{x-1} e^{-t} dt$$

for $x > 0$. More useful representations, expansions, and relations to other functions can be found in [155, 156, 157].

G.5 The Digamma function $\psi_0(x)$

The digamma function is formally defined by

$$\psi_0(x) = \frac{d}{dx} \ln(\Gamma(x)).$$

A lot of useful representations, expansions, and relations can be equally found in the literature given in the last section. We here just quote a few properties useful in the ISR

derivation:

$$\begin{aligned}
\psi_0(x) &= -\gamma + \int_0^1 \frac{1-t^{x-1}}{1-t} dt \quad (x > 1), \\
\psi_0(x+n) &= \psi_0(x) + \sum_{k=0}^{n-1} \frac{1}{x+k}, \\
\psi_0(1) &= -\gamma,
\end{aligned} \tag{G.1}$$

where γ is the Euler constant. Eq.(G.1) leads to

$$\int_0^1 \frac{1+y^2}{1-y} y^{\xi-1} dy = -\psi_0(\xi) - \psi_0(\xi+2) + 2C,$$

where

$$C = -\gamma + \int_0^1 \frac{1}{1-t} dt.$$

Another useful relation is given by

$$\psi_0(\xi+1) = \ln(\xi) + \frac{1}{2\xi} - \sum_{n=1}^{\infty} \frac{B_{2n}}{2n\xi^{2n}},$$

where B_{2n} are the Bernoulli numbers.

H References for Computer codes

We list the main literature references for all computer codes mentioned in this work (in order of appearance)

- WHIZARD [52]
- FeynArts / FormCalc [80, 81, 85, 124, 86]
- LoopTools [81]
- CompHEP [119]
- MadGraph [120]
- O'Mega [121]
- CIRCE [122]
- pythia [55]
- Sherpa [53]
- Isajet [54]
- Form [125, 126]

Bibliography

- [1] S. L. Glashow, Nucl. Phys. **22**, 579 (1961)
- [2] S. Weinberg, Phys. Rev. Lett. **19**, 1264 (1967)
- [3] A. Salam, WEAK AND ELECTROMAGNETIC INTERACTIONS, originally printed in *Svartholm: Elementary Particle Theory, Proceedings Of The Nobel Symposium Held 1968 At Lerum, Sweden*, Stockholm 1968, 367-377
- [4] S. L. Glashow, J. Iliopoulos, and L. Maiani, Phys. Rev. **D2**, 1285 (1970)
- [5] H. Fritzsch, M. Gell-Mann, and H. Leutwyler, Phys. Lett. **B47**, 365 (1973)
- [6] P. W. Higgs, Phys. Lett. **12**, 132 (1964)
- [7] F. Englert and R. Brout, Phys. Rev. Lett. **13**, 321 (1964)
- [8] P. W. Higgs, Phys. Rev. Lett. **13**, 508 (1964)
- [9] P. W. Higgs, Phys. Rev. **145**, 1156 (1966)
- [10] T. W. B. Kibble, Phys. Rev. **155**, 1554 (1967)
- [11] W. M. Yao *et al.*, J. Phys. **G33**, 1 (2006)
- [12] B. W. Lee, C. Quigg, and H. B. Thacker, Phys. Rev. **D16**, 1519 (1977)
- [13] B. W. Lee, C. Quigg, and H. B. Thacker, Phys. Rev. Lett. **38**, 883 (1977)
- [14] N. Cabibbo, L. Maiani, G. Parisi, and R. Petronzio, Nucl. Phys. **B158**, 295 (1979)
- [15] T. Hambye and K. Riesselmann, Phys. Rev. **D55**, 7255 (1997)
- [16] G. Isidori, G. Ridolfi, and A. Strumia, Nucl. Phys. **B609**, 387 (2001)
- [17] E. Witten, Nucl. Phys. **B188**, 513 (1981)
- [18] H. Georgi and S. L. Glashow, Phys. Rev. Lett. **32**, 438 (1974)
- [19] R. Haag, J. T. Lopuszanski, and M. Sohnius, Nucl. Phys. **B88**, 257 (1975)
- [20] J. Wess and J. Bagger, *Supersymmetry and supergravity* (Univ. Pr., Princeton, USA, 1992)
- [21] A. H. Chamseddine, R. Arnowitt, and P. Nath, Phys. Rev. Lett. **49**, 970 (1982)

- [22] H. P. Nilles, Phys. Rept. **110**, 1 (1984)
- [23] L. J. Hall, J. D. Lykken, and S. Weinberg, Phys. Rev. **D27**, 2359 (1983)
- [24] M. Dine and A. E. Nelson, Phys. Rev. **D48**, 1277 (1993)
- [25] M. Dine, A. E. Nelson, and Y. Shirman, Phys. Rev. **D51**, 1362 (1995)
- [26] G. F. Giudice and R. Rattazzi, Phys. Rept. **322**, 419 (1999)
- [27] L. Randall and R. Sundrum, Nucl. Phys. **B557**, 79 (1999)
- [28] G. F. Giudice, M. A. Luty, H. Murayama, and R. Rattazzi, JHEP **12**, 027 (1998)
- [29] S. Dimopoulos and H. Georgi, Nucl. Phys. **B193**, 150 (1981)
- [30] H. E. Haber and G. L. Kane, Phys. Rept. **117**, 75 (1985)
- [31] R. Barbieri, Riv. Nuovo Cim. **11N4**, 1 (1988)
- [32] M. F. Sohnius, Phys. Rept. **128**, 39 (1985)
- [33] M. Drees, hep-ph/9611409
- [34] S. P. Martin, hep-ph/9709356
- [35] B. C. Allanach *et al.*, hep-ph/0403133
- [36] G. A. Blair, W. Porod, and P. M. Zerwas, Eur. Phys. J. **C27**, 263 (2003)
- [37] J. A. Aguilar-Saavedra *et al.*, Eur. Phys. J. **C46**, 43 (2006)
- [38] M. Schmitt, Supersymmetry, Experiment
- [39] G. Weiglein *et al.*, hep-ph/0410364
- [40] B. C. Allanach *et al.*, hep-ph/0602198
- [41] A. Djouadi, M. Drees, and J.-L. Kneur, JHEP **03**, 033 (2006)
- [42] C. Adloff *et al.*, Eur. Phys. J. **C20**, 639 (2001)
- [43] M. Kuze and Y. Sirois, Prog. Part. Nucl. Phys. **50**, 1 (2003)
- [44] C. Adloff *et al.*, Phys. Lett. **B568**, 35 (2003)
- [45] J. R. Ellis, S. Heinemeyer, K. A. Olive, and G. Weiglein, JHEP **05**, 005 (2006)
- [46] B. C. Allanach *et al.*, Eur. Phys. J. **C25**, 113 (2002)
- [47] M. M. Nojiri, hep-ph/0411127
- [48] J. A. Aguilar-Saavedra *et al.*, hep-ph/0106315

- [49] K. Desch *et al.*, JHEP **02**, 035 (2004)
- [50] R. Lafaye, T. Plehn, and D. Zerwas, hep-ph/0404282
- [51] P. Bechtle, K. Desch, and P. Wienemann, hep-ph/0506244
- [52] W. Kilian, WHIZARD 1.0: A generic Monte-Carlo integration and event generation package for multi-particle processes. Manual, LC-TOOL-2001-039
- [53] T. Gleisberg *et al.*, JHEP **02**, 056 (2004)
- [54] F. E. Paige, S. D. Protopopescu, H. Baer, and X. Tata, (2003)
- [55] T. Sjostrand, S. Mrenna, and P. Skands, JHEP **05**, 026 (2006)
- [56] K. Hagiwara *et al.*, Phys. Rev. **D73**, 055005 (2006)
- [57] R. Kleiss *et al.*, in *Proceedings, Z physics at LEP 1, vol. 3* (Geneva, 1989)
- [58] Z. Was and S. Jadach, Physics Monte Carlo generators for LEP: A systematic approach, prepared for 2nd International Workshop on Software Engineering, Artificial Intelligence and Expert Systems for High-energy and Nuclear Physics, La Londe Les Maures, France, 13-18 Jan 1992
- [59] <http://epewwg.web.cern.ch>
- [60] A. Denner, S. Dittmaier, M. Roth, and D. Wackeroth, Nucl. Phys. **B587**, 67 (2000)
- [61] S. Jadach *et al.*, Comput. Phys. Commun. **140**, 475 (2001)
- [62] A. Denner, S. Dittmaier, M. Roth, and D. Wackeroth, Eur. Phys. J. direct **C2**, 4 (2000)
- [63] A. Denner, S. Dittmaier, M. Roth, and D. Wackeroth, hep-ph/0005074
- [64] T. Fritzsche and W. Hollik, Nucl. Phys. Proc. Suppl. **135**, 102 (2004)
- [65] W. Oller, H. Eberl, and W. Majerotto, Phys. Lett. **B590**, 273 (2004)
- [66] W. Oller, H. Eberl, and W. Majerotto, hep-ph/0504109
- [67] O. Nicrosini and L. Trentadue, Phys. Lett. **B196**, 551 (1987)
- [68] G. Bonvicini and L. Trentadue, Nucl. Phys. **B323**, 253 (1989)
- [69] Z. Nagy and D. E. Soper, JHEP **10**, 024 (2005)
- [70] M. Kramer, S. Mrenna, and D. E. Soper, Phys. Rev. **D73**, 014022 (2006)
- [71] S. Catani, F. Krauss, R. Kuhn, and B. R. Webber, JHEP **11**, 063 (2001)
- [72] S. Frixione and B. R. Webber, JHEP **06**, 029 (2002)

- [73] S. Frixione and B. R. Webber, hep-ph/0601192
- [74] W. Kilian, J. Reuter, and T. Robens, hep-ph/0607127, to appear in Eur. Phys. J. C
- [75] M. Skrzypek and S. Jadach, Z. Phys. **C49**, 577 (1991)
- [76] S. Y. Choi *et al.*, Eur. Phys. J. **C14**, 535 (2000)
- [77] K. Hagiwara and D. Zeppenfeld, Nucl. Phys. **B274**, 1 (1986)
- [78] S. Y. Choi, A. Djouadi, H. S. Song, and P. M. Zerwas, Eur. Phys. J. **C8**, 669 (1999)
- [79] T. Plehn, private computer program for SUSY at linear colliders
- [80] T. Hahn, The FormCalc homepage, <http://www.feynarts.de/formcalc/>
- [81] T. Hahn and M. Perez-Victoria, Comput. Phys. Commun. **118**, 153 (1999)
- [82] G. A. Ladinsky, Phys. Rev. **D46**, 2922 (1992)
- [83] F. Bloch and A. Nordsieck, Phys. Rev. **52**, 54 (1937)
- [84] T. Fritzsche, Ph.D. Thesis, 2005
- [85] T. Hahn, The FeynArts homepage, <http://www.feynarts.de/>
- [86] T. Hahn and C. Schappacher, Comput. Phys. Commun. **143**, 54 (2002)
- [87] G. 't Hooft and M. J. G. Veltman, Nucl. Phys. **B153**, 365 (1979)
- [88] M. Bohm, A. Denner, and W. Hollik, Nucl. Phys. **B304**, 687 (1988)
- [89] F. A. Berends, R. Kleiss, and W. Hollik, Nucl. Phys. **B304**, 712 (1988)
- [90] A. Denner, Fortschr. Phys. **41**, 307 (1993)
- [91] S. Dittmaier, Ph.D. thesis, RX-1526 (WURZBURG)
- [92] M. Bohm and S. Dittmaier, Nucl. Phys. **B409**, 3 (1993)
- [93] S. Dittmaier and M. Bohm, Nucl. Phys. **B412**, 39 (1994)
- [94] V. N. Gribov and L. N. Lipatov, Sov. J. Nucl. Phys. **15**, 675 (1972)
- [95] F.-z. Chen, P. Wang, C. M. Wu, and Y.-s. Zhu, Analytical approximation of radiatively corrected resonant cross-section, BIHEP-EP-90-01
- [96] M. Skrzypek, Acta Phys. Polon. **B23**, 135 (1992)
- [97] A. Denner, S. Dittmaier, M. Roth, and L. H. Wieders, hep-ph/0502063

- [98] V. S. Fadin, V. A. Khoze, and A. D. Martin, Phys. Lett. **B320**, 141 (1994)
- [99] V. S. Fadin, V. A. Khoze, and A. D. Martin, Phys. Rev. **D49**, 2247 (1994)
- [100] A. Aeppli, G. J. van Oldenborgh, and D. Wyler, Nucl. Phys. **B428**, 126 (1994)
- [101] M. Roth, Ph.D. thesis, 1999, hep-ph/0008033
- [102] K. Melnikov and O. I. Yakovlev, Nucl. Phys. **B471**, 90 (1996)
- [103] W. Beenakker, A. P. Chapovsky, and F. A. Berends, Phys. Lett. **B411**, 203 (1997)
- [104] W. Beenakker, A. P. Chapovsky, and F. A. Berends, Nucl. Phys. **B508**, 17 (1997)
- [105] A. Denner, S. Dittmaier, and M. Roth, Nucl. Phys. **B519**, 39 (1998)
- [106] S. Jadach *et al.*, Phys. Lett. **B417**, 326 (1998)
- [107] S. Jadach *et al.*, Phys. Rev. **D61**, 113010 (2000)
- [108] W. Beenakker, F. A. Berends, and A. P. Chapovsky, Nucl. Phys. **B548**, 3 (1999)
- [109] Y. Kurihara, M. Kuroda, and D. Schildknecht, Nucl. Phys. **B565**, 49 (2000)
- [110] A. Sommerfeld, *Atombau und Spektrallinien, Bd 2* (Vieweg, Braunschweig, 1939)
- [111] A. D. Sakharov, Zh. Eksp. Teor. Fiz. **18**, 631 (1948)
- [112] D. Y. Bardin, W. Beenakker, and A. Denner, Phys. Lett. **B317**, 213 (1993)
- [113] V. S. Fadin, V. A. Khoze, and A. D. Martin, Phys. Lett. **B311**, 311 (1993)
- [114] V. S. Fadin, V. A. Khoze, A. D. Martin, and A. Chapovsky, Phys. Rev. **D52**, 1377 (1995)
- [115] V. S. Fadin, V. A. Khoze, A. D. Martin, and W. J. Stirling, Phys. Lett. **B363**, 112 (1995)
- [116] A. Freitas, D. J. Miller, and P. M. Zerwas, Eur. Phys. J. **C21**, 361 (2001)
- [117] F. James, Rept. Prog. Phys. **43**, 1145 (1980)
- [118] M. A. Dobbs *et al.*, hep-ph/0403045
- [119] A. Pukhov *et al.*, hep-ph/9908288
- [120] T. Stelzer and W. F. Long, Comput. Phys. Commun. **81**, 357 (1994)
- [121] M. Moretti, T. Ohl, and J. Reuter, hep-ph/0102195
- [122] T. Ohl, Comput. Phys. Commun. **101**, 269 (1997)
- [123] J. Reuter *et al.*, ECONF **C0508141**, ALCPG0323, hep-ph/0512012

- [124] T. Hahn, Comput. Phys. Commun. **140**, 418 (2001)
- [125] J. A. M. Vermaseren, The Symbolic manipulation program FORM, KEK-TH-326
- [126] J. A. M. Vermaseren, math-ph/0010025
- [127] S. Dittmaier, Phys. Rev. **D59**, 016007 (1999)
- [128] T. Robens, (2006), internal DESY notes (in preparation)
- [129] P. Skands *et al.*, JHEP **07**, 036 (2004)
- [130] J. P. Alexander, G. Bonvicini, P. S. Drell, and R. Frey, Phys. Rev. **D37**, 56 (1988)
- [131] S. Catani and M. H. Seymour, Phys. Lett. **B378**, 287 (1996)
- [132] S. Catani and M. H. Seymour, Nucl. Phys. **B485**, 291 (1997)
- [133] S. Dittmaier, Nucl. Phys. **B565**, 69 (2000)
- [134] A. Denner, S. Dittmaier, M. Roth, and D. Wackeroth, Nucl. Phys. **B560**, 33 (1999)
- [135] Z. Nagy and D. E. Soper, JHEP **09**, 055 (2003)
- [136] D. R. Yennie, S. C. Frautschi, and H. Suura, Ann. Phys. **13**, 379 (1961)
- [137] V. N. Gribov and L. N. Lipatov, Sov. J. Nucl. Phys. **15**, 438 (1972)
- [138] E. A. Kuraev and V. S. Fadin, Sov. J. Nucl. Phys. **41**, 466 (1985)
- [139] D. Bailin and A. Love, *Supersymmetric gauge field theory and string theory* (IOP, Bristol, UK, 1994)
- [140] A. Bartl, H. Fraas, W. Majerotto, and N. Oshimo, Phys. Rev. **D40**, 1594 (1989)
- [141] S. Y. Choi, J. Kalinowski, G. Moortgat-Pick, and P. M. Zerwas, Eur. Phys. J. **C22**, 563 (2001)
- [142] J. F. Gunion and H. E. Haber, Nucl. Phys. **B272**, 1 (1986)
- [143] F. Schwabl, *Advanced quantum mechanics (QM II)* (Springer, Berlin, Germany, 1997)
- [144] J. D. Bjorken and S. D. Drell, *RELATIVISTIC QUANTUM MECHANICS. (GERMAN TRANSLATION)* (Bibliograph.Inst. (B.I.- Hochschultaschenbuecher), Mannheim, 1966)
- [145] C. Itzykson and J. B. Zuber, *QUANTUM FIELD THEORY* (McGraw-Hill, New York, USA, 1980)
- [146] R. Kleiss and W. J. Stirling, Nucl. Phys. **B262**, 235 (1985)

- [147] H. E. Haber, hep-ph/9405376
- [148] R. Kleiss, Z. Phys. **C33**, 433 (1987)
- [149] S. Jadach, M. Skrzypek, and B. F. L. Ward, Phys. Lett. **B257**, 173 (1991)
- [150] S. Jadach, M. Skrzypek, and B. F. L. Ward, EXPONENTIATION, HIGHER ORDERS AND LEADING LOGS, presented at 25th Rencontre de Moriond: Electroweak Interactions and Unified Theories, Les Arcs, France, Mar 4- 11, 1990
- [151] A. Prudnikov, Y. Brychkov, and O. Marichev, *Integrals and Series: Volume 4* (Gordon and Breach Science Publishers, USA, 1992)
- [152] A. Prudnikov, Y. Brychkov, and O. Marichev, *Integrals and Series: Volume 5* (Gordon and Breach Science Publishers, USA, 1992)
- [153] A. Erdelyi, W. Magnus, F. Oberhettinger, and F. Tricomi, *Tables of Integral Transforms* (McGraw-Hill Book Company, USA, 1954)
- [154] W. Szpankowski, *Average Case Analysis of Algorithms on Sequences* (Wiley and Sons, USA, 2001)
- [155] J. Spanier and K. Oldham, *An atlas of functions* (Hemisphere Publishing Corporation, USA, 1987)
- [156] A. Erdelyi, W. Magnus, F. Oberhettinger, and F. Tricomi, *Higher transcendental Functions* (McGraw-Hill Book Company, USA, 1953)
- [157] I. Gradshteyn and I. Ryzhik, *Tafeln/ Tables (Volume 2)* (Verlag Harri Deutsch, Frankfurt, 1981).

Acknowledgements

First of all, I want to thank my advisor Wolfgang Kilian for supervision and encouragement throughout my whole time at DESY. I furthermore thank Jürgen Reuter, Peter Zerwas, Seong Youl Choi, Jan Kalinowski, Markos Maniatis, Markus Diehl, Alexander Westphal and Frank Steffen for help and discussions. I am grateful for the support I got from the theory group at MPI Munich and the provision of their code, especially Thomas Fritzsche, Wolfgang Hollik, Thomas Hahn, Markus Roth, and Stefan Dittmaier. Thanks for further help and advice goes to Ayres Freitas, Heidi Rzehak, and Michael Spira. Finally, I want to thank Birgit Eberle, Oleg Lebedev, Adam Falkowski, Yann Mambrini, Iman Benmachiche, Yvonne Wong, Koichi Hamaguchi, Paolo Merlatti, Riccardo Catena, Tobias Kleinschmidt, and the rest of the DESY theory group for an open, friendly, and encouraging period at DESY Hamburg. I thank Jürgen Reuter, Frank Deppisch, and Tobias Kleinschmidt for carefully reading the manuscript.

I am greatly indebted to my parents for moral and financial support throughout all of my studies.